North Carolina Agricultural and Technical State University

Aggie Digital Collections and Scholarship

2012

Kinetic And Mechanistic Studies On The Simultaneous Removal Of Nox And So2 By Aqueous Persulfate Activated By Temperature And Fe(Ii) Ions

Nana Y. Sakyi
North Carolina Agricultural and Technical State University

Recommended Citation

KINETIC AND MECHANISTIC STUDIES ON THE SIMULTANEOUS
REMOVAL OF NO$_X$ AND SO$_2$ BY AQUEOUS PERSULFATE
ACTIVATED BY TEMPERATURE AND Fe(II) IONS

by

Nana Y. Sakyi

A thesis submitted to the graduate faculty in partial fulfillment
of the requirements for the degree of
MASTER OF SCIENCE

Department: Chemical and Bioengineering
Major: Chemical Engineering
Major Professor: Dr. Yusuf G. Adewuyi

North Carolina A&T State University
Greensboro, North Carolina
2012

School of Graduate Studies
North Carolina Agricultural and Technical State University

This is to certify that the Master's Thesis of

Nana Y. Sakyi

has met the thesis requirements of
North Carolina Agricultural and Technical State University

Greensboro, North Carolina
2012

Approved by:

Dr. Yusuf G. Adewuyi	Dr. Vinayak Kabadi
Major Professor	Committee Member

Dr. Leonard Uitenham	Dr. Leonard Uitenham
Committee Member	Department Chairperson

Dr. Sanjiv Sarin
Associate Vice Chancellor for Research
and Dean of Graduate Studies

DEDICATION

I dedicate this thesis to my family.

BIOGRAPHICAL SKETCH

Nana Sakyi was born on July 4, 1974 in Accra, Ghana. He received the Bachelor of Science degree in Chemical Engineering from Kwame Nkrumah University of Science and Technology, Kumasi, Ghana in 2006. He is a candidate for the Master of Science degree in Chemical Engineering at North Carolina Agricultural and Technical State University, Greensboro, NC.

ACKNOWLEDGMENTS

TABLE OF CONTENTS

LIST OF FIGURES

FIGURE **PAGE**

LIST OF TABLES

ABSTRACT

Sakyi, Nana Y. KINETIC AND MECHANISTIC STUDIES ON THE SIMULTANEOUS REMOVAL OF NO_X AND SO_2 BY AQUEOUS PERSULFATE ACTIVATED BY TEMPERATURE AND Fe(II) IONS. **(Major Advisor: Yusuf G. Adewuyi),** North Carolina Agricultural and Technical State University.

Nitric Oxide (NO) is regarded as a pollutant with multiple effects. These include visibility impairment, respiratory problems, declined crop yield, greenhouse effect and stratospheric ozone depletion. Together with SO_2, NO is a major contributor to acid rain, ground-level ozone and photochemical smog. Of much recent concern for NO_x (all oxides of nitrogen together) is its ability to form ground-level ozone with volatile organic compounds (VOC) in the presence of heat and sunlight. Consequently, the Environmental Protection Agency (EPA) is becoming stringent in terms of standards for NO_x emissions to protect human health and the environment. Past and current existing methods for NO_x control have high operating cost, strict temperature requirements, and disposal problems. Current federal regulations require that all the utility power plants (some were previously exempted) control their emissions, therefore, much attention has shifted to a less expensive alternative; the use of scrubbing solutions. In this research work, the absorption and oxidation of NO by aqueous $Na_2S_2O_8$ activated by temperature and Fe^{2+} have been studied in a bubble column reactor operated in a semi-batch mode. Experiments were conducted to investigate the effects of persulfate (0.01-0.2 M), Fe^{2+} (0-0.1 M), and gas-phase NO (500-1000 ppm) concentrations. The effects of temperature (23-90°C), presence of SO_2 and the scrubbing solution's pH were also investigated. In addition, mechanistic reaction pathways were proposed, and a previously developed

model was applied to include the case of temperature-Fe^{2+} activation. From these the kinetic rate constants were determined and the activation energies were subsequently estimated. The absorption rate model was also used to obtain the kinetic rate expression. In the presence of 0.01 M Fe^{2+}, 0.1 M persulfate remains the suitable concentration for NO removal by activated persulfate. Overall, presence of 0.01 M Fe^{2+} significantly improved NO removal by about 10% compared to temperature alone activation. The presence of SO_2 gas greatly improved NO removal for temperature activated persulfate and worked best at near neutral pH. SO_2 gas was completely absorbed in all cases, and the rate of reaction of NO with persulfate ($S_2O_8^{2-}$) was found to be first order with respect to NO and zero order with respect to $S_2O_8^{2-}$ ($r_A = k_{mn}C_{NO}$) at 23, 40 and 50°C. The results demonstrate the feasibility of removing NO_x and SO_2 by activated persulfate.

CHAPTER 1

INTRODUCTION

1.1 Background

Nitric Oxide (NO) is one of the seven groups of compound of nitrogen oxides (NO_x). NO and NO_2 form the major components of NO_x [1]. Since NO readily oxidizes to NO_2 by reacting with oxygen in the atmosphere, Environmental Protection Agency (EPA) regulates NO_x emissions by setting standards for NO_2 as a representative of the NO_x family under National Ambient Air Quality Standards (NAAQS) for criteria pollutants. It is therefore acceptable to control NO as a measure to mitigate NO_2 and subsequently NO_x emissions into the atmosphere.

NO_x is emitted during fuel combustion processes. It is produced as a result of either nitrogen being present in the fuel or air used in the high temperature combustion. Due to this, its emission sources could be traced to industrial boilers, power plants (mainly uses coal in US), steel mills, automobile combustion engines, and incinerators. High temperature combustion engines in automobile contribute the most NO_x emissions in the United States. The chart in Figure 1.1 shows NO_x emissions breakdown for Guilford County, North Carolina.
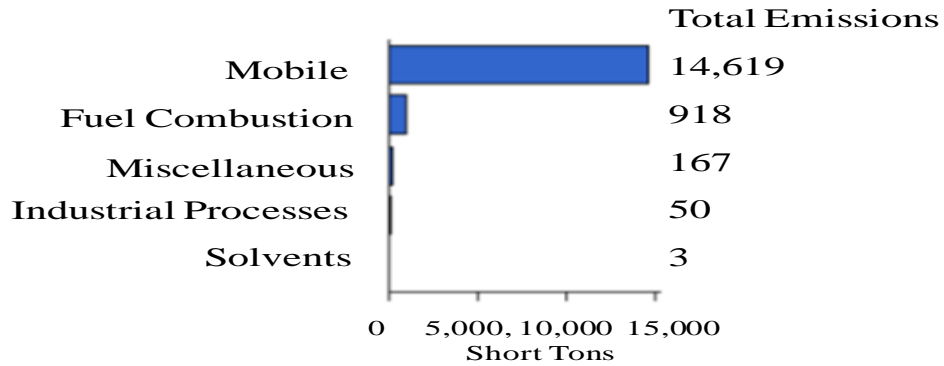
Figure 1.1. Nitrogen Oxides Emissions by Source Sector in Guilford County, NC (Environmental Protection Agency, 2011)

Although NO_x emissions have for the past years fallen below the national average emission standard (see Figure 1.2), the increase in travel has offset much of the efforts directed towards control programs for vehicle emissions.
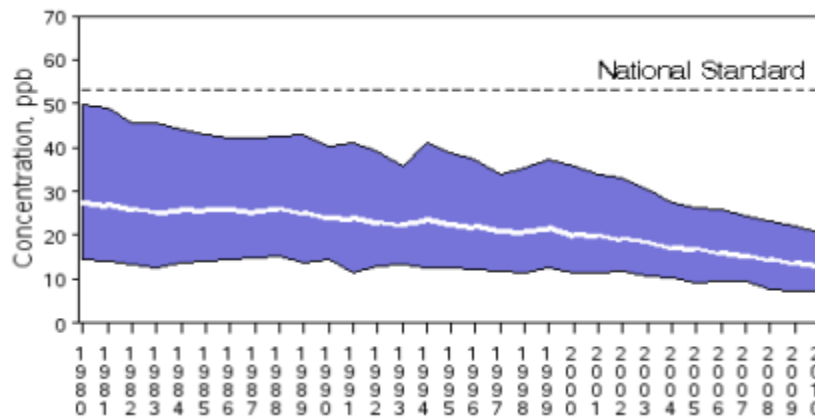
Figure 1.2. NO_2 air quality, 1990-2010 (Based on Annual Arithmetic Average). NationalTrend based on 81 sites (Environmental Protection Agency, 2011)

NO_x combines with ammonia gas, moisture and other compounds to form small particles that are able to penetrate deep into the aveoli of the human lungs. This results in severe

2

respiratory infections, and vulnerable lung issues of children, elderly and asthmatic patients become worse. NO_x is also a major contributor of acid rain which finds its way into fresh waters, estuarine and coastal waters. In addition to aquatic species extinction due to acidification of the water body, nutrient enrichment in the form of nitrates occurs. This leads to Eutrophication where algae growth is promoted. Subsequently, the oxygen level of the water is depleted and more harmful substances are entrapped. The aesthetic value of the water body greatly reduces and the possibility of emerging odor becomes very high. Currently, much concern for NO_x emissions is its ability to form ground-level ozone with volatile organic compounds in the presence of heat and sunlight. This primarily causes visibility impairment in urban areas. Despite the fact that current emissions level fall below the national average standard, NO_x has been identified as a pollutant with multiple effects as shown in Figure 1.3. Therefore, continual efforts are still being devoted to research that will help reduce its emissions to further minimum levels.
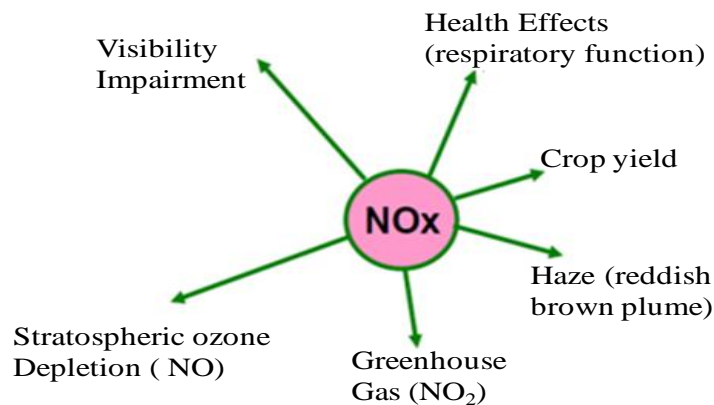
**Figure 1.3. Multiple effects of Nitrogen Oxides Emissions
(Environmental Protection Agency, 2011)**

Both NO_x and SO_2 contribute to the formation of ground-level ozone, urban photochemical smog, acid rain, eutrophication, respiratory and cardiovascular diseases. Since the adoption of Clean Air Act of 1970, whereas the levels of many air pollutants such as NO_2 and SO_2 have decreased, the level of NO has actually increased by 20% [2].

Many control technologies for NOx emissions including selective catalytic reduction (SCR), selective non-catalytic reduction (SNCR), flue gas recirculation (FGR) and thermal NOx control have been attempted [3, 4]. Several other dry adsorption combinative techniques such as SCR with copper and iron based zeolite catalysts have also been used [5]. Due to high operating costs, strict temperature requirements, and disposal problems with these control methods, a less expensive alternative which involves the use of scrubbing solutions have emerged [6]. Numerous chemical oxidants such as $NaClO_2$, sodium hypochlorite, sulfites, $KMnO_4$, and oxone all of which oxidize NO into more soluble forms; NO_2, N_2O_4 etc have been used in a number of scrubbing solutions [1, 5, 7-13]. However, the cost of chemicals, disposal issues, and the complexity of the methods involved did not encourage commercial applications; therefore, current treatment methods have shifted to the use of Advanced Oxidation Processes (AOPs). An AOP involves the generation of reactive radical species that are more powerful than their parent oxidants.

Persulfate ($S_2O_8^{2-}$) oxidant can be activated to produce a more powerful sulfate radical either thermally or by use of transition metal ions. The oxidant is very soluble in water (730 g/l), does not produce odor and has effective oxidation capability over wide temperature range [14]. It is environmentally safe, relatively inexpensive with minimal

4

impact on soil microorganisms [15]. Therefore, it has become the ultimate choice for remediating variety of contaminants. It has also been widely applied in the in situ chemical oxidation (ISCO) remediation of soil, groundwater or subsurface contamination [16, 17].

Although $S_2O_8^{2-}$ is a strong oxidizing agent, it is kinetically slow at ordinary conditions, but can be activated by heat, light, ultrasound or transition ions such as Co(II), Mn, Ce, Fe(II), Cu(I) and Ag(I) to generate intermediate sulfate free radical ($SO_4^{\bullet-}$) [18-28]. Of all the transition metal ions, ferrous iron (Fe^{2+}) is the most common and naturally present in most soils [29, 30] and pollutant systems. Also, just like persulfate, a great deal of information has been documented on ferrous iron. For these reasons we deemed it fit to investigate Fe^{2+} activated persulfate on NO removal from flue gas system. Previous work using thermally activated persulfate for NO absorption, the first of its kind, was conducted from the same laboratory and with the same set of equipment by Khan and Adewuyi [3]. Upon thorough literature survey at the time of doing this research, no work had been done on Fe^{2+} activation of persulfate for NO removal. In this work, the chemistry and effects of temperature and iron (II) activation of persulfate on the fractional conversion of NO were determined via experimental and modeling studies in a bubble column reactor operated in the semibatch mode. In addition, mechanistic reaction pathways were proposed, and previously developed model was applied to correlate the experimental data and determined kinetic rate constants [3]. The activation energies for the NO_x-persulfate-iron (II) reactions were also estimated. Effects of SO_2 and the scrubbing solution pH on NO removal were also evaluated.

1.2 Objectives

The objectives of this research were:

- o To investigate the capability of temperature and/or Fe^{2+} activated persulfate for removal of NO present in flue gases

- o To compare Fe^{2+} activation with temperature activation in NO removal

- o To observe the combined effect of both temperature and Fe^{2+} activations

- o To apply a simple model to correlate and explain experimental data for the temperature-Fe^{2+} activation

- o To develop absorption rate model and obtain kinetic rate expressions

- o To study the effect of NO concentration, presence of SO_2 and pH on NO removal

CHAPTER 2

LITERATURE REVIEW

2.1 Nitric Oxide

Nitric Oxide (NO) is one of the seven member group of oxides of Nitrogen (NO_x). The other members in the family are NO_2, N_2O, N_2O_2, N_2O_3, N_2O_4 and N_2O_5. NO_x is produced from combustion of nitrogen in fuels (coal or heavy oils) or high temperature oxidation of molecular nitrogen when air is used for combustion (thermal NO_x) [31]. Due to the production processes of NO_x, its major emissions sources could be traced to industrial boilers, power plant boilers, incinerators, iron and steel mills, vehicle combustion engines, glass manufacture, cement manufacture and petroleum refineries. NO and NO_2 are the major components of NO_x with NO forming about 90-95% of NO_x in a typical flue gas [5, 10, 13, 32]. NO is rapidly converted to NO_2 by a reaction with oxygen, therefore, EPA regulates NO_2 as a representative of the NO_x family. As stated on EPA's website (http://www.epa.gov/air/nitrogenoxides/health.html), emissions that lead to NO_2 formation also lead to formation of other NO_x components in the family. Hence, control measures to reduce NO formation will help mitigate NO_2 and entire NO_x emissions. Gaseous and aqueous phase reactions of NO_x are shown in equations 2.1 through 2.5 and 2.6 to 2.14 respectively [5].

In the atmosphere, NO_x reacts with ammonia, moisture, and other compounds to form small particles which are able to penetrate deeply into human lungs. NO_x also react with volatile organic compounds in the presence of heat and sunlight to form ground-level

ozone. This, together with the small particles formed from reaction with ammonia has severe and adverse effects on human respiratory system, and can further worsen respiratory problems in asthmatic patients. NO readily converts to NO_2, a very poisonous gas which contributes to the formation of acid rain in the atmosphere [6].

Gaseous-phase reactions of NO_x

$$2NO_{(g)} + O_{2(g)} \longrightarrow 2NO_{2(g)} \tag{2.1}$$

$$2NO_{2(g)} \rightleftarrows N_2O_{4(g)} \tag{2.2}$$

$$NO_{(g)} + NO_{2(g)} \rightleftarrows N_2O_3 \tag{2.3}$$

$$NO_{(g)} + NO_{2(g)} + H_2O_{(g)} \rightleftarrows 2HNO_{2(g)} \tag{2.4}$$

$$3NO_{(g)} + H_2O_{(g)} \rightleftarrows 2HNO_{3(g)} + NO_{(g)} \tag{2.5}$$

Interfacial and Liquid-phase Reactions of NO_x

$$N_2O_{4(g)} \rightleftarrows N_2O_{4(l)} \tag{2.6}$$

$$N_2O_{3(g)} \rightleftarrows N_2O_{3(l)} \tag{2.7}$$

$$NO_{2(g)} \rightleftarrows NO_{2(l)} \tag{2.8}$$

$$HNO_{3(g)} \rightleftarrows HNO_{3(l)} \tag{2.9}$$

$$HNO_{2(g)} \rightleftarrows HNO_{2(l)} \tag{2.10}$$

$$2NO_{2(l)} + H_2O_{(l)} \longrightarrow HNO_{3(l)} + HNO_{2(l)} \tag{2.11}$$

$$N_2O_{3(l)} + H_2O_{(l)} \longrightarrow 2HNO_{2(l)} \longrightarrow 2H^+ + 2NO_2^- \qquad\qquad 2.12$$

$$N_2O_{4(l)} + H_2O_{(l)} \longrightarrow HNO_{2(l)} + HNO_{3(l)} \longrightarrow 2H^+ + NO_2^- + NO_3^- \qquad 2.13$$

$$3HNO_{2(l)} \rightleftarrows HNO_{3(l)} + 2NO_{(l)} + H_2O_{(l)} \qquad\qquad 2.14$$
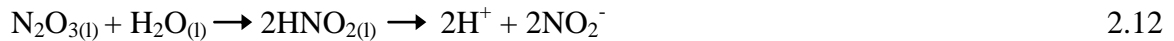
2.2 NOx Emissions Control

Owing to the damaging effects of NO_x on human health and the ecosystem, there has been over the years continuous effort by research scientists to find a cost-effective ways to control emissions into the atmosphere. The best way to control NO_x emissions would have been to reduce or eliminate nitrogen contained fuels and air (molecular nitrogen) used for combustion processes. Pre-combustion methods have not yet been explored; therefore, current control technologies focus on emissions from combustion engines. After the 1990 Clean Air Act Amendments, popular NO_x control methods like SCR, SNCR, FGR and thermal NO_x removal emerged [3]. Several other dry adsorption techniques including SCR with copper based zeolite and iron based zeolite catalysts have also been used [5]. However, these technologies have high operating cost, strict temperature requirements and controls, and disposal problems as major drawbacks. Scrubbing solutions provide less expensive alternative for NO_x removal. While scrubbing solutions are able to easily remove over 90% of SO_2 and NO_2 in a flue gas system, NO absorption by this method is difficult due to its low solubility in aqueous solutions, which decreases with increasing temperature [5]. The sparingly soluble characteristic of NO in aqueous solutions also increases the liquid phase resistance to mass transfer [5, 32]. NO

is easily oxidized to the soluble form of NO_2 (plus N_2O_3, N_2O_4, N_2O_5, or N_2O_2), therefore, current scrubbing methods make use of aqueous solution of oxidants that offer efficient and inexpensive NO_x control technologies and can be easily retrofitted to existing power plants [5]. Adewuyi et al. [5] in 1999 investigated the use of aqueous solutions of sodium chlorite ($NaClO_2$) to simultaneously absorb NO and SO_2 gas in a bubble column reactor. Their results showed complete removal of NO for all aqueous solutions of $NaClO_2$ used at about room temperature. They also observed that NO_2 was generated as a product of NO absorption and oxidation. They further found buffered solutions of $NaClO_2$ to be more effective in simultaneous absorption of NO and SO_2 than $NaClO_2$ in pure water alone or aqueous solutions of NaOH. Optimum pH from their work was between 6 and 7. The results demonstrated NO oxidation into NO_2 which is soluble in aqueous solution [5]. On the contrary, Chu et al., 2001 [9] discovered that the addition of NaOH into solution of $NaClO_2$ decrease the absorption rate of NO. Kinetic study analysis from their work showed the absorption of NO into $NaClO_2$ to be proportional to the squares of partial pressure of NO and $NaClO_2$ concentration, respectively. In addition, they concluded that absorption rate of NO at 25°C was lower than that at 50°C, and independent of gas flow rate [9]. Other investigators like Sada et al. and Brogren et al. have successfully proved $NaClO_2$ to be effective in absorbing NO gas [33, 34]. Solutions of sulphite and permanganate ions, with or without other chemicals have also been discovered to be good oxidants and are able to efficiently absorb NO gas [8, 10-12]. Although good efforts have been made towards NO control, the cost of chemicals,

disposal issues and complexity of the methods involved did not encourage commercial applications of these control technologies [6].

2.3 Current Methods of NOx Control

Current treatment methods focus on processes that are efficient, inexpensive and environmentally friendly. Advanced Oxidation Processes (AOP) is the modern method of pollution control that has been applied to various pollutants including NO_x. It involves the generation of radicals which in chemical and environmental processes have stronger oxidation capability than the parent compounds.

2.3.1 *The Hydroxyl Radical*

The hydroxyl radical ($OH^{\bullet}$) can be produced through sonolysis, use of H_2O_2/ultra violet (UV) light, or by using H_2O_2/Fe^{2+} (Fenton's reagent). Sonochemistry is the use of ultrasound to generate $OH^{\bullet}$ radicals from water. This idea of using $OH^{\bullet}$ radicals to curb emissions is not new. Acid rain formation is a naturally occurring process in which $OH^{\bullet}$ radicals (from UV/water vapor) oxidize NO_x and SO_2 to the corresponding nitric acid (HNO_3) and sulfuric acid (H_2SO_4) respectively. The same phenomenon is being used currently where highly reactive radical species are generated to curb anthropogenic emissions of NO_x and SO_2 from various sources.

Owusu and Adewuyi, 2006 [6] investigated absorption of NO into water with simultaneous oxidation induced by ultrasonic irradiation at a frequency of 20kHz at room temperature in a bubble column reactor. Their results showed that this method could

absorb 65 to 80% of NO gas with complete removal of SO_2 gas at room temperature. They also found NO removal to increase with presence of moderate SO_2 gas concentrations and increasing ultrasound intensity. However, they recommended that the use of this technique for just small scale operations and short term emergency needs. This limits its acceptability for commercial use.

The use of ultrasound to treat pollutants is energy intensive, thereby making it economically unattractive. Therefore sonochemistry has not yet received much attention as an alternative pollution control technique for commercial applications [25]. Equations 2.15 to 2.28 show some sonochemical reactions of OH· radical [26]. See Adewuyi , 2005 [26] for detailed Sonophotochemical reactions.

Sonolysis only (Ultrasound) reactions

$$H_2O +))) \longrightarrow H\cdot + OH\cdot \qquad \text{(where }))) \text{ denotes ultrasonic irradiation)} \qquad 2.15$$

$$OH\cdot + OH\cdot \longrightarrow H_2O + O\cdot \qquad 2.16$$

$$OH\cdot + H_2O \longrightarrow H_2O_2 + H\cdot \qquad 2.17$$

$$H\cdot + OH\cdot \longrightarrow H_2O \qquad 2.18$$

$$O\cdot + O\cdot \longrightarrow O_2 \qquad 2.19$$

$$OH\cdot + OH\cdot \longrightarrow H_2 + O_2 \qquad 2.20$$

$$OH\cdot_{(aq)} + OH\cdot_{(aq)} \longrightarrow H_2O_{2(aq)} \qquad 2.21$$

$$H\cdot + O_2 \longrightarrow HO_2\cdot \qquad\qquad 2.22$$

$$HO_2\cdot + H\cdot \longrightarrow H_2O_2 \qquad\qquad 2.23$$

$$HO_2\cdot + HO_2\cdot \longrightarrow H_2O_2 + O_2 \qquad\qquad 2.24$$

$$O_2 \longrightarrow 2O\cdot \qquad\qquad 2.25$$

$$O_2 + O\cdot \longrightarrow O_3 \qquad\qquad 2.26$$

Fenton reactions

$$Fe^{2+} + H_2O_{2(aq)} \longrightarrow OH\cdot_{(aq)} + Fe^{3+} + OH^-_{(aq)} \qquad\qquad 2.27$$

$$Fe^{2+}_{(aq)} + OH\cdot \longrightarrow Fe^{3+}_{(aq)} + OH^-_{(aq)} \qquad\qquad 2.28$$
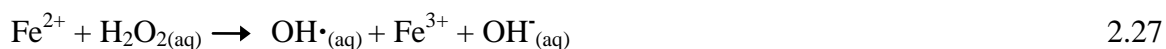
An AOP that has been widely applied and accepted for the degradation of most organic pollutants in water treatment fields is UV/H_2O_2 [35]. Unlike sonochemical approach for generating $OH^{\bullet}$ radicals, UV/H_2O_2 does not require much energy input. It is less complicated and has also been applied effectively in purifying multiple pollutants from flue gas systems. Cooper et al., 2002 [36] looked into NO absorption and oxidation by injecting aqueous solutions of H_2O_2 into flue gas with UV lamp as the initiator. Their results showed NO conversion to vary from below 10 to above 70% for the various combinations of H_2O_2 to NO ratios and UV lamps (none, one or two) at temperatures of 117 to 350°C. Higher conversions occurred at higher temperatures, increased dosages of H_2O_2 and with both UV lamps turned on. They also discovered that, NO or NO_x absorption was not inhibited by the presence of SO_2 gas [36]. Liu et al., 2010 [37] studied

the simultaneous removal of NO and SO_2 gases from coal-fired flue gas by UV/H_2O_2 AOP. Their objective was to check effects of UV lamp power and H_2O_2 concentrations on removal efficiencies. The results indicated higher NO removal with increased UV power or H_2O_2 concentration, and complete removal was observed for SO_2 gas under all conditions studied [37]. Liu et al., 2011 [35] also looked into the kinetics of NO removal from simulated flue gas by wet UV/H_2O_2 AOP using the steady state approximation technique and the two-film theory. The results showed a pseudo-first-order reaction for NO by this removal technique. Also, NO absorption rate primarily depended on the chemical reaction rate, the diffusion rate, and the NO partial pressure, but was independent of the liquid-phase mass-transfer coefficient [35].

A third form of $OH^{\bullet}$ radical generation involving the use of Fenton's reagent has rarely been investigated in the literature for NO removal. However, it has popular applications to many organic pollutants, such as trichloroethylene (TCE) removal in groundwater treatments.

Although Fenton's reagent is effective in treating many of the organic pollutants in groundwater systems, its application to gaseous pollutants, such as NO_x and SO_2 has not been really studied and acknowledged. Even in water treatments using Fenton applications, the pH has to be less than 4 to keep iron in solution. At higher pH, say greater than 6, iron speciation and precipitation occurs, and the efficiency of the Fenton reagent is drastically reduced [38]. Also, $OH^{\bullet}$ radical is non-selective in terms of reactivity and may be scavenged in the presence of other non-target contaminants or ions. Therefore higher doses of oxidant might be required which increases the overall cost of

water treatment. A more recent radical with almost the same oxidation capability as the OH$^\bullet$ radical but with broader range of efficacy on pollutants has been discovered to be the sulfate radical ($SO_4^{\bullet-}$).

2.3.2 *The Sulfate radical*

The $SO_4^{\bullet-}$ radical can be generated either from peroxomonosulfate (reaction shown in equation 2.19), commonly called oxone (HSO_5^-) or persulfate ($S_2O_8^{2-}$). The latter has been used more extensively due to its stability. Studies have shown that cobalt/oxone system is more efficient than Fenton reagent in degrading 2,4-dichlorophenol and atrazine. $SO_4^{-\bullet}$ radical, from persulfate or oxone, has also been found to be more stable than OH· radical from Fenton reaction [38].

$$Co^{2+} + HSO_5^- \longrightarrow Co^{3+} + SO_4^{-\bullet} + OH^- \qquad\qquad 2.29$$

Oxone in itself is a strong oxidizing agent which could be applied directly for the oxidation of NO_x, SO_2, H_2S and organic pollutants. According to Adewuyi and Owusu, 2003 [1], oxone concentration of 0.02M could remove 84% NO (initial of 1040ppm) and 100% SO_2 (initial of 2520ppm) when the gas flow rate is 0.1 standard liters per minute (SLPM) at pH of 6.1 and 22°C temperature. Their kinetic analysis showed the rate of NO reaction with oxone to be first-order with respect to NO and zero order with respect to HSO_5^-. They further observed higher NO removal with the presence of moderate SO_2 gas, but independent of the temperature for the range (22-55°C) studied [1].

2.4 The Persulfate Anion

A more popular and effective way of radical oxidation is by using persulfate. Persulfate is the recent ISCO oxidant that has received wide acceptance. The oxidant was discovered in 1878 by French scientist Marcelin Berthelot. It can be produced from electrolysis of sulfate salts [29]. Persulfate is a strong oxidant with an excellent shelf life when stored properly, and is relatively inexpensive with environmentally friendly end products [3]. The persulfate ion has high solubility in water (730g/l), no odor, and effective oxidation capability over wide temperature range [14]. Prior to activation, it is very stable, a property that has famously rewarded its applications in ISCO including decontamination of groundwater [15-17]. Persulfate exhibits widespread reactivity toward organic compounds, is relatively stable near neutral aqueous solutions, and has minimal impact on soil microorganisms [15]. All these advantages make persulfate a promising choice among the AOPs [39].

The persulfate anion ($S_2O_8^{2-}$) is a strong and non-selective oxidant (E^o = 2.01 V, see redox reaction in equation 2.30) comparable to ozone and hydrogen peroxide, both of which are widely used in water and wastewater treatment. It is kinetically slow when applied directly [3], therefore, can only degrade limited pollutants.

$$S_2O_8^{2-} + 2e^- \longrightarrow 2SO_4^{2-} \quad E^o = 2.01V \tag{2.30}$$

However, when activated according to reaction in equation 2.31, $SO_4^{\bullet-}$ radical which is a stronger oxidant (E^o =2.6V) than the persulfate ion is produced [21]. The $SO_4^{\bullet-}$ radical enhances the kinetics of persulfate oxidation. It is a very potent tool for remediating a

variety of contaminants; chlorinated solvents (of ethenes, ethanes and methanes), BTEX (Benzene, Toulene, Ethylbenzene, Xylene) , MTBE, 1,4-dioxane, PCBs, polyaromatic hydrocarbons, carbon tetrachloride (CTC), 1,1,1-trichloroetane (TCA), TCE, and 2,4-dichlorophenol (2,4-DCP) [21, 30, 40, 41]. Activated persulfate has also found use in olefin polymerization, measurement of total organic carbon (TOC), and as a bleaching agent in the pulp and paper industry [27, 41]. The $SO_4^{\bullet-}$ radical reaction is 10^3 to 10^5 times faster than $S_2O_8{}^{2-}$ [29].

$$S_2O_8{}^{2-} + \text{activator} \longrightarrow SO_4^{\bullet-} + (SO_4^{\bullet-} \text{ or } SO_4{}^{2-}) \hspace{3cm} 2.31$$
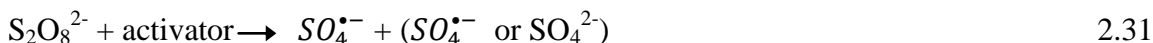
In comparison with $OH^{\bullet}$, $SO_4^{\bullet-}$ radical is more stable in aqueous solutions [23] and has a longer half-life [39]. It also has a unique property of multiple radical effects in applications. Table 2.1 shows the oxidation potential of these associated radicals and oxidants from persulfate [30].

Table 2. 1. Redox Potential for Reactive Species in Activated Persulfate System

Potential Reactive Species in an Activated Persulfate System		
Species		**Potential (V)**
Persulfate anion	$S_2O_8{}^{-2}$	+2.1
Sulfate radical	$SO_4^{\bullet-}$	+2.6
Hydrogen peroxide	H_2O_2	+1.8
Hydroxyl radical	$OH^{\bullet}$	+2.7
Monopersulfate	HSO_5^-	+1.4
Hydroperoxide	HOO^-	
Superoxide	$O_2^-\cdot$	-0.2

$SO_4^{\bullet-}$ radical when generated in aqueous solutions reacts with water according to the reactions in equations 2.32 and 2.33 to produced $OH^{\bullet}$ radicals [42].

All pHs $\quad: SO_4^{\bullet\bullet} + H_2O \longrightarrow SO_4^{2-} + OH\cdot + H^+$ $\qquad\qquad$ 2.32

Alkaline pH : $SO_4^{\bullet\bullet} + OH^- \longrightarrow SO_4^{2-} + OH\cdot$ $\qquad\qquad$ 2.33
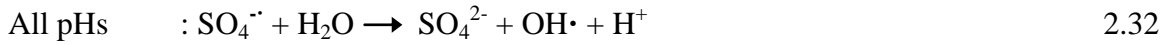
2.5 Persulfate Activation techniques

Several techniques such as use of alkaline [43], activated carbon [14], H_2O_2 , transition metal ions, heat and UV radiation have been used to activate persulfate. Alkaline and H_2O_2 activations by previous researchers did not prove to be efficient [29]. The two main activation methods that have well been investigated and widely applied are temperature (heat or thermal) and transition metal ion activations.

2.5.1 *Thermal Activation of Persulfate*

The persulfate anion can be thermally decomposed according to reaction in equation 2.34 to produce $SO_4^{\bullet\bullet}$ [3, 44].

$S_2O_8{}^{2-} \xrightarrow{\text{heat}} 2SO_4^{\bullet\bullet}$ $\qquad\qquad\qquad\qquad$ 2.34

Heat or thermally activated persulfate has been demonstrated to be able to degrade wide range of contaminants [30] as well as nitric oxide [3]. In studies by Liang and Bruell [44], it was found that thermally activated persulfate could be effective in oxidizing TCE. Kinetic analysis by Liang and Bruell [44] showed thermally activated persulfate reaction with TCE to be pseudo zero order with respect to TCE and 0.8 with respect to persulfate.

Rachel et al. [45] successfully applied thermally activated persulfate for remediation of groundwater contaminated with chlorinated ethenes. In another study, Liang et al., 2003 [46] established the ability of thermally activated persulfate to degrade TCA and TCE at a temperature range of 40 to 99°C. They concluded that good degradation occurs at higher temperatures, and reported the reaction kinetics to be first order with respect to TCA/TCE degradation [46].

In a more recent work, Khan and Adewuyi, 2010 [3] looked into absorption and oxidation of NO by aqueous solutions of sodium persulfate in a bubble column reactor. The process variables studied were $S_2O_8^{2-}$ concentration (0.01-0.2 M), temperature (23-90°C), pH(4-12), sodium chloride concentration (0-0.5 M), and NO concentration (500-1000 ppm). They found that NO removal increased with temperature and $S_2O_8^{2-}$ concentrations (up to 0.1 M), but no significant effect could be attributed to initial NO gas concentrations. They also observed moderate effect from NaCl and solution pH except at higher temperatures. Khan and Adewuyi [3] demonstrated the feasibility of NO removal by aqueous solutions of sodium persulfate.

2.5.2 Transition Metal Activation of Persulfate

As mentioned earlier, the persulfate anion can be activated by transition metals to produce free $SO_4^{-\cdot}$ radicals at room temperature. Examples of transition metals that have so far been investigated are Fe^{2+}, Ag^+, Cu^{2+}, manganese, cerium, and Co^{2+} [20, 27-29, 40]. Transition metal activation can be represented by the reaction in equation 2.35 [14] .

$$S_2O_8{}^{2-} + M^{n+}{}_{(aq)} \longrightarrow M^{(n+1)+}{}_{(aq)} + SO_4{}^{-\cdot}{}_{\textbf{(aq)}} + SO_4{}^{2-}{}_{(aq)} \qquad\qquad 2.35$$

where M = Transition metal

Among the transition metal activators, Fe^{2+} is the most common and readily available [30]. In ISCO applications, Fe^{2+} has mostly been used as activator due to its natural abundance in the soil and benign nature [29]. Because iron has extensively been used in Fenton system with no significant problems and due to its presence in flue gas system, it is regarded as a good choice of activator for NO_x removal by persulfate. Other metal activators, such as Ag^+ and Cu^{2+} may pose subsequent environmental problems due to their toxic nature [29] and can be expensive. Fe^{2+} activation can be described by the reactions shown in equations 2.36, 2.37 and 2.38.

$$Fe^{2+} + S_2O_8{}^{2-} \longrightarrow Fe^{3+} + SO_4{}^{-\cdot} + SO_4{}^{2-} \qquad\qquad 2.36$$

$$Fe^{2+} + SO_4{}^{-\cdot} \longrightarrow Fe^{3+} + SO_4{}^{2-} \qquad\qquad 2.37$$

$$2Fe^{2+} + S_2O_8{}^{2-} \longrightarrow 2Fe^{3+} + 2SO_4{}^{2-} \qquad\qquad 2.38$$

One major advantage of Fe^{2+} activated persulfate is that it can be applied at ambient temperatures. Because of this it has attracted increasingly attention in recent years.

Liang and Lee, 2008 [21] worked on remediation studies by applying Fe^{2+} activated persulfate to TCE removal in a soil column. The results showed TCE degradation efficiency up to 42%. Oh et al., 2009 [47] used Fe^{2+} activated persulfate to oxidize polyvinyl chloride via batch experiments. They reported complete degradation efficiency within 10 minutes. According to Cao et al., 2008 [23], Fe^{2+} activated persulfate can

completely remove lindane, a carcinogenic, persistent organic pollutant from the environment. In another study of Fe^{2+} activated persulfate system, Killian et al., 2007 [48] revealed that up to 85% and 95% of polycyclic aromatic hydrocarbons (PAH) and BTEX respectively could be removed from contaminated soils. Near complete degradation of polychlorinated biphenyls (PCBs) in aqueous and sediment systems could be achieved with Fe^{2+} activated persulfate [39]. In a model wastewater, Kusic et al., 2011 [24] predicted 54.38% degradation of azo dye with Fe^{2+} activated persulfate system. Despite the numerous applications, Fe^{2+} activated persulfate systems have Fe^{2+} applicability challenges just like encountered in Fenton reagent.

One major drawback of Fe^{2+} activated persulfate systems is the antagonistic effect of excess iron. According to the stoichiometry of the overall reaction in equation 2.38, a molar concentration ratio of $Fe^{2+}/S_2O_8^{2-}$ of 2 is required for Fe^{2+} reaction with persulfate. The rate-determining step for $SO_4^{\cdot-}$ radical generation is the reaction shown in equation 2.36 [49]. However, the reaction between Fe^{2+} and $SO_4^{\bullet-}$ according to equation 2.37 occurs so rapidly that any excess Fe^{2+} in the system consumes the $SO_4^{\cdot-}$ radical produced. This limits the amount of $SO_4^{\bullet-}$ radicals available for pollutant oxidation. Liang and Lee, 2008 [21] reported the degradation of TCE to be less in a relatively higher Fe^{2+} concentration than that in lower Fe^{2+} systems. In another study of Fe^{2+} molar concentration effect for oxidation of PVA, degradation efficiency was about 70% for $Fe^{2+}/S_2O_8^{2-}$ molar concentration ratio of 1/1. Further increase of Fe^{2+} concentration to molar ratios of 2/1 or 5/1 dramatically reduced PVA removal [47]. Oh et al., 2009 [47] noticed that unlike heat-activated persulfate, Fe^{2+} activated persulfate did not completely oxidize

PVA. They attributed the decrease in removal efficiency to excess Fe^{2+} that might be working as an intrinsic scavenger to $SO_4^{\bullet-}$ radicals. Similar to the observation made by Oh et al. [47], Cao et al. [23] also found out that maximum degradation of Lindane occurred at Fe^{2+} /$S_2O_8^{2-}$ molar concentration ratio of 1/1.

On the account of evidences from the works of [23], [21] and [47], the Fe^{2+} /$S_2O_8^{2-}$ ratio must be optimized for any Fe^{2+} activated persulfate systems so as to avoid or minimize the occurrence of reaction shown in equation 2.37. Numerous approaches including sequential addition of the Fe^{2+}, use of thiosulfate ($S_2O_3^{2-}$), and providing alternative source of Fe^{2+} have been investigated.

The gradual addition of Fe^{2+} is perceived as a technique that limits the existence and availability of any excess Fe^{2+} ions in Fe^{2+} activated persulfate systems. Liang et al., 2004 [50] demonstrated that adding the Fe^{2+} in small increments resulted in an increased TCE removal efficiency. This method was also used by Killian et al. , 2007 [48] in oxidation of PAH and BTEX compounds found in manufactured gas plants (MGP), and it was successful.

In some cases, $S_2O_3^{2-}$ has been added to solve the excess Fe^{2+} problem. It is conceptualized that $S_2O_3^{2-}$ converts the Fe^{3+} formed back to Fe^{2+}, thus creating a recycling of Fe^{2+}. See the reaction in equation 2.39. According to Liang et al., 2004 [50], sequential addition of $S_2O_3^{2-}$ after the initial Fe^{2+} activated persulfate system had stalled resulted in an improvement in TCE removal to a fairly complete degradation.

$$Fe^{3+} + S_2O_3{}^{2-} \longrightarrow Fe^{2+} + \frac{1}{2}S_4O_6{}^{2-}$$ 2.39

Other researchers have looked into providing a source for Fe^{2+} instead of applying it directly in Fe^{2+} activated persulfate systems. This is to enable slow release of Fe^{2+} ions. Liang and Lai , 2008 [51] successfully applied zerovalent iron (Fe^0) in $Fe^0/S_2O_8{}^{2-}$ system to mineralize TCE. They reported slower decomposition of $S_2O_8{}^{2-}$ in $Fe^0/S_2O_8{}^{2-}$ system than $Fe^{2+}/S_2O_8{}^{2-}$ system, and attributed the observation to slow release of Fe^{2+} from self corrosion of Fe^0. The proposed reaction mechanism for Fe^0 activated persulfate according to Liang and Lai [51] are shown in equations 2.40 through 2.44.

$$Fe^0 \longrightarrow Fe^{2+} + 2e^-$$ 2.40

Under aerobic and anaerobic conditions, we have

$$Fe^0 + \frac{1}{2}O_2 + H_2O \longrightarrow Fe^{2+} + 2OH^-$$ 2.41

$$Fe^0 + 2H_2O \longrightarrow Fe^{2+} + 2OH^- + H_2$$ 2.42

Also,

$$Fe^0 + S_2O_8{}^{2-} \longrightarrow Fe^{2+} + 2SO_4{}^{2-}$$ 2.43

Fe^{2+} recycling from Fe^{3+} possibly occur on the Fe^0 surface through the following reaction.

$$2Fe^{3+} + Fe^0 \longrightarrow 3Fe^{2+}$$ 2.44

The above reactions show a possible way of producing Fe^{2+} from Fe^0 to generate $SO_4^{\bullet-}$ radical through activation of persulfate.

In another Fe^0 study, Liang and Guo, 2010 [52] were able to oxidize naphthalene particles with Fe^0 activated persulfate. They determined the rate constant of Fe^0 activated persulfate degradation of naphthalene to be first order and equal to 3.74 min^{-1}. Another interesting but contradictory discovery by Liang and Guo [52] was that, sequential addition additions of Fe^0 at lower concentrations helped slowed down the formation of $SO_4^{\bullet-}$ radical, hence prevented scavenging of $SO_4^{\bullet-}$ radical by Fe^0 and improved removal of naphthalene particles. Ironically, this is the same problem that occurred with Fe^{2+} and for which Fe^0 was meant to solve. There would have been a good platform for assessment of the two systems had Liang and Guo [52] concurrently worked on Fe^{2+} activated persulfate degradation of naphthalene. Oh et al., 2009 [47] attempted to provide the answer to this issue by comparing the two systems; $Fe^{2+}/S_2O_8^{2-}$ and $Fe^0/S_2O_8^{2-}$ activated persulfate systems for the oxidation of PVA. They reported 70% and approximately 100% of PVA degradation for $Fe^{2+}/S_2O_8^{2-}$ and $Fe^0/S_2O_8^{2-}$ systems respectively for the same conditions studied. Therefore, instead of Fe^{2+}, Fe^0 could be used to effectively enhance the oxidation of PVA by persulfate [47]. Also, in a model studies of persulfate oxidation of azo dye in model wastewater, Kusic et al., 2011 [24] predicted higher performance for $Fe^0/S_2O_8^{2-}$,system over $Fe^{2+}/S_2O_8^{2-}$, confirming the superiority of Fe^0. Pyrite (FeS_2) has been proposed as another source for Fe^{2+}, and been used in oxidation of MTBE [53]. Liang et al., 2010 [53] used pyrite activated persulfate to completely degrade

MTBE under sufficient reaction time at 20°C. They proposed the following reactions pathway, equations 2.45 to 2.49 for $S_2O_8^{2-}$ activation by pyrite.

$$2FeS_2 + 7O_2 + 2H_2O \longrightarrow 2Fe^{2+} + 4SO_4^{2-} + 4H^+ \qquad \qquad 2.45$$

$$4Fe^{2+} + O_2 + 4H^+ \longrightarrow 4Fe^{3+} + 2H_2O \qquad \qquad 2.46$$

$$FeS_2 + 14Fe^{3+} + 8H_2O \longrightarrow 15Fe^{2+} + 2SO_4^{2-} + 16H^+ \qquad \qquad 2.47$$

$$2FeS_2 + 15S_2O_8^{2-} + 16H_2O \longrightarrow 2Fe^{3+} + 34SO_4^{2-} + 32H^+ \qquad \qquad 2.48$$

$$FeS_2 + 2S_2O_8^{2-} \longrightarrow Fe^{2+} + 2SO_4^{\cdot -} + 2SO_4^{2-} + 2S \qquad \qquad 2.49$$
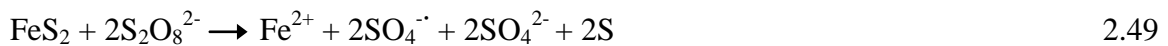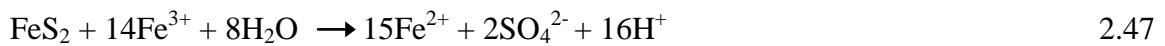
The second major limitation to Fe^{2+} as an activator in Fe^{2+} activated persulfate systems is that iron speciation and precipitation occurs at near-neutral and higher pHs [38]. Therefore there must be a way to keep Fe^{2+} in solution. Various chelating agents have been tried for this purpose [29]. Liang et al., 2004 [54] using the same target pollutant investigated the ability of different kinds of chelating agents to hold Fe^{2+} in solution for Fe^{2+} activated persulfate oxidation of TCE in both soil slurries and aqueous systems. Of all the chelating agents tested under same conditions, citric acid emerged as the most efficient for Fe^{2+} activated persulfate oxidation of TCE [54]. The results of their work [54] is summarized in table 2.2.

Table 2. 2. Chelating agents effect on TCE degradation by Fe^{2+} activate persulfate

	Observed TCE Degradation	
Chelating agent	**Soil Slurries (%)**	**Aqueous system (%)**
Ethyldiamintetraacetic acid (EDTA)	33	34
Sodium triphosphate (STPP)	67	73
Citric Acid	80	90
1-hydroxyethane-1,1-diphosphonic acid (HEDPA)	54	41

[54]

In the same study, Liang et al., 2004 [54] observed approximately 100% destruction of TCE after one hour for both aqueous and soil systems using citric acid as chelating agent. Therefore they concluded that using a citric acid chelated Fe^{2+} ion produces a superior result than that of unchelated Fe^{2+}. In addition, Rastogi et al.,2009 [55] investigated the effectiveness of three chelating agents; citrate, ethyldiaminedisuccinate (EDDS), and pyrophosphate on three common Fe^{2+} activated oxidants; peroxomonosulfate, persulfate and hydrogen peroxide in oxidation of chlorophenols at neutral pH condition. The results showed that each of the Fe^{2+} chelating agents was superior in activating a particular oxidant, and consequently chlorophenols degradation. Pyrophosphate and EDDS were found to be most efficient for Fe^{2+}/peroxomonosulfate and Fe^{2+}/H_2O_2 systems, respectively. Overall, citrate with Fe^{2+}/$S_2O_8^{2-}$ system gave the maximum contaminant removal, and Fe^{2+}/citrate complex was effective in activating all three oxidants to varying degrees [55].

Although the different solution methods outlined in previous paragraphs for resolving the excess Fe^{2+} problem and keeping Fe^{2+} in solution were effective in operation, there might be somewhat associated issues with applications. Sequential addition of Fe^{2+} may not be favorable in high temperature systems. At high temperatures, more $SO_4^{\bullet-}$ radicals may be produced and could even scavenged itself according to the reaction in equation 2.50 [29]. Therefore introducing Fe^{2+} sequentially into such a pool of $SO_4^{\bullet-}$ radicals, generated through temperature activation, may cause an even more scavenging from both Fe^{2+} and the radical itself.

$$SO_4^{\bullet-} + SO_4^{\bullet-} \longrightarrow 2SO_4^{2-} \qquad\qquad 2.50$$

Use of $S_2O_3^{2-}$ may form complex with Fe^{2+} thereby limiting its availability for $S_2O_8^{2-}$ activation. Optimizing for the best $S_2O_8^{2-}/S_2O_3^{2-}/Fe^{2+}$ may also be complicated. Liang et al., 2004 [50] interestingly reported that sequential addition of $S_2O_3^{2-}$ improved TCE removal. This indicates that the method is not all that efficient in solving Fe^{2+} scavenging problem. Fe^0 or FeS_2 as a source of Fe^{2+} introduces additional solid phase. From experience with reaction chemistry, homogenous phase (all liquid) reactions are better than heterogeneous ones. Also, mechanism of Fe^0 or FeS_2 activated persulfate discussed earlier indicated more persulfate requirements for such systems. Moreover, after Fe^0 or FeS_2 produces Fe^{2+}, it still remains in the system and competes with Fe^{2+} for the oxidant according to reactions in equations 2.43 and 2.49. Furthermore, colloidal sulfur may be formed introducing more end waste that would increase treatment cost. In all, not enough information has been documented in this area to guarantee their effectiveness. While the

use of chelating agents to keep Fe^{2+} in solution is a good approach, complicated optimization for $Fe^{2+}/S_2O_8^{2-}$/chelate ratios might be encountered. There may be cases where very efficient chelating agents will be toxic to the environment. This will also increase end treatment cost.

It is clear from literature of Fe^{2+} activated persulfate systems that different pollutants require different levels of Fe^{2+} molar concentration. Pollutants are specific to treatments, and the fact that $S_2O_3^{2-}$, Fe^0, FeS_2 or use of a particular chelating agent worked for some contaminants does not mean they will work automatically well for others. Also, use of these chemicals complicates understanding of the mechanisms and might lead to erroneous conclusions. With regards to the issues of concern for Fe^{2+} as an activator for persulfate, the best alternative will be to optimize the Fe^{2+} concentration for any pollutant treatment by persulfate.

CHAPTER 3

MATERIALS AND METHODS

3.1 Materials

All gases used for this work including N_2, SO_2 and NO were obtained from Airgas National Welders, Charlotte, NC. The SO_2 (5000 ppm) and NO (500-1000 ppm) cylinders contained gases with ultrapure nitrogen as the carrier gas. The water used in preparing scrubbing solutions, samples and standards was deionized (DI) with Milli-Q Advantage A10 Elix 5 system as the purification unit. The unit had a specific resistance of $18.2M\Omega$ at 25°C, and was obtained from Millipore Corporation (Bedford, MA). Total Organic Compounds (TOC), silicates and heavy metals were reduced to a very low parts-per-billion levels. The sodium persulfate ($Na_2S_2O_8$, powder, > 98%) and iron(II) heptahydrate ($FeSO_4.7H_2O$, 99+%) were both obtained from Acros Organics, Morris Plain in NJ and the 5.0N sulphuric acid was purchased from Labchem Inc., Pittsburg, PA.

3.2 Experimental setup and equipments

3.2.1 *Experimental Setup*

The schematic diagram of the experimental setup used for this project is shown in Figure 3.1, and the actual images are depicted in Figure 3.2. The setup mainly consists of a bubble column reactor, dyna-blender and FTIR. The reactor is made from pyrex glass with dimensions of 5.1cm ID and 61cm long (Ace Glass Inc., Vineland, NJ). The gases

from the cylinders go through a flow control unit made of Dynablender and two flow

transducers before the blend is introduced into the bubble column reactor.
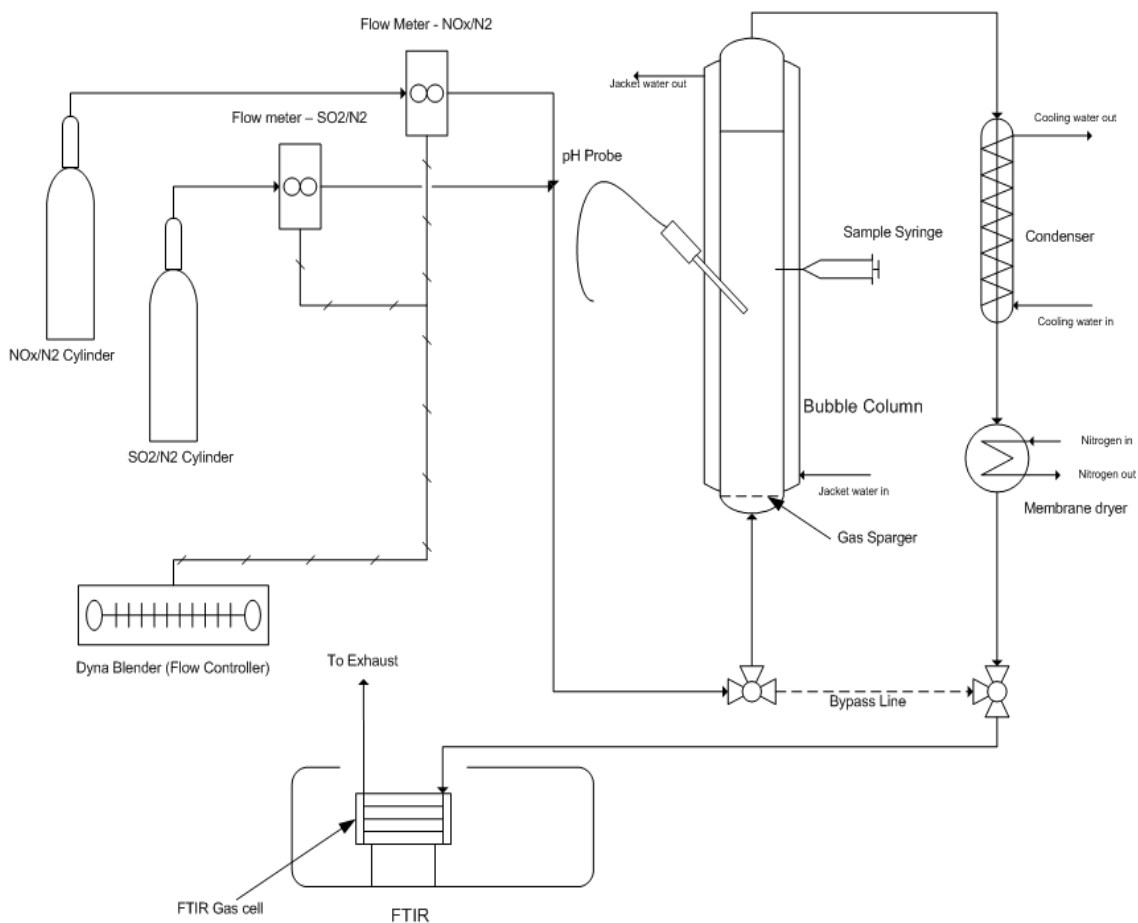
Figure 3.1. Schematic diagram of experimental setup (Khan & Adewuyi, 2010a)

At the entrance of the reactor is a connected gas sparger fitted with 25-50um filter in a

tube (8-mm o.d x 150-mm length). The sparger is connected to a 25 mm diameter disk at

the discharge end. The reactor has been designed in a way to allow continuous flow of

gas in upward direction while the liquid could either be in a batch or continuous mode.

Semi-batch operation in which the gas flowed upward whilst the liquid remained stationary was adopted for all experiments in this work. The total volume of scrubbing solution used was 1 L, and was at a liquid height of about 0.5 m. The FTIR which is the main analytical equipment in this study will be described in the next section.

**Figure 3.2. Images of Column Reactor and FTIR used for experiments
(Room 338, McNair Building, NCA&TSU)**

3.2.2 *Fourier Transform Infrared Spetrophotometer (FTIR)*

The FTIR (Tensor 27, Bruker optics) together with its gas cell from FTIR.com (Benton, ME) was used for online monitoring of the inlet and outlet gas of the column reactor. The technique of the FTIR is basically obtaining information on infrared radiation absorbed by the sample versus wavelength. Each substance absorbs in different specific wavelength ranges depending on the functional group. As shown in Figure 3.3, the FTIR consists mainly of an interferometer, mirrors, IR source and a sample compartment. The beam splitter of the interferometer directs about 50% of the beam (modulation) from the IR source to the sample compartment. The two light beams will be out of phase with one another. Since light consists of waves, the out of phase waves can cancel one another or lessen the overall wave intensity through interference. The pattern that results from the interaction of the two beams is known as an interferogram.
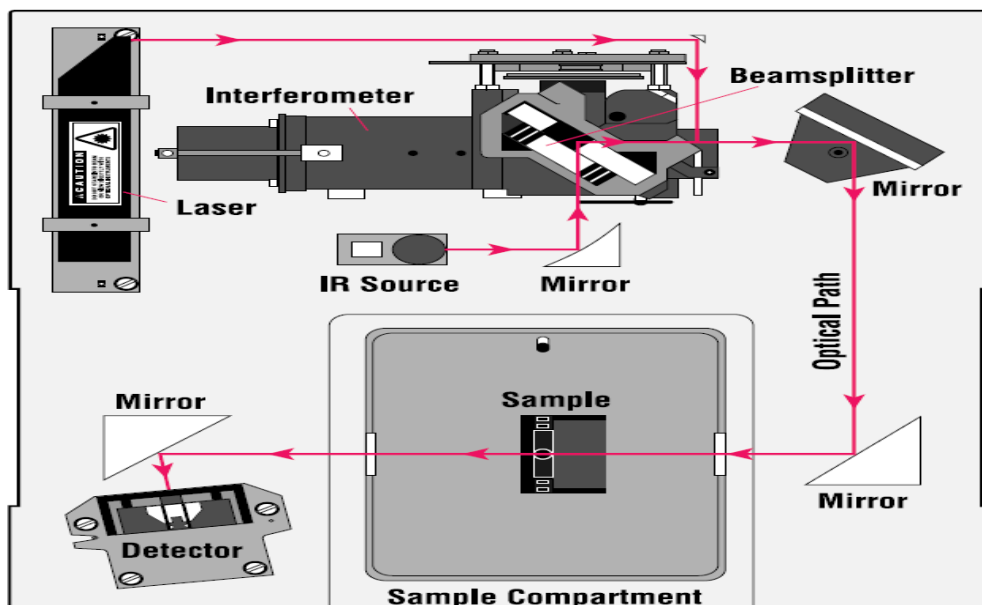
Figure 3.3. Schematic diagram of FTIR

The IR radiation excites the sample molecules into higher vibrational state. The intensity of the transmitted or reflected light versus wavenumber (reciprocal of wavelength) from the sample molecules are plotted to give the FTIR spectra. The computer uses an in-built mathematical tool, Fourier Transformation, to decode the interferogram to the desired spectra information for analysis. The collection and quantitative analysis of the FTIR spectrum data were performed by the proprietary software called Enformatic FTIR Collection Manager (EFCM) from FTIR.com. Once the software is calibrated with standard gases it is able to perform online monitoring of the different species in the gas phase. Figure 3.4 shows the calibration spectrums used for calibrating EFCM.
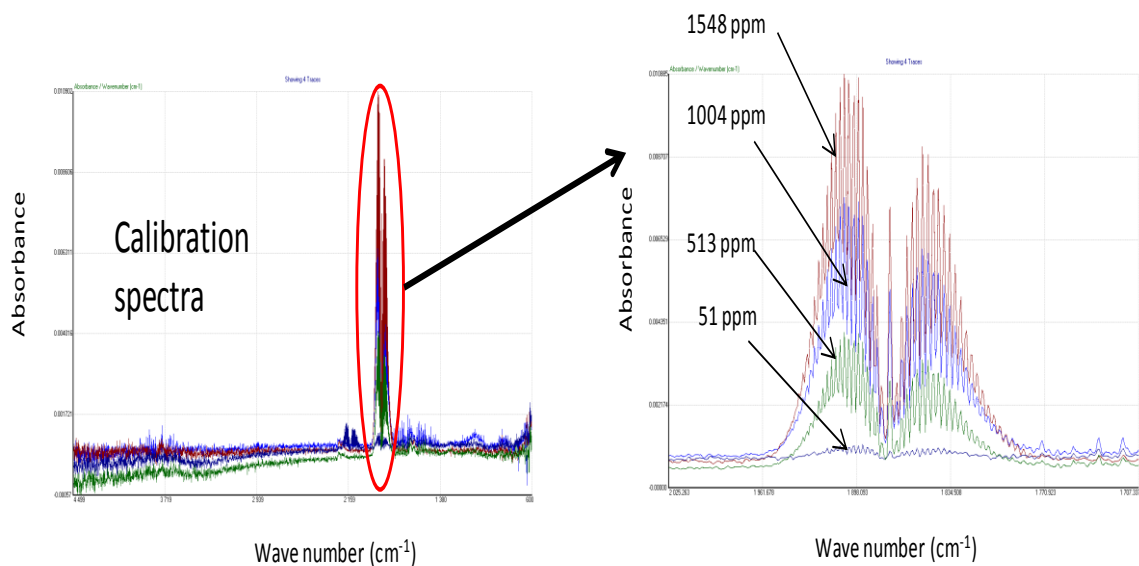
Figure 3.4. Calibration spectra for the standard of NO concentrations [3]

The NO bands appear in the region between 1825 and 1949 cm^{-1}, the water bands in the two regions between 1446 and 1754 cm^{-1} and between 3617 and 3878 cm^{-1} and NO$_2$

absorbs at about 1600 cm^{-1}. These regions were specified in EFCM along with the corresponding concentrations for online monitoring of NO and NO$_2$ (if any) concentrations.

3.3 Methods

3.3.1 *Experimental Procedure*

The tubes connecting the cylinders to the bubble column reactor and FTIR were purged daily to remove water vapor by passing through ultra pure nitrogen gas before the start of experiments. The temperature of each experimental run was maintained by means of cooling/heating water from a refrigerated cooler (Neslab RTE7D1; Thermo Scientific, Waltham, MA). Initially, 750 ml of water was introduced into the column, and when the desired temperature had been attained, pure, dry nitrogen gas was passed through the scrubber for at least 15 minutes to remove any dissolved oxygen. At the same time, the simulated flue gas was passed through the bypass line until a stabilized reading was observed. Once that was achieved, a freshly prepared sodium persulfate that would make up the desired concentration in 1 L of water was introduced into the column. Additional water was then added, up to the mark on the reactor that corresponded to 1 L volume of solution. For all iron (II) experiments appropriate amount of 5.0N sulfuric acid was used to adjust the solution pH to below 3.5. Both sodium persulfate and iron (II) sulfate dissolved quickly with the help of warmness of the solution and the mixing action of the bubbling nitrogen. The simulated flue gas was then switched to the inlet of the reactor and data acquisition was started immediately. Accumet pH meter 50 was used to measure

pHs before and after experiments, and appropriate buffer concentrate was used to keep the pH at the desired level. The exit gas from the reactor was passed through a condenser (cooled to 0.1C) and a membrane dryer (MD-050-48P; Perma Pure LLC, Toms River, NJ) before it entered the FTIR. These were done to avoid moisture interference with gas concentration analysis. The membrane dryer and the FTIR spectrometer were both purged with dry, CO_2-free air from a laboratory gas generator (Parker Balston, Haverhill, MA) which continuously removed moisture from the units. The FTIR calibration had been reported in previous work by Khan and Adewuyi , from the same laboratory with the same set of equipment. [3]

CHAPTER 4

RESULTS AND DISCUSSION

4.1 Persulfate Decomposition

The persulfate anion is a strong oxidant with redox potential of 2.01V [3, 48, 50] . It breaks down in the presence of an oxidizable compound according to the reaction in equation 4.1 to produce sulfate ions.

$$S_2O_8^{2-} + 2e^- \longrightarrow 2SO_4^{2-} \quad E^o = 2.01V \quad [48] \tag{4.1}$$

However, a more powerful oxidant, sulfate radical can be generated when the persulfate anion is thermally or Fe^{2+} activated. The sulfate radical has a higher redox potential and reacts just like the persulfate but faster to produce sulfate ions. See reaction in equation 4.2.

$$SO_4^{\cdot\cdot} + e^- \longrightarrow SO_4^{2-} \quad E^o = 2.6V \quad [44] \tag{4.2}$$

The reactions shown in equations 2.34 through 2.38 can be used to describe thermal and Fe^{2+} activation of persulfate.

Equation 2.34 shows thermal activation whiles equations 2.36 to 2.38 explain Fe^{2+} activation of persulfate. The overall reaction for Fe^{2+} activation is represented by equation 2.38. In equation 2.36, one mole of $S_2O_8^{2-}$ reacts with one mole of Fe^{2+} ions to produce sulfate radicals. In the presence of excess Fe^{2+} ions, equation 2.37 which is undesirable occurs.

4.2 Determination of optimum Fe^{2+} concentration

It is evident from many studies as well as the reaction shown in equation 2.37 that excess Fe^{2+} ions scavenge or consume some of the $SO_4^{\bullet-}$ radicals meant for contaminant oxidation. Owing to this fact, the first major task of this research was to find the best Fe^{2+} concentration level upon which all other experiments would be based. Previous persulfate studies for NO removal from the same laboratory by Khan and Adewuyi [3] reported 0.1 M to be the most suitable persulfate concentration. They did not find appreciable effect from NO gas-phase concentration on NO removal efficiency. With regards to this information and the fact that commercial flue gas removal systems operate at about 50° C, all preliminary experiments to find the best Fe^{2+} concentration level were conducted with 1000 ppm NO gas concentration at 50 °C. The results obtained for 0.05 M and 0.1 M persulfate concentrations are shown in Figures 4.1 and 4.2 respectively. As can be observed from these plots, 0.01 M Fe^{2+} concentration appears to be optimum for both 0.05 M and 0.1 M persulfate concentrations. The fractional conversion of NO was calculated using the final steady state value attained according to the expression

$$X_{NO} = \frac{[NO]_{in} - [NO]_{out}}{[NO]_{in}} \times 100 \qquad\qquad 4.3$$

where NO_{in} and NO_{out} are the steady state concentrations in parts per million (ppm) of NO at the inlet and outlet of the bubble column reactor respectively.
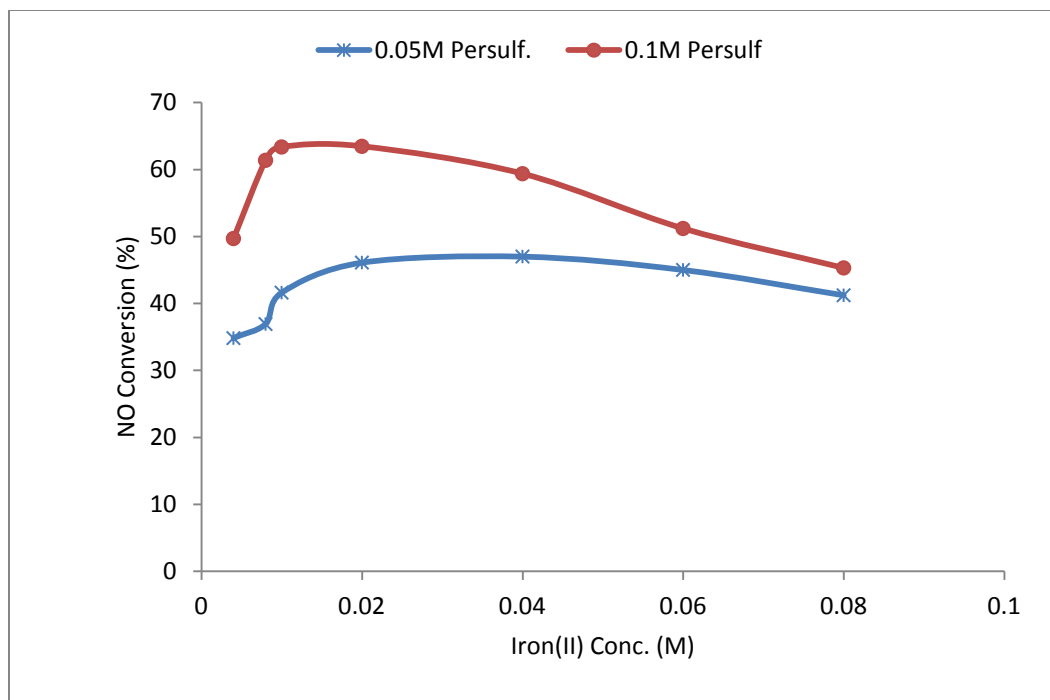
Figure 4.1. Effect of ferrous ion concentration on NO conversion for different persulfate concentrations
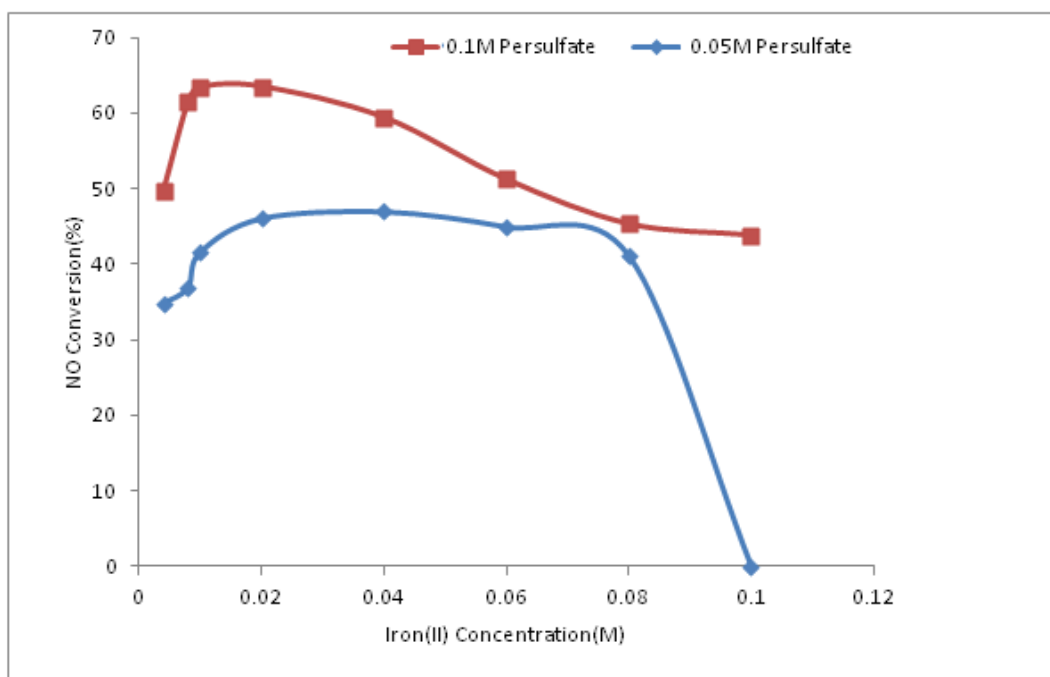
Figure 4.2. Scavenging effect of excess ferrous ion concentration

Although 0.02 M Fe^{2+} concentration appears to produce a slightly higher NO fractional conversion than 0.01 M, that is twice the amount, therefore, 0.01 M of the Fe^{2+} is preferred for practical applications to avoid end use iron separation problems. It can also be seen from the plot in Figure 4.1 that concentrations higher than 0.02 M Fe^{2+} result in declining NO removal. This could be attributed to the presence of excess Fe^{2+} ions which act as scavengers to $SO_4^{\bullet-}$ radicals meant for NO oxidation. The results indicate that 0.02 M Fe^{2+} is the threshold Fe^{2+} concentration level for our system, beyond which sulfate radical scavenging occurs.

Similar Fe^{2+} scavenging of sulfate radical issue had been observed by other authors. Liang et al., 2008 [21] in their work of TCE degradation with Fe^{2+} activated persulfate noticed that, when relatively higher Fe^{2+} concentration was present, TCE degradation enhancement was less than when lower Fe^{2+} concentration was used. In a different study, Liang et al., 2004 [50] observed reduction in TCE destruction by about 20% when increasing Fe^{2+} content was applied. Further increases in Fe^{2+} concentration resulted in no improvement in TCE degradation. The optimum persulfate/Fe^{2+} ratio for maximum TCE degradation in aqueous solution occurred at 15/1[50]. Rastogi et al., 2009 [39] found the molar concentration ratio to be 1/1 for Fe^{2+} activated peroxymonosulfate oxidation of polychlorinated biphenyls (PCB). Oh et al., 2009 [47] in their research, oxidation of polyvinyl alcohol (PVA) using Fe^{2+} activated persulfate observed maximum PVA degradation at Fe^{2+}/persulfate molar concentration ratio of 1/1 [47]. It is evident from the literature that optimizing for appropriate Fe^{2+} concentration level constitutes the most challenging aspect of Fe^{2+} activated persulfate systems oxidation. Nevertheless, this is

largely dependent on the pollutant of concern. For our system, $Fe^{2+}/S_2O_8^{2-}$ molar concentration ratio of 1/10 was the most appropriate for NO absorption and oxidation in aqueous persulfate solution. Block et al., 2004 [30] indicated 100 to 250mg/l as the most effective Fe^{2+} concentration level in Fe^{2+} activated persulfate systems. Unfortunately, Block and his group did not give the equivalent persulfate amount.

Another interesting discovery that can be observed in Figure 4.3 is that, increasing Fe^{2+} concentration beyond 0.08 M, say 0.1 M Fe^{2+} in excess for 0.05 M persulfate, results in no NO removal at all within the experimental period. The scrubbing solution absorbs for sometime but loses its potency completely after 20 minutes. This could be due to the fact that the entire $SO_4^{\bullet-}$ radicals responsible for NO oxidation have been eaten out totally by the excess Fe^{2+} ions present. However, this did not occur with 0.1 M persulfate concentration shown in Figure 4.2. The same 0.1 M Fe^{2+} concentration, which is excess for 0.05 M persulfate concentration cannot be perceived to be in excess for 0.1 M persulfate concentration. More persulfate ions exist at 0.1 M concentration level, therefore, unlike 0.05 M persulfate where scavenging occurred, enough persulfate would be activated by the supposedly excess Fe^{2+} ions (for 0.05 M persulfate) to produce $SO_4^{\bullet-}$ radicals. Even at 50°C, thermal activation could still produce more $SO_4^{\bullet-}$ radicals from the enough (0.1 M) persulfate. These reasons account for why the scrubbing solution stayed potent for the duration of experiment in the case of 0.1 M persulfate. Despite the maintenance of potency of the scrubbing solution, 1/1 molar concentration ratio of $Fe^{2+}/S_2O_8^{2-}$ did not in any way match up with high NO removal efficiency observed at

1/10 molar concentration ratio. Therefore, 1/1 molar concentration ratio stipulated in the stoichiometry reaction of equation 2.36 cannot be accepted as universal for all Fe^{2+} activated persulfate oxidation systems. Again, it significantly depends on the pollutant of concern.
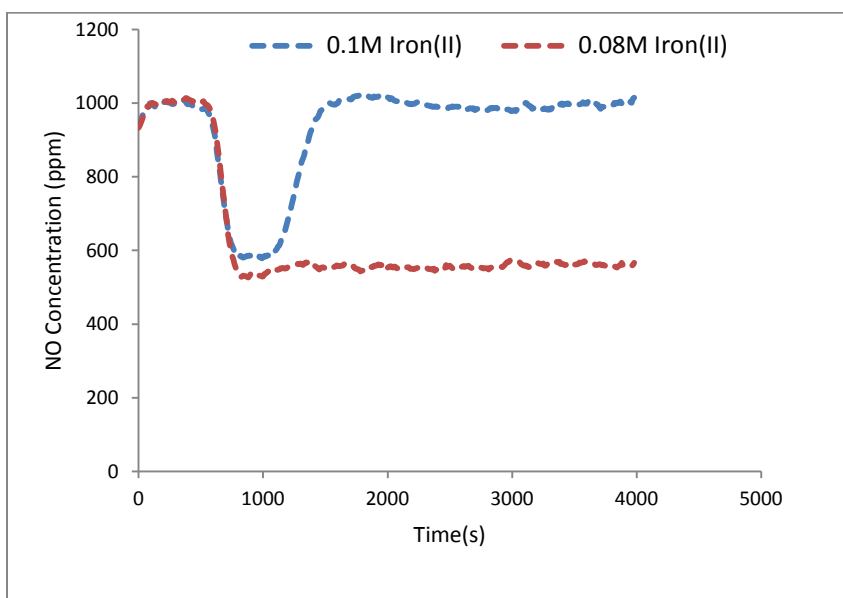
Figure 4.3. Antagonistic effect of 0.1 M ferrous ion on NO removal efficiency

4.3 Influence of Persulfate Concentration

With the established 0.01 M Fe^{2+} concentration as the optimum, experiments were performed for varying initial persulfate concentrations. Figure 4.4 shows the plots of these experiments for temperatures 23, 30, 40, 50, 60 and 70° C. The plots indicate increases in NO removal efficiencies for increasing initial persulfate concentrations in the presence of 0.01 M Fe^{2+} ions. Similar observation without Fe^{2+} ions was reported by

Adewuyi and Khan, 2010 [3] from the same laboratory. Also, it is worth mentioning, and can be observed from Figure 4.4 that, the fractional NO conversion greatly improved for every temperature increase. This is clearly shown in Figure 4.5 as NO profiles over time for individual temperatures.
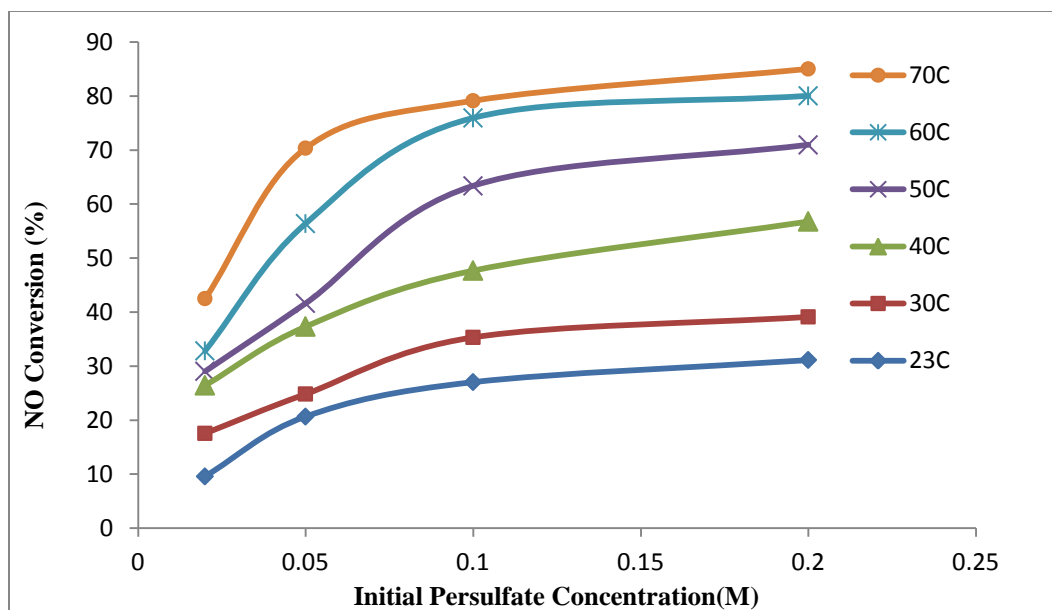
Figure 4.4. Dependence of NO conversions on initial persulfate concentrations for 0.01 M ferrous ion at different temperatures
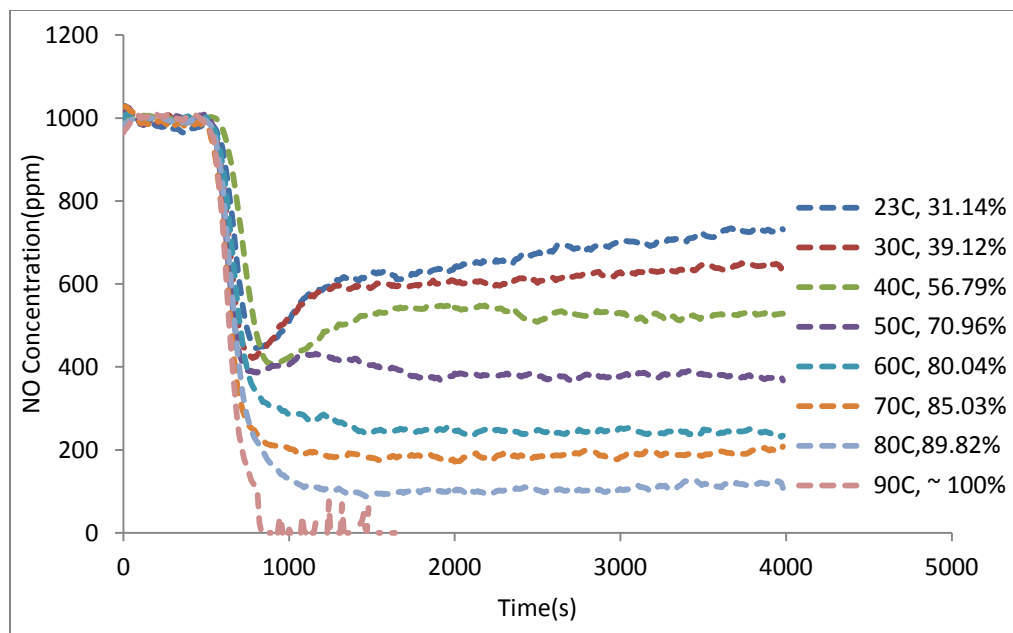
Figure 4.5. Dependence of NO removal efficiency on temperature for 0.1 M persulfate and 0.01 M ferrous ion concentrations

At both elevated temperatures and higher persulfate concentrations, reactant molecules increase their kinetic energy and collisions per second respectively. Therefore molecular interaction occurs more frequently, and subsequently reaction rates increase. This accounts for higher NO removal for either temperature or oxidant concentration increase. Accordingly, the rate of PVA degradation happened to dramatically increase from 30% to 92% when the temperature increased from 30 to 40°C respectively. Further increasing the temperature to 60° C produced complete PVA oxidation [47]. As shown in Figure 4.5 for this project, increasing the temperature of the scrubbing solution significantly improved NO absorption by Fe^{2+} activated persulfate. More $SO_4^{\bullet-}$ radicals could be produced at elevated temperatures to carry out pollutant oxidation. Similar studies by Khan and Adewuyi [3] showed improvement in fractional NO conversion for higher temperatures and oxidant concentrations in NO removal by aqueous persulfate. Again 0.1

43

M persulfate concentration appears to be the optimum even in the presence of Fe^{2+} ions. Beyond this level (0.1 M persulfate), as shown in Figure 4.4, no appreciable NO removal is achieved with even times two of the oxidant concentration at all temperatures studied. Therefore, using 0.1 M persulfate concentration to optimize the Fe^{2+} ions level is justified. It can be partially concluded from Figure 4.4 that 0.01 M $S_2O_8^{2-}$ and 0.01 M Fe^{2+} concentrations at 60°C form the most appropriate conditions for absorbing NO gas into aqueous solutions of persulfate.

A clearer way to ascertain persulfate concentration effects on NO removal are plotted in Figures 4.6 through 4.9. These plots show how NO gas concentration with online monitoring by the FTIR reduces over time after passing through persulfate solution. Three different NO profiles at a specified temperature are shown for 0.05, 0.1, and 0.2 M persulfate concentrations. Figure 4.6, 4.7, 4.8, and 4.9 represent the plots for 40, 50, 60, and 70 °C respectively. In all four temperatures, NO removal efficiency increases with increasing persulfate concentrations. Increasing persulfate concentration of 0.05 M to 0.1 M, and subsequently to 0.2 M as can be observed from the graphs of figure 4.6 through 4.9, the marginal NO fractional conversion increase for 0.05 M to 0.1 M oxidant concentrations is by far greater than that of 0.1 M to 0.2 M persulfate amount increase. Therefore, using 0.1 M persulfate concentration might have some economic advantage, and could be accepted as the most suitable for NO absorption.
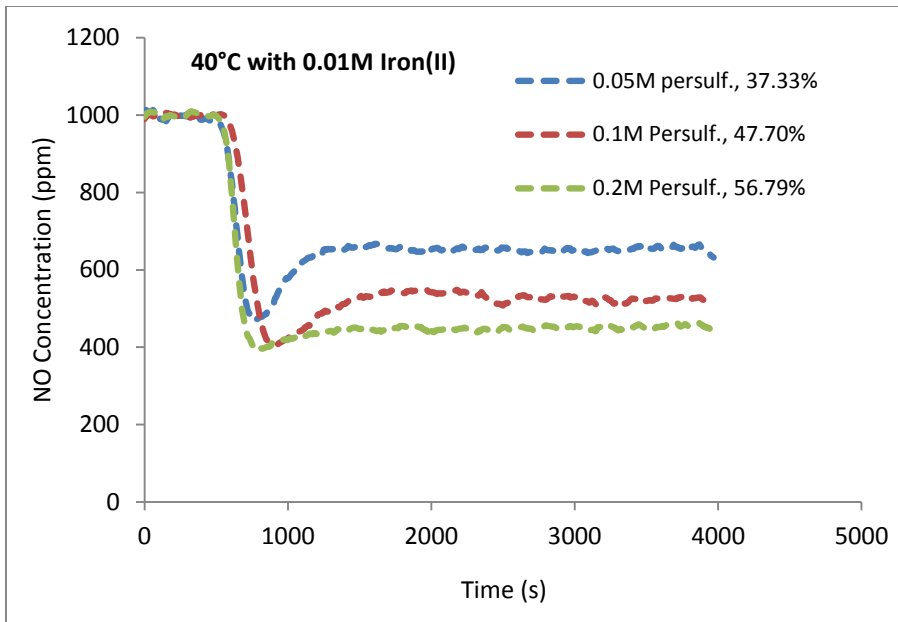
Figure 4.6. NO removal efficiency for different persulfate concentrations at 0.01 M ferrous ion and 30° C
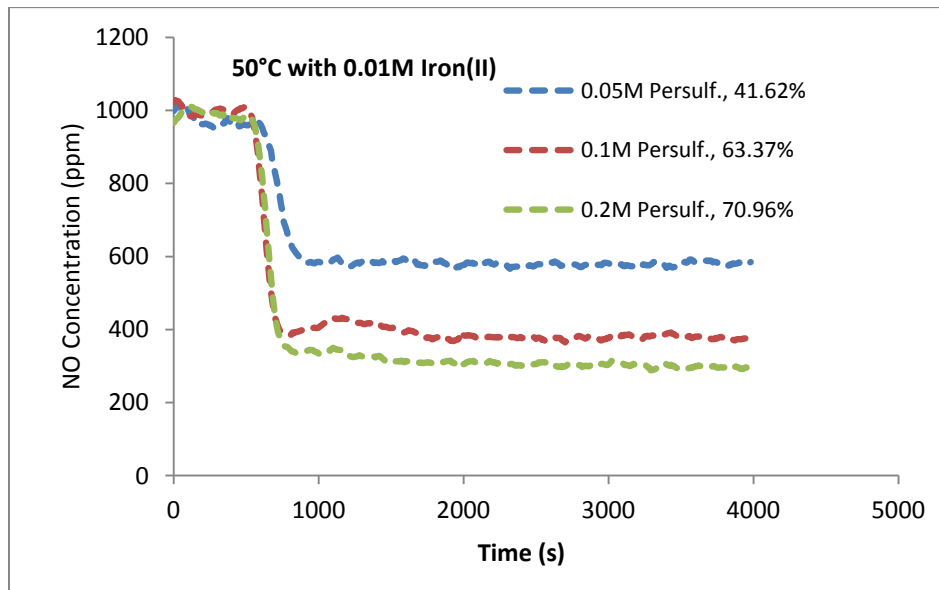
Figure 4.7. NO removal efficiency for different persulfate concentrations at 0.01 M ferrous ion and 50° C
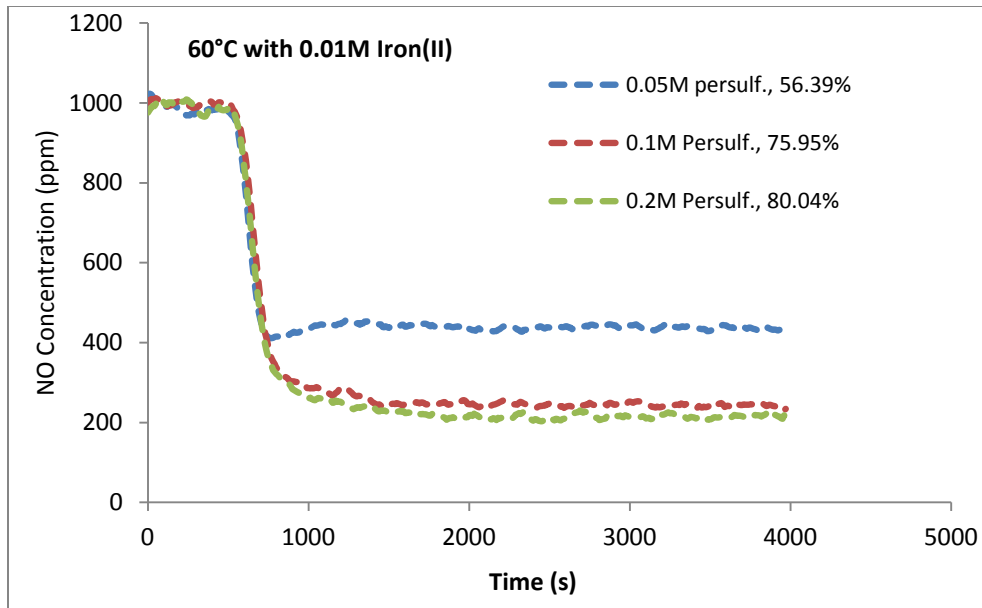
Figure 4.8. NO removal efficiency for different persulfate concentrations at 0.01 M ferrous ion and 60° C
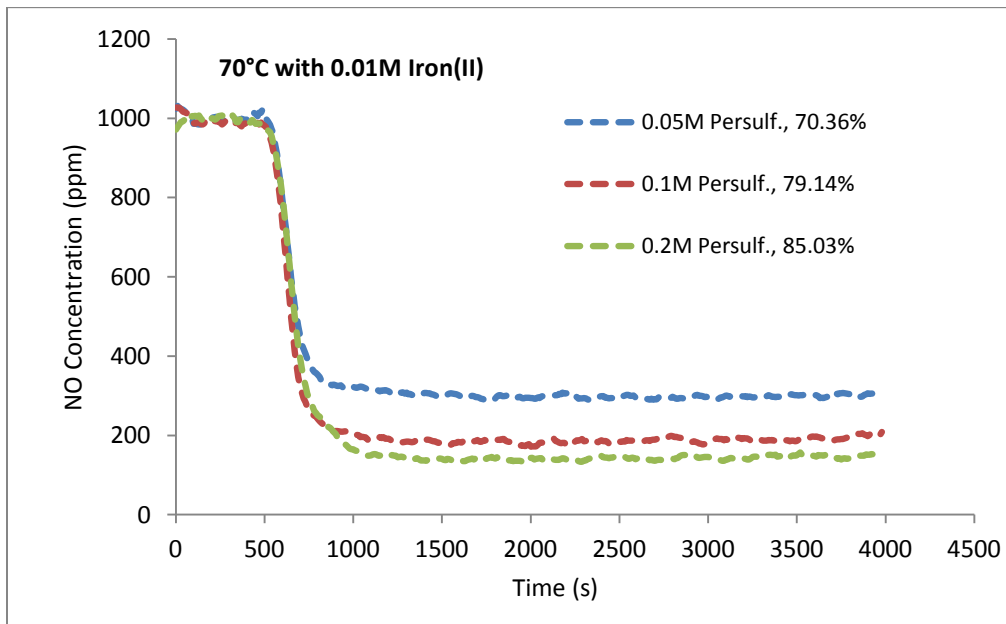
Figure 4.9. NO removal efficiency for different persulfate concentrations at 0.01 M ferrous ion and 70° C

Cost of oxidant forms majority of the total expenses for pollution treatment with scrubbing solutions [3]. In practical terms, economical benefits could be chosen over slight improvement in NO conversions provided by the 0.2 M over 0.1 M persulfate concentrations. After all, lower levels of the pollutant within emission standards might not pose significant danger to the environment or society.

Figure 4.10 combines all the individual temperatures of Figures 4.6 through 4.9 in one graph. It can be inferred from this figure that, by extrapolating to higher temperatures beyond 70°C, conversions for all three concentrations; 0.05 M, 0.1 M and 0.2 M are likely to become very close and eventually the same. This makes temperature a significant factor in NO removal by aqueous solutions of persulfate.
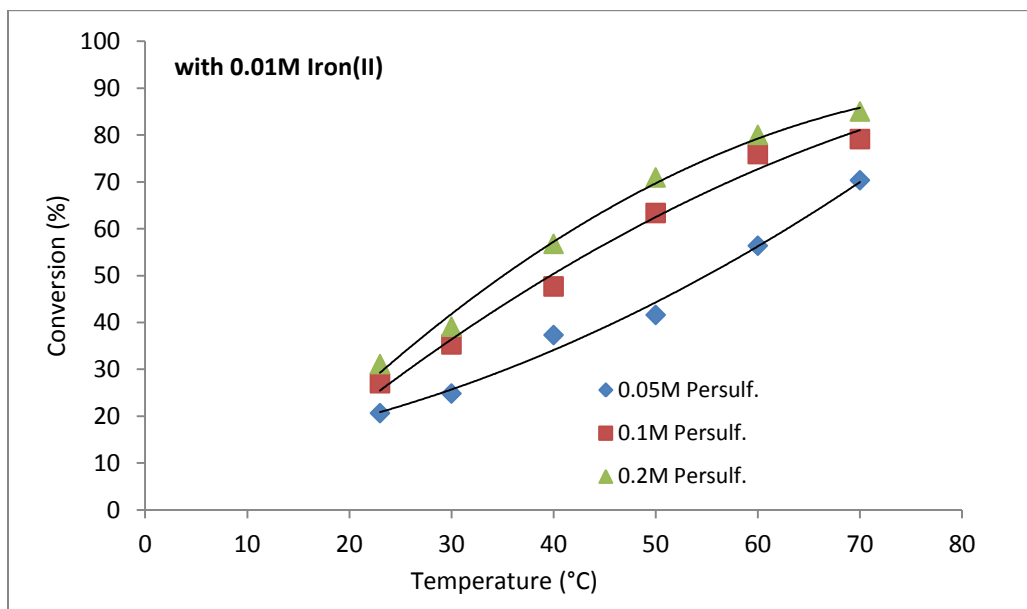
Figure 4.10. NO conversion dependency on temperature at different persulfate concentrations for 0.01 M ferrous ion

4.4 Effect of NO Concentration

So far, appropriate operable concentration levels of Fe^{2+} and $S_2O_8^{2-}$ for NO removal have been determined. The next parametric effect to discuss here is gas-phase NO concentration. Figure 4.11 depicts NO gas concentration effect on pollutant removal efficiency over the temperature range of 23 to 70° C. For the two NO gas-phase concentrations (500 ppm and 1000 ppm), the NO fractional conversions observed at 1000 ppm were slightly higher than 500 ppm. This is to be expected because higher NO gas-phase concentration results in larger amount of NO liquid-phase concentration. This subsequently increases the reaction rates in the liquid phase [3]. However, the differences in NO conversions noticed for 500 and 1000 ppm for the temperature range are very small and can be assumed to be negligible. This indicates the absorption was mainly liquid-phase controlled and the scrubbing system could be used for both low and high gas-phase NO concentration levels [3].
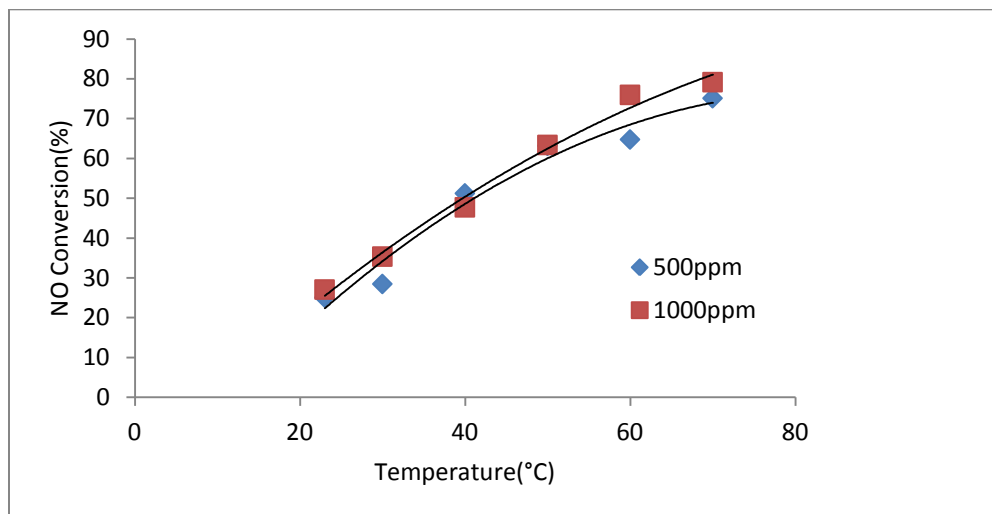
Figure 4.11. Dependence of NO conversion on temperature for different initial NO gas phase concentration

48

4.5 Combined effect of temperature and Fe^{2+} activations

In the presence of 0.01 M Fe^{2+} ions, NO removal by 0.1 M persulfate significantly increased with temperature elevation. As can be observed in Figure 4.5, each temperature increase correspondingly resulted in improved NO removal efficiency with the greatest NO conversion difference occurring between 40 and 50 °C. Similar results have been reported by [47] in which they applied Fe^{2+} activated persulfate to oxidize polyvinyl alcohol.

Unlike heat activated persulfate where complete removal of NO could not be reached even at 90 °C [3], combined temperature-Fe^{2+} activated persulfate was able to achieve total NO degradation. Thus, at the same condition of 0.1 M persulfate at 90°C, 92% and about 100% NO fractional conversions were recorded for temperature-alone and combined temperature-Fe^{2+} activations. Also, irrespective of the persulfate concentration, whether 0.1 M or 0.2 M, the presence of 0.01 M Fe^{2+} was able to further enhance NO removal efficiencies for all the temperatures studied. Figures 4.12 and 4.13 clearly show this for the two concentrations of persulfate where the presence of 0.01 M Fe^{2+} was able to, on the average, improve NO removal efficiency by a superior 10% over temperature range of 23 to 70 °C.
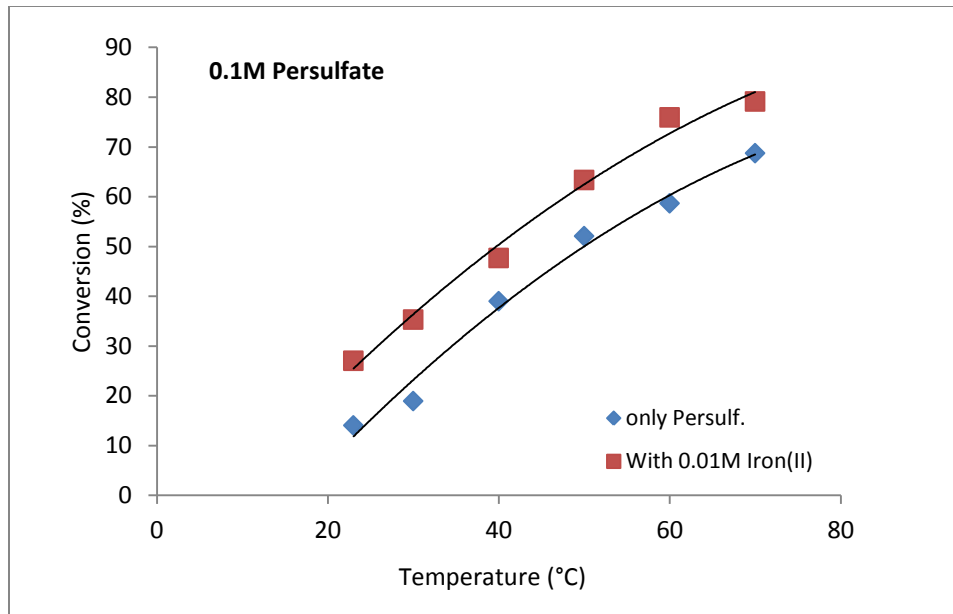
Figure 4.12. The effect of temperature on NO removal by 0.01 M ferrous ion using 0.1 M persulfate
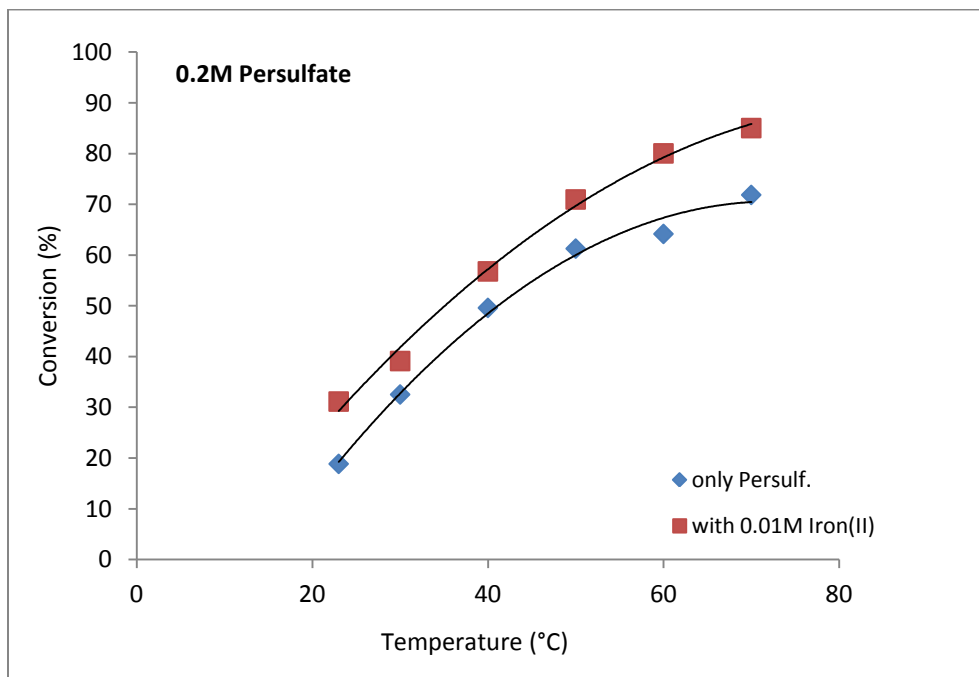
Figure 4.13. The effect of temperature on NO removal by 0.01 M ferrous ion using 0.2 M persulfate

50

Thermal (temperature-alone) activation of persulfate is known to occur at temperatures of 40°C and above, therefore, at these higher temperatures both thermal and Fe^{2+} activation of persulfate would be occurring to produce sulfate radicals that are able to oxidize and subsequently absorb NO into aqueous solutions of persulfate. Radical scavenging according to equation 2.5 did not manifest here. The results indicate that, 0.01 M Fe^{2+} activation at higher temperatures produces a synergy with thermal activation for a more effective NO removal by persulfate. However, when only persulfate (0.2 M) was used, the plot for NO conversion over temperature in Figure 4.13 started to level off after 60° C. Both high temperatures and low pH levels have been reported to increase radical generation, a synergy that might more favor radical-to-radical reactions than radical-to-contaminant reactions [29]. This could explain the observation in figure 4.13 because our scrubbing solution was acidic (pH below 4) and the experiment was conducted at temperatures beyond 40° C. Also, since there were more persulfate ions in 0.2 M than 0.1 M, it could be that more persulfate ions remained unactivated for the temperature-alone activation within the time of experiment. Nevertheless, this case of leveling off of NO conversion when 0.2 M persulfate was used did not happen in the presence of 0.01 M Fe^{2+}, because the Fe^{2+} ions were able to activate the remaining persulfate to produce $SO_4^{\bullet-}$ radicals for further NO removal. Hence, NO removal efficiency improved even at higher temperatures. Moreover, persulfate activation by Fe^{2+} ions is faster and more effective than thermal decomposition, and at higher temperatures, a synergy is formed which results in dramatic increase in NO removal efficiencies. For the temperatures studied, 23 to 70° C, NO oxidation by persulfate with and without Fe^{2+} were compared.

Figures 4.14 to 4.19 show the plots from this study. In all six cases, 0.01 M Fe^{2+} ions were able to synergistically improve NO removal efficiency with the greatest differences occurring at 23, 30 and 60° C. Those results at the lower temperatures (23 and 30° C) could be attributed to the fact that at those temperatures, thermal activation does not to a significant extent occur. Therefore the low conversion values, 14.07% and 18.96% observed for 23 and 30° C respectively, when only persulfate was used might have come from direct NO oxidation by persulfate and not supposedly sulfate radicals. The results of this study indicate that, while the absorption capacity of the 0.1 M persulfate scrubbing solution with or without 0.1 M Fe^{2+} is sufficient to maintain a constant absorption rate throughout the experiment without depleting significantly, Fe^{2+} activation further improved NO removal by about 10% at all temperatures. At 0.1 M $Na_2S_2O_8$ and 0.01 M Fe^{2+} concentrations, conversions of up to 79% and approximately 100% were observed at 70° C and 90° C, respectively.
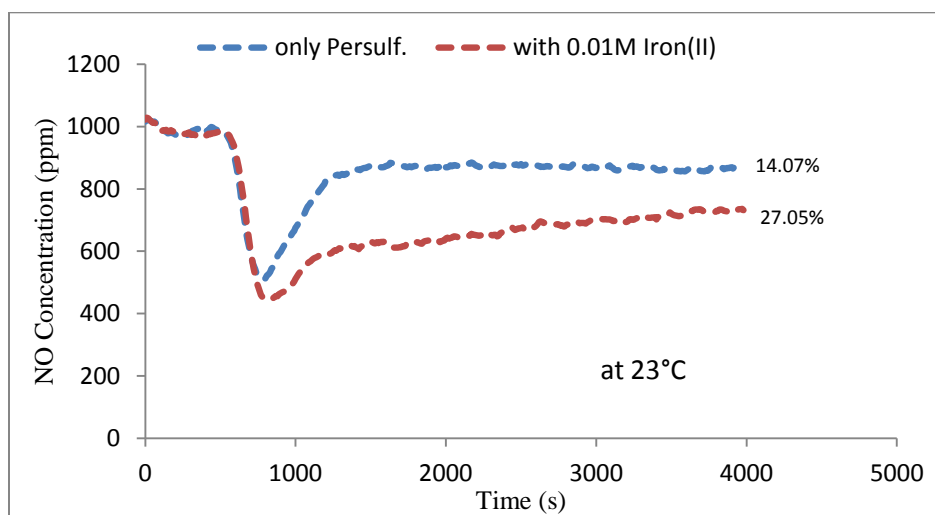
Figure 4.14. Change in NO removal by 0.01 M ferrous ion activated persulfate at 23° C
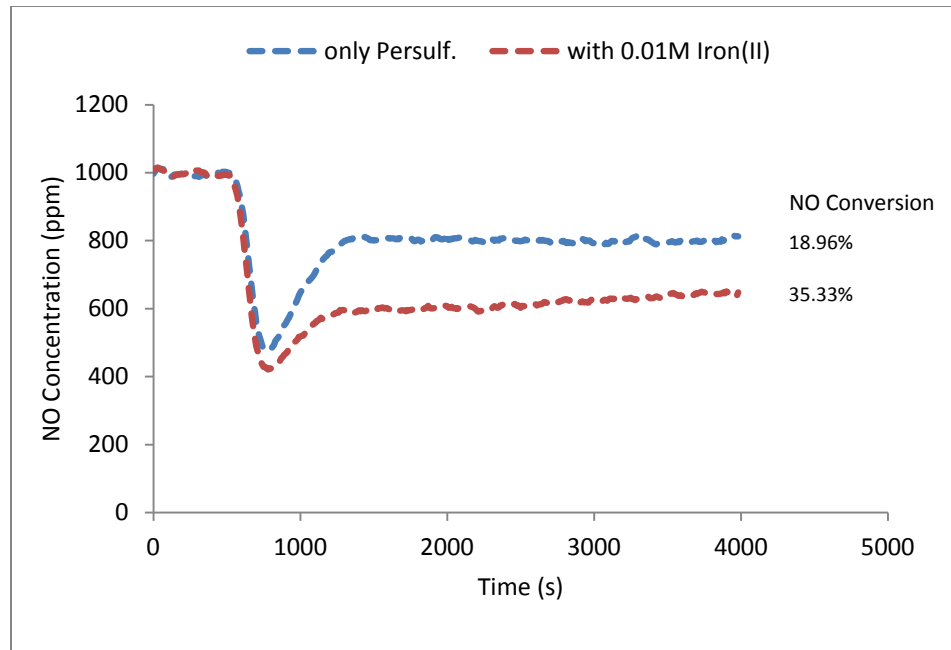
Figure 4.15. Change in NO removal by 0.01 M ferrous ion activated persulfate at 30° C
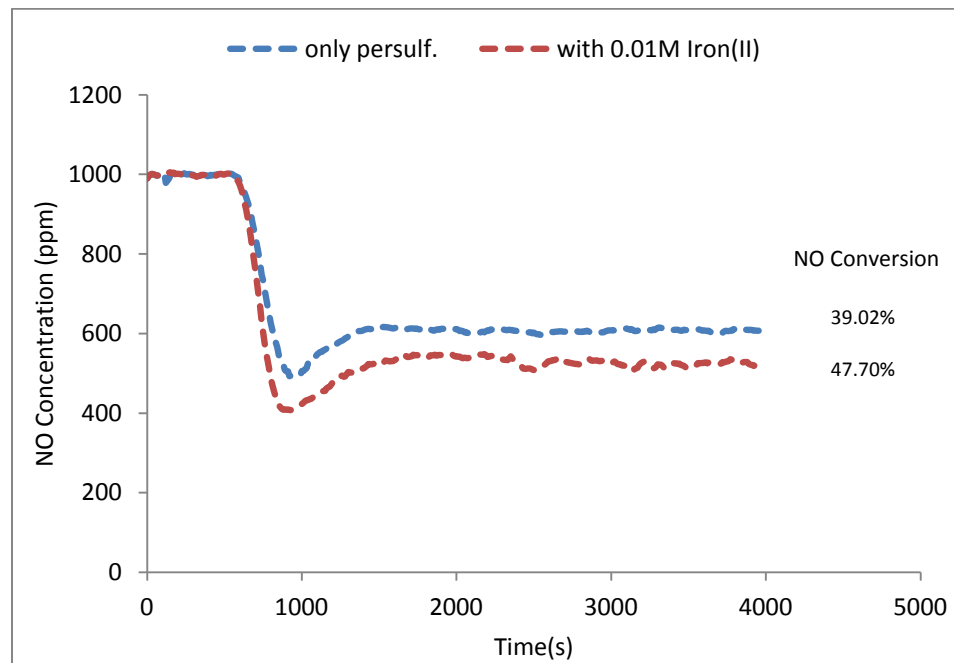
Figure 4.16. Change in NO removal by 0.01 M ferrous ion activated persulfate at 40° C
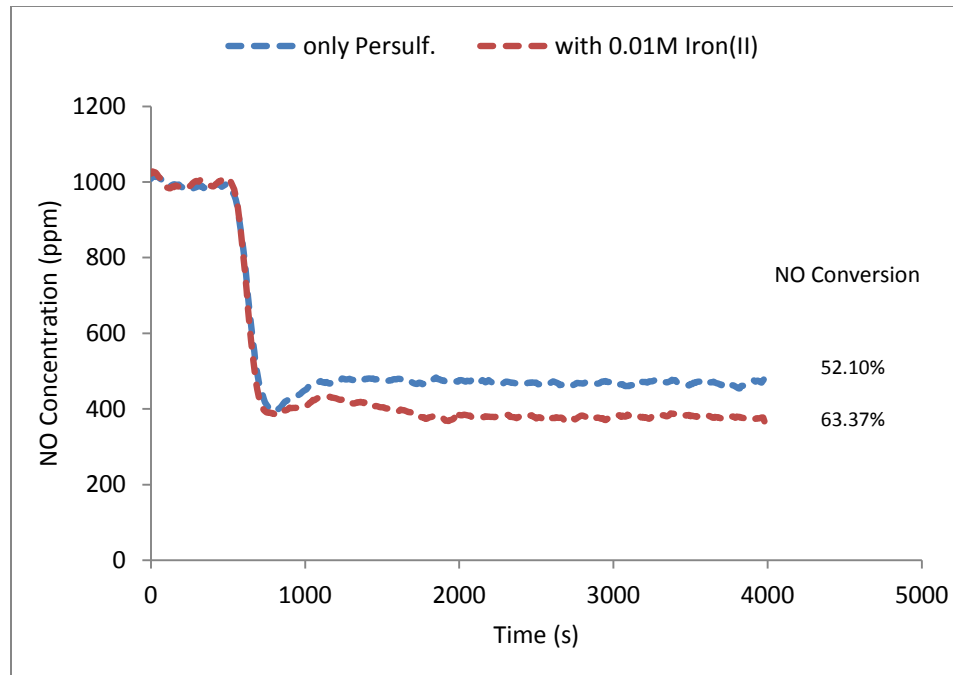
Figure 4.17. Change in NO removal by 0.01 M ferrous ion activated persulfate at 50° C
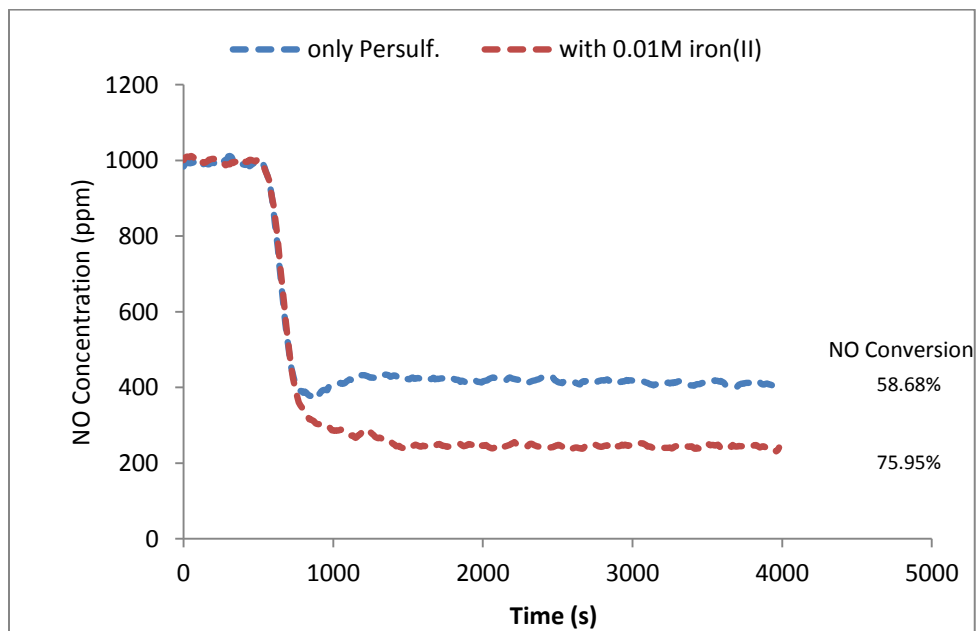
Figure 4.18. Change in NO removal by 0.01 M ferrous ion activated persulfate at 60° C
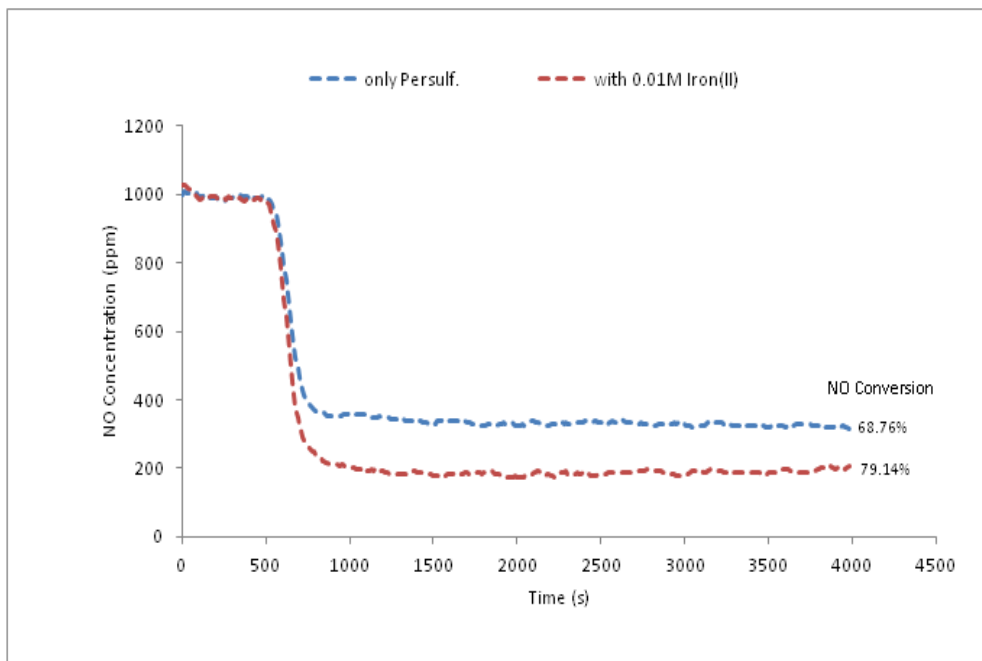
Figure 4.19. Change in NO removal by 0.01 M ferrous ion activated persulfate at 70° C

The maximum synergistic effect of temperature and Fe^{2+} activations of 0.1 M persulfate for NO removal occurred at 60° C. This could be explained from two perspectives; either Fe^{2+} activation works best at 60° C or the temperature-alone activation does not do too well at 60°C. This led to investigation of NO conversion values for all the temperature-alone activation experiments. Removal efficiencies of 14.07, 18.96, 39.02, 52.01, 58.68, and 68.76 % were recorded for 23, 30, 40, 50, 60, and 70 °C respectively. These values show for each temperature increment, a corresponding improved NO fractional conversion by an average of more than 10% except at 50 to 60 °C which recorded a lower than 10 % average NO fractional conversion difference over the previous temperature. Therefore it can be accepted that the highest improvement in synergistic NO conversions from these comparisons observed at 60° C resulted from poor performance of

temperature-alone activation run at 60° C. Fortunately, around 60° C is deemed suitable temperature for flue gas pollution control systems. At this temperature, an appreciable amount of 72-76 % of 1000 ppm NO could be absorbed from flue gas by persulfate.

4.6 Mechanism and model of NO absorption by Fe^{2+} activated persulfate

4.6.1 *Mechanism*

Mechanisms of NO reactions and persulfate decomposition (by either heat or Fe^{2+}) have been well documented in literature. House and Block [20, 30] presented exhaustive review on mechanism of persulfate activation by heat, Fe^{2+} and other transition metal ions. On the other hand mechanism of NO absorption into aqueous solutions have been extensively investigated by [5, 10, 32, 35, 56] . The absorption of NO by persulfate solution is thought to be dependent on the reaction of dissolved NO with the reactive radicals generated by thermal [3] and Fe^{2+} activations of persulfate. In general, the consumption of NO by reactions in the liquid phase maintains the driving force needed for absorption [5, 57]. Khan and Adewuyi, 2010 [3] recently presented the mechanism for the absorption-oxidation of NO by aqueous solution of sodium persulfate decomposition under different conditions of temperature, pH and NaCl concentrations with plausible explanations for the effects of these process parameters [3]. This mechanism is readily extendable to the case in which Fe^{2+} is present in the aqueous phase. Based on this mechanism, the following set of reactions (with their corresponding rate constants [58-61] can be assumed to be responsible for consumption of NO in the presence of Fe^{2+} ions.

$$S_2O_8^{2-} + heat \xrightarrow{k_1=1.0 \times10^{-7}\ (25°C)\ or\ 5.7 \times10^{-7}s^{-1}(70°C)} 2\ SO_4^{\bullet-} \qquad\qquad 4.4$$

$$S_2O_8^{2-} + Fe^{2+} \xrightarrow{k_2=1.7-2.7\ or\ 2.0 \times10^{1}M^{-1}s^{-1}(70°C)} SO_4^{2-} + SO_4^{\bullet-} + Fe^{3+} \qquad\qquad 4.5$$

$$SO_4^{\bullet-} + H_2O \xrightarrow{k_3 = 6.6\times10^{2}s^{-1}} HSO_4^{-} + OH^{\bullet} \qquad\qquad 4.6$$

$$OH^{\bullet} + NO \xrightarrow{k_4 = 2\times10^{10}M^{-1}s^{-1}} H^{+} + NO_2^{-} \qquad\qquad 4.7$$

$$S_2O_8^{2-} + NO_2^{-} \xrightarrow{k_5} SO_4^{2-} + SO_4^{\bullet-} + NO_2 \qquad\qquad 4.8$$

$$NO_2^{-} + SO_4^{\bullet-} \xrightarrow{k_6 = 9.8\times10^{8}M^{-1}s^{-1}} SO_4^{2-} + NO_2 \qquad\qquad 4.9$$

$$NO_2 + OH^{\bullet} \xrightarrow{k_7 = 4.5\times10^{9}M^{-1}s^{-1}} H^{+} + NO_3^{-} \qquad\qquad 4.10$$
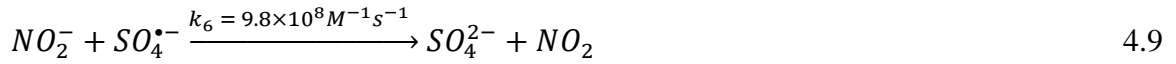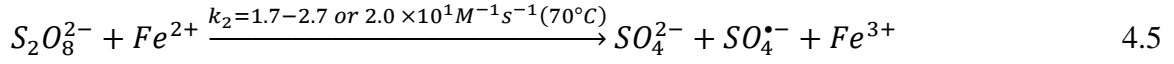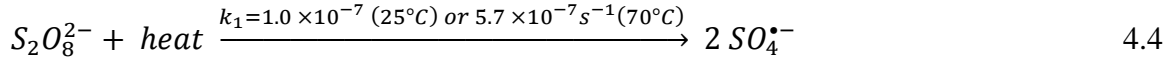
Applying Pseudo-Steady State Approximation (PSSA) to $SO_4^{\bullet-}$ in the equations above results in

$$\frac{dC_{SO_4^{-}}}{dt} = 2k_1Cs_2\,o_8^{2-} + k_2\,Cs_2\,o_8^{2-}C_{Fe^{2+}} - k_3Cso_4^{-} + k_5Cs_2\,o_8^{2-}C_{NO_2^{-}} - k_6Cso_4^{-}C_{NO_2^{-}}$$
$$4.11$$

That of NO_2^{-} is

$$\frac{dC_{NO_2^{-}}}{dt} = k_4C_{OH^{\cdot}}C_{NO} - k_5Cs_2\,o_8^{2-}C_{NO_2^{-}} - k_6Cso_4^{-}C_{NO_2^{-}} \qquad\qquad 4.12$$

And that of NO yields

$$\frac{dC_{NO}}{dt} = k_4C_{OH^{\cdot}}C_{NO} - k_2'\,Cs_2\,o_8^{2-}C_{NO} \qquad\qquad 4.13$$

From equation 4.12, and assuming steady state NO_2^- since it is an intermediate species and reaches a constant value fairly quickly implies,

$$k_4 C_{OH} \cdot C_{NO} = k_5 Cs_2 o_8^{2-} C_{NO_2^-} + k_6 Cso_4^- C_{NO_2^-} \qquad 4.14$$

and

$$2k_1 Cs_2 o_8^{2-} + k_2 Cs_2 o_8^{2-} C_{Fe^{2+}} + k_5 Cs_2 o_8^{2-} C_{NO_2^-} - k_3 Cso_4^- = k_6 Cso_4^- C_{NO_2^-} \qquad 4.15$$

This implies,

$$k_6 Cso_4^- C_{NO_2^-} = \left(2k_1 + k_2 C_{Fe^{2+}} + k_5 C_{NO_2^-}\right) Cs_2 o_8^{2-} - k_3 Cso_4^- \qquad 4.16$$

Therefore,

$$k_4 C_{OH} \cdot C_{NO} = k_5 Cs_2 o_8^{2-} C_{NO_2^-} + \left(2k_1 + k_2 C_{Fe^{2+}} + k_5 C_{NO_2^-}\right) Cs_2 o_8^{2-} - k_3 Cso_4^- \qquad 4.17$$

k_1 and k_3 are small compared to k_2 and k_5, implies

$$k_4 C_{OH} \cdot C_{NO} = k_5 Cs_2 o_8^{2-} C_{NO_2^-} + k_2 Cs_2 o_8^{2-} C_{Fe^{2+}} + k_5 Cs_2 o_8^{2-} C_{NO_2^-} \qquad 4.18$$

Or

$$k_4 C_{OH} \cdot C_{NO} = (2k_5 C_{NO_2^-} + k_2 C_{Fe^{2+}}) ly Cs_2 o_8^{2-} = (k_5' + k_2 C_{Fe^{2+}}) Cs_2 o_8^{2-}$$
4.19

Therefore,

$$\frac{dC_{NO}}{dt} = -\left(k_5' + k_2 C_{Fe^{2+}}\right) Cs_2 o_8^{2-} - k_2' Cs_2 o_8^{2-} C_{NO} \qquad 4.20$$

Or

$$\frac{dC_{NO}}{dt} = -k_1' C_{S_2O_8^{2-}} - k_2' C_{S_2O_8^{2-}} C_{NO} - k_3' C_{S_2O_8^{2-}} C_{Fe^{2+}} \qquad 4.21$$

Equation 4.21 describes the overall oxidation of NO by persulfate. Similarly, the rate of consumption of persulfate can be expressed as

$$\frac{dC_{S_2O_8^{2-}}}{dt} = -k_1' C_{S_2O_8^{2-}} - k_2' C_{S_2O_8^{2-}} C_{NO} - k_3' C_{S_2O_8^{2-}} C_{Fe^{2+}} \qquad 4.22$$

4.6.2 *Model*

Based on the results in equation 4.21 and the assumption that the gas and liquid phases of the experiment were completely back-mixed, a simple model previously developed by Khan and Adewuyi [3] was modified to include the case of Fe^{2+}, and applied to explain the experimental data. Another assumption for this model was that the transfer of NO from gas to liquid was liquid-phase controlled.

Using the film theory the rate of transfer of NO from gas to liquid can be expressed as

$$R_A = K_L a \left(\frac{P_{NO}}{H} - C_{NO} \right) \qquad 4.23$$

where $K_L a$ is the mass transfer coefficient, H is the Henry's law coefficient, P_{NO} is the partial pressure of NO at the outlet, C_{NO} is the aqueous concentration of NO. P_{NO} is calculated from

$P_{NO} = ppm_{NO} x 10^{-6} x P_{total}$ where P_{total} is 1 atm and ppm_{NO} is molar ppm.

The material balance of NO in the gas phase can also be described by the following equation [3]

$$\frac{V_G}{RT}\frac{dP_{NO}}{dt} = \frac{Q}{RT}\left(P_{NO}^{in} - P_{NO}\right) - R_A V_L \qquad 4.24$$

where V_G is the gas holdup volume, R is the gas constant, T is the temperature, Q is the gas flow rate, P_{NO}^{in} is the partial pressure of NO at the inlet, V_L is the liquid volume.

Combining equations 4.23 and 4.24 yields

$$\frac{dP_{NO}}{dt} = \frac{Q}{V_G}\left(P_{NO}^{in} - P_{NO}\right) - \frac{V_L RT}{V_G}K_L a\left(\frac{P_{NO}}{H} - C_{NO}\right) \qquad 4.25$$

From equations 4.21 and 4.23, the material balance of NO in the aqueous phase results in the equation

$$\frac{dC_{NO}}{dt} = K_L a\left(\frac{P_{NO}}{H} - C_{NO}\right) - k_1' C_{S_2 O_8^{2-}} - k_2' C_{NO} C_{S_2 O_8^{2-}} - k_3' C_{S_2 O_8^{2-}} C_{Fe^{2+}} \qquad 4.26$$

Now, solving equations 4.25 and 4.26 simultaneously with 4.22, this simple model was able to at least match the experimental data. The three equations were solved with Matlab, and the codes, previously developed by Khan [62] and modified for this case are included in appendix D. The values of the parameters $K_L a$, k_1', k_2' and k_3' were varied until a good fit for the data was obtained. Figures 4.20 to 4.23 show the experimental and model plots at different temperatures; 30, 40, 50 and 60°C for the case of 0.1 M persulfate in the presence of 0.01 M Fe^{2+} ions.
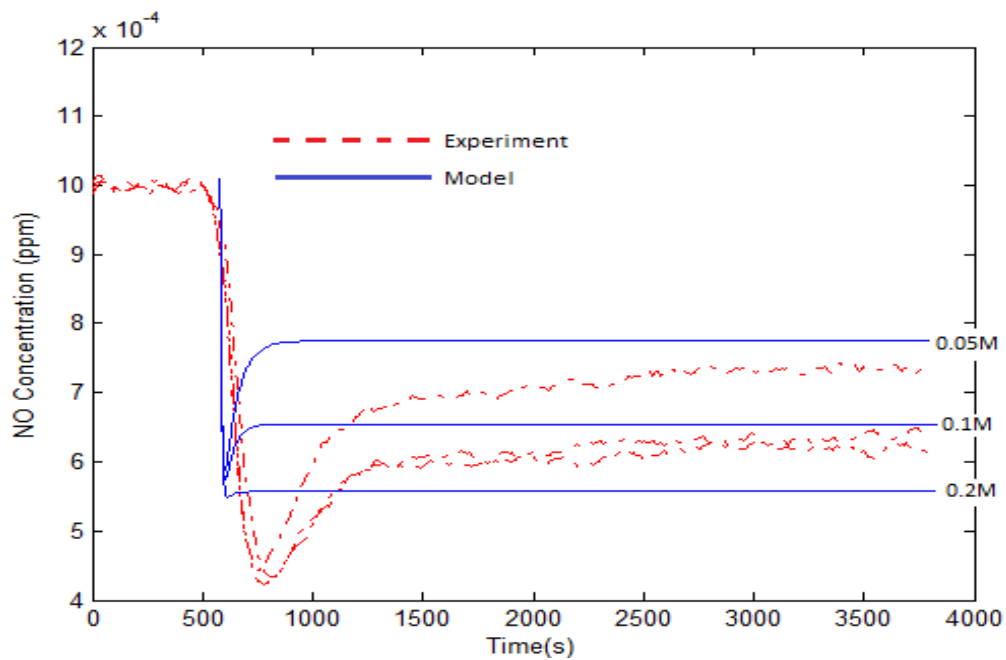
Figure 4.20. Experimental data and model prediction for different persulfate concentrations at 30° C
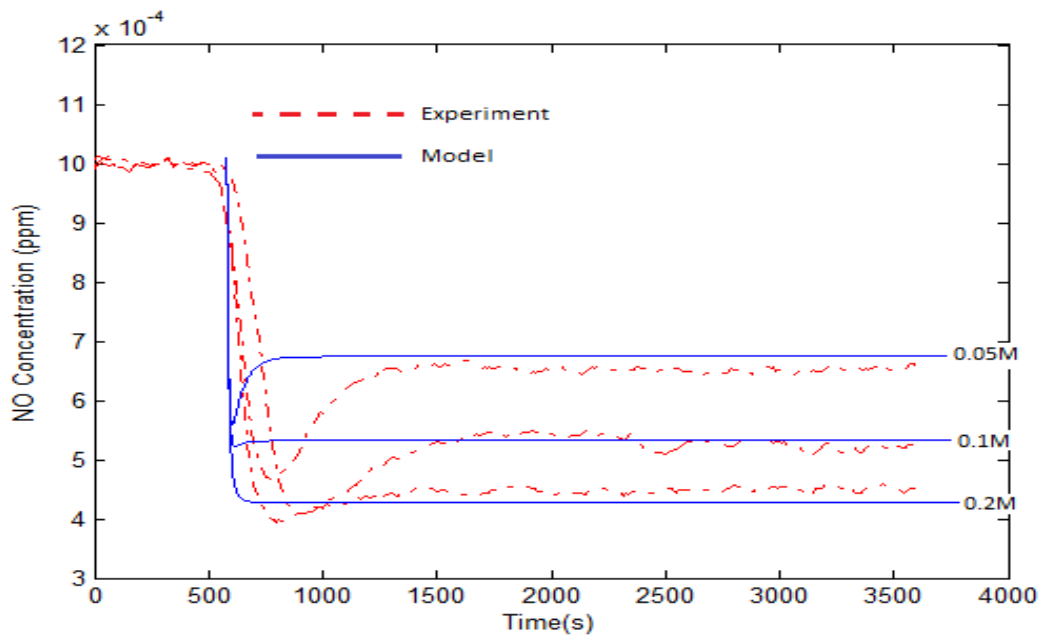
Figure 4.21. Experimental data and model prediction for different persulfate concentrations at 40° C
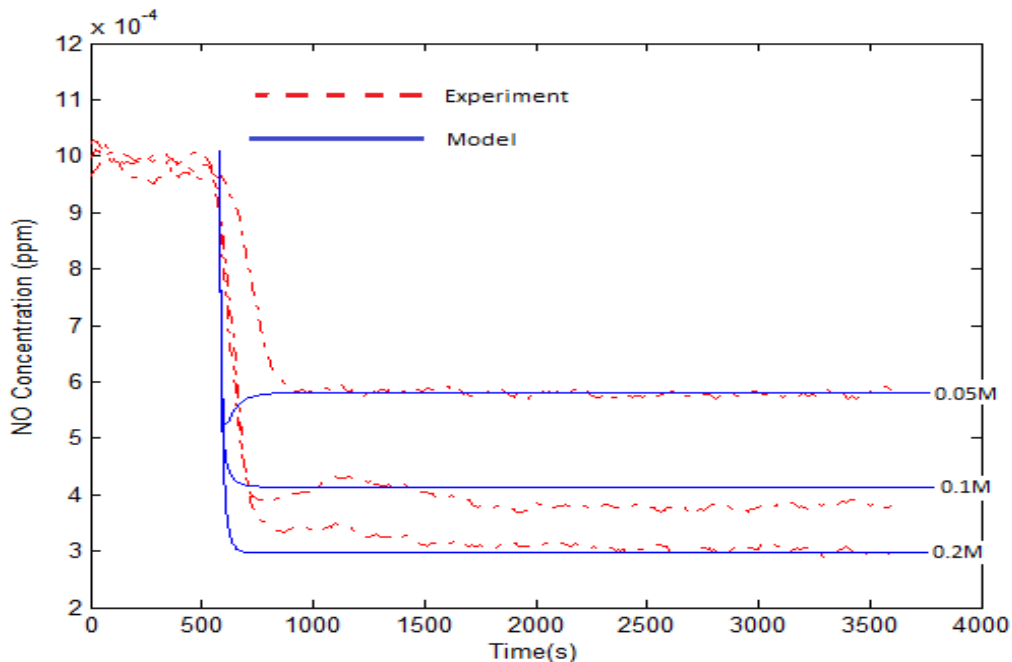
Figure 4.22. Experimental data and model prediction for different persulfate concentrations at 50° C
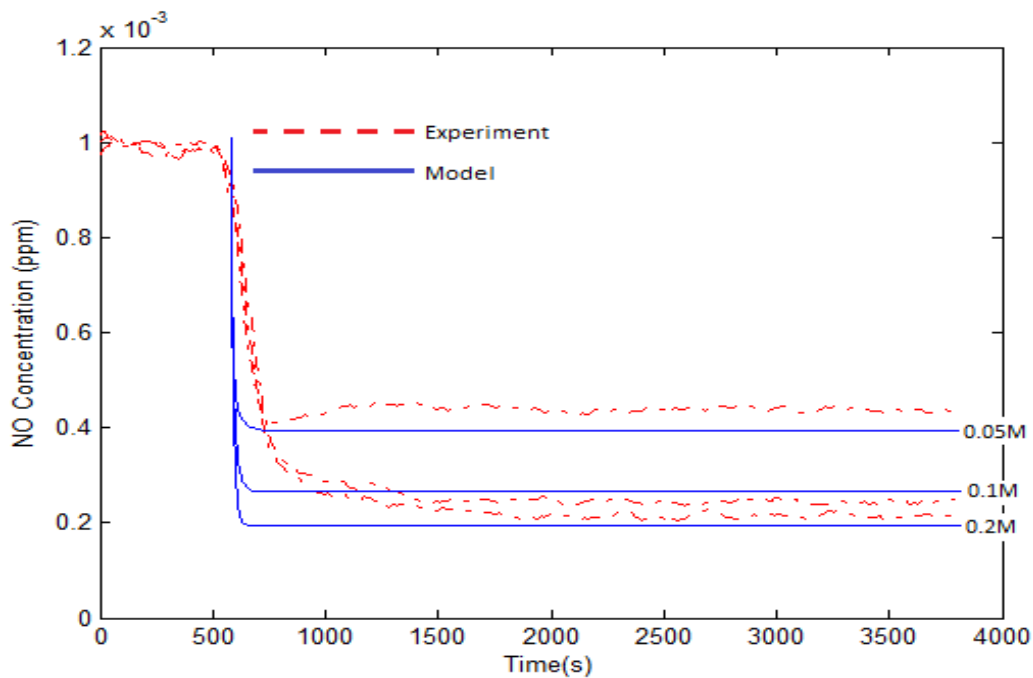
Figure 4.23. Experimental data and model prediction for different persulfate concentrations at 60° C

It is obvious from Figures 4.20 to 4.23 above that this simple model, from the film theory and NO balance in gas and aqueous phases, adequately fits the experimental data. The final values of $K_L a$ was 2.83×10^{-2} s^{-1} and the values recorded for k_1', k_2' and k_3' at the various temperatures have been used to obtain the Arrhenius plot shown in Figure 4.24. The form of Arrhenius equation used is shown in equation 4.27 and the individual values for k_1', k_2' and k_3' are depicted in Table 4.1.

$$\ln\left(\frac{k}{k_{30^oC}}\right) = -\frac{E}{RT} - \frac{E}{RT_{30^oC}} \qquad\qquad 4.27$$

Table 4. 1. The values of rate constants k₁', k₂' and k₃'

Temp(°C)	k′₁(s⁻¹)	k′₂(M⁻¹s⁻¹)	k′₃(M⁻¹s⁻¹)
30	5.00E-09	1.90E-01	1.90E-02
40	5.00E-08	2.50E-01	2.40E-02
50	1.10E-07	2.75E-01	3.10E-02
60	2.50E-07	6.00E-01	3.60E-02
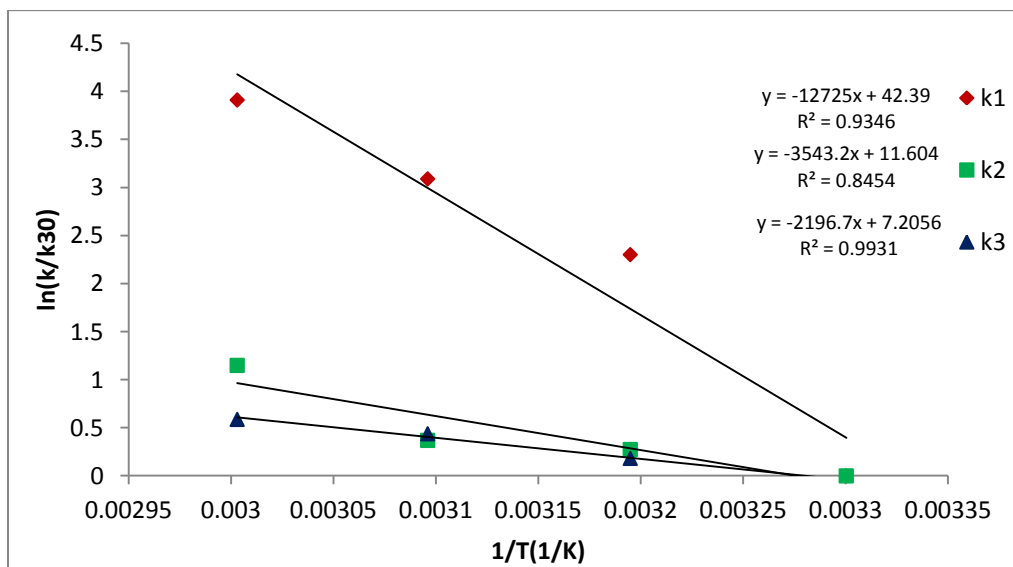
Figure 4.24. Arrhenius plots for the reaction rate constants k₁', k₂', and k₃'

From the plot of $\ln\left(\dfrac{k}{k_{30^oC}}\right)$ being y-axis and $\dfrac{1}{T}$ as x-axis, the activation energies can be calculated. The activation energies determined for the rate constants $k_1^{'}$, $k_2^{'}$ and $k_3^{'}$ were 105,796, 24,458 and 18,263 J/mol respectively. $k_1^{'}$, $k_2^{'}$ and $k_3^{'}$ are correspondingly the rate constants for thermal activation, direct persulfate reaction with NO, and Fe^{2+} activation. $k_1^{'}$ term which requires heat to take place recorded the highest activation energy, followed by $k_2^{'}$ which is a direct reaction. The lowest activation energy value for $k_3^{'}$ could be attributed to catalytic action by the Fe^{2+} ions.

4.7 Kinetic analysis

The steady state absorption of a gas A (NO) into liquid B (aqueous persulfate) with a chemical reaction is usually considered to be fast and irreversible, and can be described by the pseudo-mth, nth order reaction below.

$$aA + bB \xrightarrow{k_{mn}} products \tag{4.28}$$

where $r_a = k_{mn} C_A^m C_B^n$ is the kinetic rate expression

According to two-film model, the rate of absorption, R_A of gas component A into liquid stream B with a chemical reaction enhancement is related by the expression [1]

$$R_A = N_A a = k_G a(P_A - P_{Ai}) = E k_L a(C_{Ai} - C_{Ab}) \tag{4.29}$$

where N_A = average rate of transfer of gas per unit area (flux)

E is the enhancement factor

P_A, P_{Ai} = Partial pressures of soluble gas in the bulk gas and the interface respectively

C_{Ai} = Concentration of dissolved gas corresponding to equilibrium with P_{Ai}

C_{Ab} = Average concentration of dissolved gas in the bulk of the liquid

k_G = The gas side mass transfer coefficient

k_L = The physical liquid side mass transfer coefficient that applies in the absence of

    chemical reaction

a = The interfacial area

Determination of the physical parameters k_G, k_L and a have been well explained in previous work [1] in which the same apparatus was used from the same laboratory to study NO absorption by oxone.

Using Henry's law $C_{Ai} = P_{Ai}/H$ $where$ H equals Henry's or solubility coefficient to define the interfacial concentration of NO, C_{Ai}, equation 4.29 can be reduced to:

$$R_A = \frac{a(HP_A - C_{Ab})}{\dfrac{H}{k_G} + \dfrac{1}{Ek_L}} \qquad\qquad 4.30$$

Initially, there is no bulk liquid concentration of NO, which implies $C_{Ab} = 0$
Therefore,

$$R_A = \frac{aHP_A}{\dfrac{H}{k_G} + \dfrac{1}{Ek_L}} \qquad\qquad 4.31$$

Rearranging equation 4.31 gives

$$R_A = \frac{aP_A}{\frac{1}{k_G} + \frac{1}{HEk_L}} \qquad \text{or} \qquad R_A = \frac{aP_A}{(k_G)^{-1} + (HEk_L)^{-1}} \qquad\qquad 4.32$$

Normally, a pseudo-mth, nth order reaction of gas absorption into liquid using the film theory with a chemical reaction enhancement can also be described by [1, 63, 64]

$$E = \frac{Ha(\frac{Ei-E}{Ei-1})^{n/2}}{\tanh\{Ha(\frac{Ei-E}{Ei-1})\}^{\ n/2}} \qquad\qquad 4.33$$

E_i is enhancement factor for instantaneous chemical reaction.

Ha is the Hatta number defined as the ratio of chemical reaction rate to physical absorption rate in the liquid film [1, 64].

$$Ha = \frac{1}{k_L}\{\left[\frac{2}{m+1}\right]k_{mn}D_A C_{Ai}^{m-1}C_{Bo}^{n}\}^{1/2} \qquad\qquad 4.34$$

It has been established that, when the order of reaction is *m*=1, *E*= Ha/tanh(Ha), and when *m* = 0,2,or 3, $E = (1+Ha^2)^{1/2}$. But when 1<Ha>Ei, and E=Ha, equation 4.32 can be written as [32]

$$N_A = {R_A}/{a} = P_A \left(\frac{1}{k_G} + \frac{1}{H\{\left[\frac{2}{m+1}\right]k_{mn}D_A C_{Ai}^{m-1}C_{Bo}^{n}\}^{\frac{1}{2}}}\right)^{-1} \qquad\qquad 4.35$$

Thus, for pseudo mth, nth order rate expression, measuring the gas absorption rate for different NO and persulfate concentrations, the reaction orders, m and n, and the rate

constant k_{mn} can be estimated from equation 4.35. Equation 4.35 can be rearranged to give

$$\frac{N_A k_G}{H(P_A k_G - N_A)} = \left(\frac{2 D_A k_{mn} C_{Ai}^{m-1} C_{Bo}^n}{m+1} \right)^{1/2}$$

4.36

Representing $\dfrac{N_A k_G}{H(P_A k_G - N_A)}$ by $N_A^{'}$ and taking logarithms of both sides of equation

4.36 implies

$$log N_A^{'} = \frac{1}{2} log \left(\frac{2 D_A k_{mn} C_{Bo}^n}{m+1} \right) + \frac{m-1}{2} log C_{Ai}$$

4.37

4.7.1 *Determination of Reaction Orders and Rate constant*

In order to determine m, n, and k_{mn}, the flux N_A for absorption of NO into persulfate was determined for NO concentrations of 502, 753, and 1004 ppm in nitrogen gas, and persulfate concentrations of 0.05, 0.1, and 0.2 M. The interfacial concentration of NO in water C_{Ai} was determined by the relations:

$R_A = k_G a (P_A - P_{Ai})$ and the Henry's law $C_{Ai} = P_{Ai}/H_{NO}$

The rate of absorption of NO can be determined as

$$R_A = \frac{(Moles\ of\ NO)_{in} - (Moles\ of\ NO)_{out}}{Volume\ X\ time}$$

4.38

and

The number of moles, $n = \dfrac{PV}{RT} = \dfrac{PQt}{RT}$ 4.39

Using the following values;

Temperature, T = 25°C = 298.15K

Pressure Total in, P_{Tin} = 25 psig = 34.7 psia = 2.361 atm

Pressure Total out, P_{Tout} = 1.0 atm

Molar gas constant, R = 0.08057 atm.L/mol.K

Volumetric flow rate of gas, Q = 0.1 L/min and

Duration of experiment, t = 60 min,

The total moles in, n = 0.589691 mmoles, and for 14.07% conversion,

moles of NO absorbed = 0.1407x 0.589691= 0.082969 mmoles. Therefore,

$$R_A = \frac{moles\ absorbed}{volume\ X\ time} = \frac{0.082969 mmoles}{1000 Cm^3 X\ 60X\ 60\ s} = 2.304709x10^{-8} \frac{mmoles}{cm^3 sec}$$

The flux, N_A was determined by the relation,

$$N_A = D_{A,L} \frac{dC_A}{dz} = D_{A,L} \frac{(C_{A_i} - C_{A_{out}})}{z_1 - z_o} = D_{A,L} \frac{(P_{A_i} - P_{A_{out}})}{RT(z_1 - z_o)}$$ 4.40

and the estimation of the diffusivity, $D_{A,L}$ by the Wilke-Chang equation has been shown in appendix A. Table 4.2 shows the absorption rates of NO, R_A for 0.05 M persulfate concentration at different initial NO concentrations that were used to calculate the interfacial concentrations, C_{Ai} at 23°C. The table of values for 0.1 and 0.2 M persulfate concentrations at 23°C can be found in Tables C-1 and C-2 respectively of appendix C.

In Tables C-3 to C-11 of appendix C, the values of R_A and C_{Ai} have been shown for the different NO and persulfate concentrations at 40, and 50°C.

Table 4. 2. Estimation of Interfacial Concentration, C_{Ai} at 23°C for 0.05 M Persulfate

NO(ppm)	mole fraction	PA (atm)	RA/kGa	PAi(atm)	CAi=PAi/H	logCAi
502	0.000502	0.00118463	0.0001183	0.0010664	2.062E-06	-5.685695
753	0.000752	0.0017765	0.0002081	0.0015684	3.033E-06	-5.518137
1004	0.001003	0.00236807	0.0003516	0.0020164	3.899E-06	-5.409023

Table 4. 3. Determination of reaction order, m at 23°C

N_A	$P_A k_G - N_A$	$N_A k_G$	N'_A	$\log N'_A$
		$[S_2O_8^{2-}] = 0.05M$		
1.54817E-11	4.6317E-11	8.0768E-19	3.37208E-11	-10.472103
2.34823E-11	6.9192E-11	1.2251E-18	3.42373E-11	-10.465500
3.19443E-11	9.1591E-11	1.6665E-18	3.51851E-11	-10.453642
		$[S_2O^8_{2.}] = 0.1M$		
1.55284E-11	4.627E-11	8.1012E-19	3.38567E-11	-10.470356
2.37959E-11	6.8878E-11	1.2414E-18	3.48526E-11	-10.457764
3.18870E-11	9.1648E-11	1.6635E-18	3.51000E-11	-10.454693
		$[S_2O_8^{2-}] = 0.2M$		
1.60594E-11	4.5739E-11	8.3782E-19	3.54208E-11	-10.450742
2.44217E-11	6.8253E-11	1.2741E-18	3.60971E-11	-10.442528
3.29247E-11	9.061E-11	1.7177E-18	3.66574E-11	-10.435839

The plots of log N'$_A$ vs log C_{Ai} shown in Figures 4.25, 4.26, and 4.27 for 23, 40, and 50°C respectively appear to fit a straight line from which the reaction order m can be calculated. With the different linear plots shown for 0.05 M, 0.1 M and 0.2 M persulfate concentrations at 23°C (Figure 4.25), the average of the slopes is 0.0582, therefore,

$(m-1)/2 = 0.0582$ (m=1.1164) from equation 4.37, which approximately gives $m = 1$.

The same type of analysis has been used to find m at 40 and 50°C from the graphs shown in Figures 4.26 and 4.27 respectively.
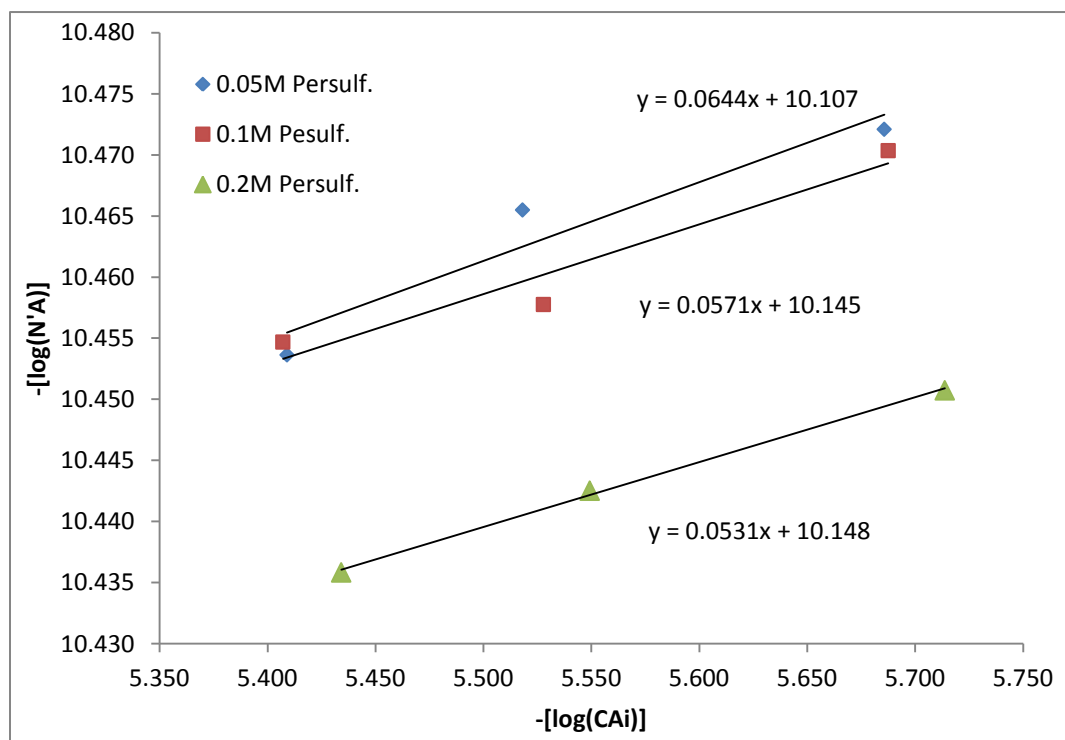
Figure 4.25. Plot of logN'$_A$ vs log C$_{Ai}$ for determining reaction order, m at 23° C
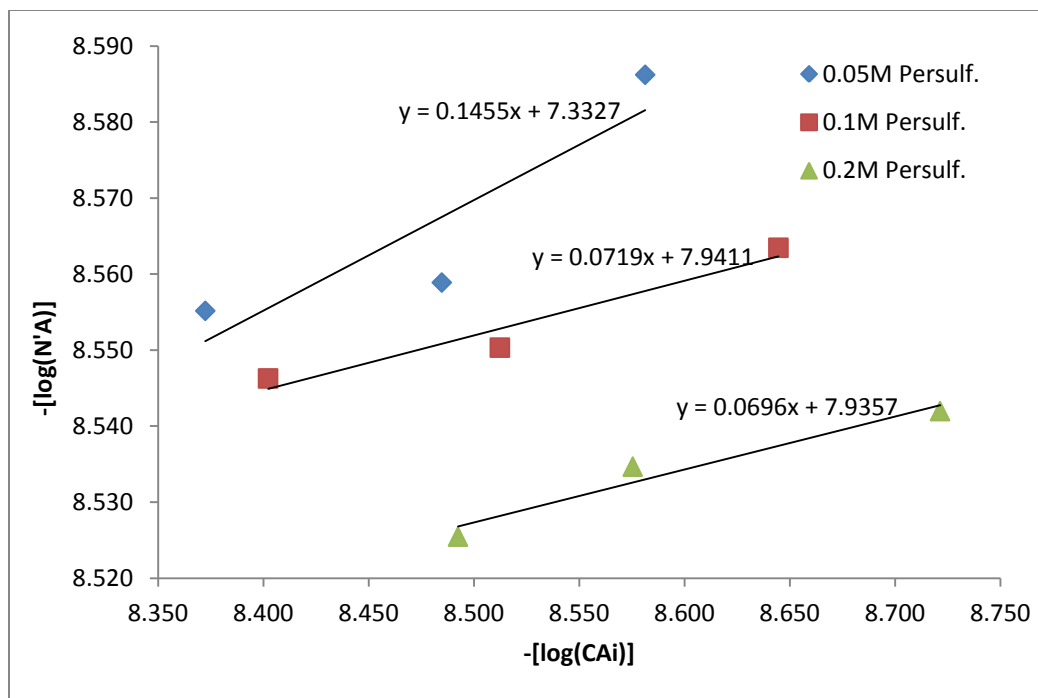
Figure 4.26. Plot of logN'$_A$ vs log C$_{Ai}$ for determining reaction order, m at 40° C
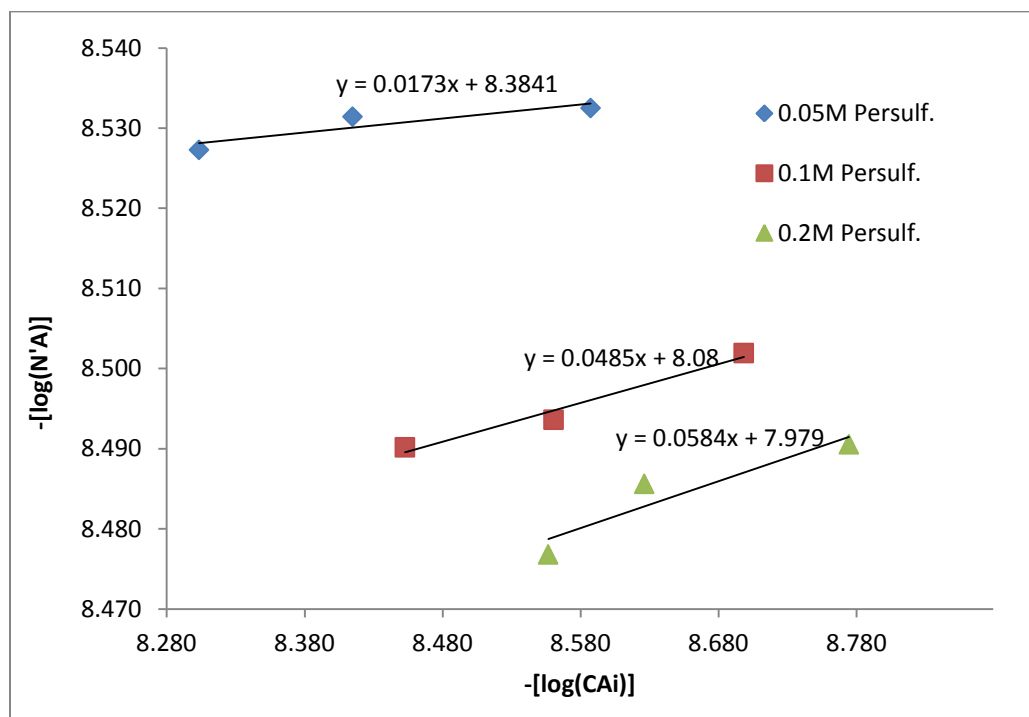
Figure 4.27. Plot of logN'$_A$ vs log C$_{Ai}$ for determining reaction order, m at 50° C

By substituting the $m = 1$, equation 4.37 reduces to

$$logN'_A = \frac{1}{2}\log\left(k_{mn}D_AC_{Bo}^n\right) \qquad\qquad 4.41$$

Rearranging equation 4.41 gives

$$\log\left(N'_A\bigg/\sqrt{D_A}\right) = \frac{1}{2}\log k_{mn} + \frac{n}{2}\log C_{Bo} \qquad\qquad 4.42$$

Thus, a plot of $\log(N'_A/D_A^{0.5})$ versus $\log C_{Bo}$ for the different concentrations of persulfate can be used to estimate reaction order n, and rate constant k_{mn}. Table 4.4 shows the data at 23°C used for the plots shown in Figure 4.30. The data that were used to produce similar plots at 40 and 50°C in Figures 4.30 and 4.31 respectively can be found in tables C-12 through C-15 of appendix C.

Table 4. 4. Values for determining Reaction order, n and rate constant k_{mn} at 23°C

C_{Bo}(M)	N'_A	$N'_A/(D)^{0.5}$	$Log((N'_A/(D)^{0.5})$	$logC_{Bo}$
		[NO]= 502ppm		
0.05	1.25694E-11	2.50091E-09	-8.601901478	-1.30103
0.1	1.36657E-11	2.71904E-09	-8.565584901	-1
0.2	1.41265E-11	2.81073E-09	-8.551181635	-0.69897
		[NO]= 753ppm		
0.05	1.26062E-11	2.50824E-09	-8.600631483	-1.30103
0.1	1.39829E-11	2.78215E-09	-8.555618847	-1
0.2	1.43214E-11	2.8495E-09	-8.545230621	-0.69897
		[NO]= 1004ppm		
0.05	1.27492E-11	2.53668E-09	-8.59573394	-1.30103
0.1	1.41166E-11	2.80875E-09	-8.551486767	-1
0.2	1.46771E-11	2.92027E-09	-8.534577496	-0.69897

Figure 4.28. Plot of $\log(N'_A/(D^{0.5}))$ vs $\log C_{Bo}$ for determining n and k_{mn} at 23° C

From Figure 4.28, the average of the slopes is 0.0926, from which *n* is estimated as *n*/2 = 0.0926 (equation 4.42), therefore n is 0.1852 (approximately zero). The average of the intercepts is 8.371, which implies ½ log k_{mn} = -8.371, therefore k_{mn} = 1.8113 x 10^{-17}s^{-1} at 23°C. See Figures 4.29 and 4.30 for plots used in determining *n* and k_{mn} at 40 and 50°C respectively.

Figure 4.29. Plot of log(N'$_A$/(D$^{0.5}$)) vs logC$_{Bo}$ for determining n and k$_{mn}$ at 40° C

Figure 4.30. Plot of log(N'$_A$/(D$^{0.5}$)) vs logC$_{Bo}$ for determining n and k$_{mn}$ at 50° C

From the plots in Figure 4.29 and 4.30 and data in Tables C-16 through C-19 of appendix C, the values of m, n, and k_{mn} determined for 23, 40, and 50°C have been tabulated in table 4.5. The corresponding Arrhenius plot is shown Figure 4.31, from which activation energy is estimated to be 57,136 J/mol.

Table 4. 5. Values of m, n, and k_{mn} at different temperatures

Temp., °C	m	n	k_{mn}, s^{-1}
23	1.1	0.2	1.1260E-17
40	1.2	0.1	1.8113E-17
50	1.0	0.2	9.3139E-17
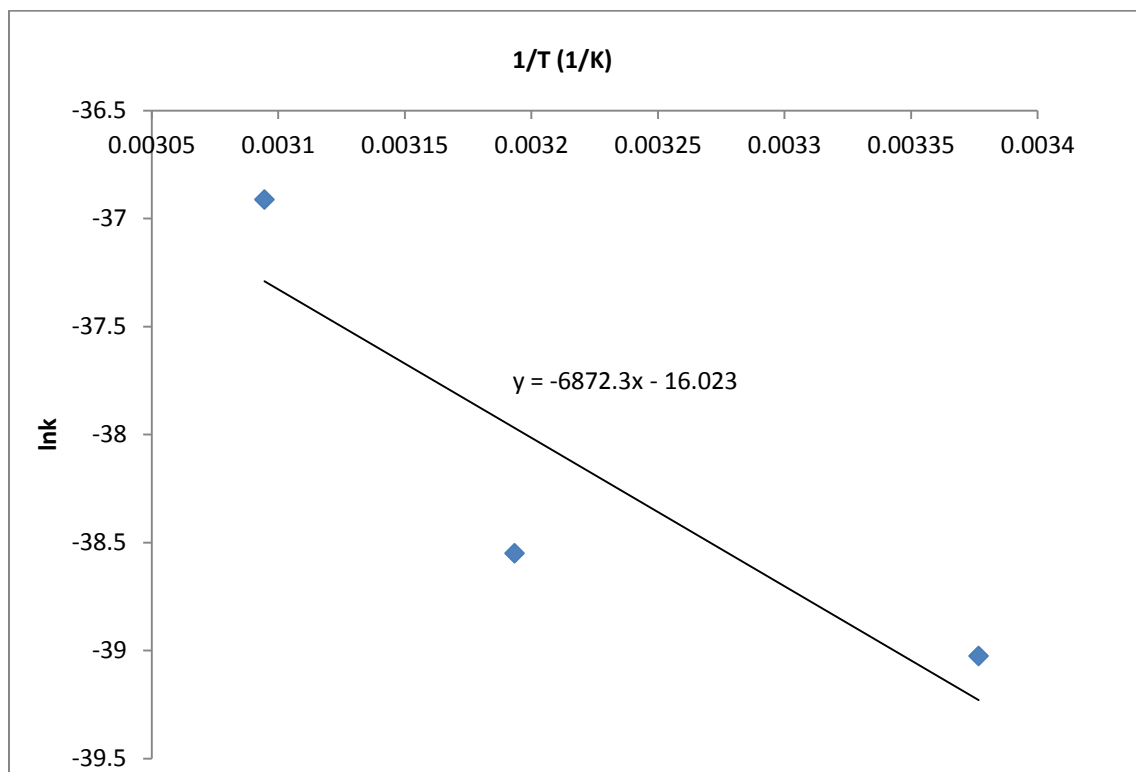
Figure 4.31. Arrhenius plot of rate constants

4.8 Impact of SO$_2$ gas presence on NO absorption

In a flue gas system SO$_2$ is always present with NO; therefore it is necessary to test how well the scrubbing solution for this project performs in the presence of SO$_2$ gas. The concentration of SO$_2$ in a typical flue gas system is around 2000 ppm and that of NO$_x$ is about 800 ppm [65]. Based on this fact, a number of experiments was conducted with NO-SO$_2$ blend in which the SO$_2$ and NO gas concentrations were about 1550 ppm and 1000 ppm respectively. Figure 4.32 shows profiles of NO gas concentration in the presence of SO$_2$ gas at various temperatures when 0.1 M persulfate concentration was used. The plots do not show any significant differences in NO fractional conversions as temperature increases unlike the case of Fe^{2+} studies graph shown in Figure 4.5. The presence of SO$_2$ in NO absorption studies showed NO fractional conversions to be in range of 77 to 83% for temperatures 23 to 70° C respectively, thus, higher conversions at even lower temperatures.
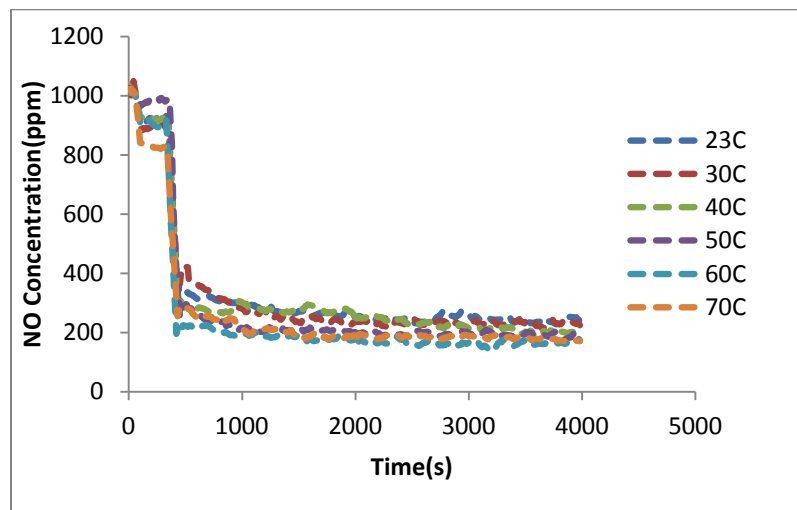
Figure 4.32. NO removal by 0.1 M persulfate in the presence of about 1550 ppm SO$_2$ gas at different temperatures

In Figure 4.33, the NO conversions for different initial persulfate concentrations have been compared for presence and absence of SO_2 at 50° C. It can be observed from the plots that lower persulfate concentrations absorbed way less NO gas than higher concentrations when SO_2 was present. Unlike when SO_2 was absent, a big gain in conversion occurred when the persulfate concentration increased from 0.05 M to 0.1 M in the presence of SO_2. This indicates that 0.1 M persulfate concentration as observed with earlier experiments still remains the optimum concentration level for NO gas removal by persulfate even in the presence of SO_2 gas.
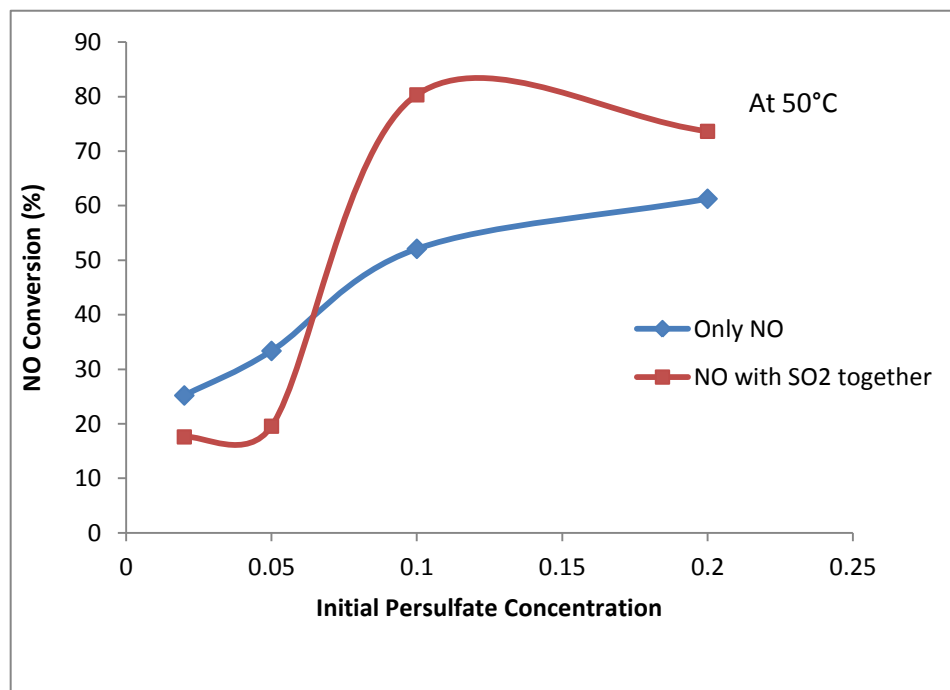
Figure 4.33. NO conversion dependency on initial persulfate concentration in the presence/absence of 1550 ppm SO_2 at 50° C

To better elucidate the effect of SO_2 gas, Figures 4.34 to 4.39 have been plotted to compare NO gas absorption when SO_2 was present and absent for the individual temperatures; 23, 30, 40, 50, 60, and 70° C. In all cases, presence of SO_2 dramatically improved NO gas absorption into aqueous persulfate with the greatest effect occurring at lower temperatures of 23 and 30° C.
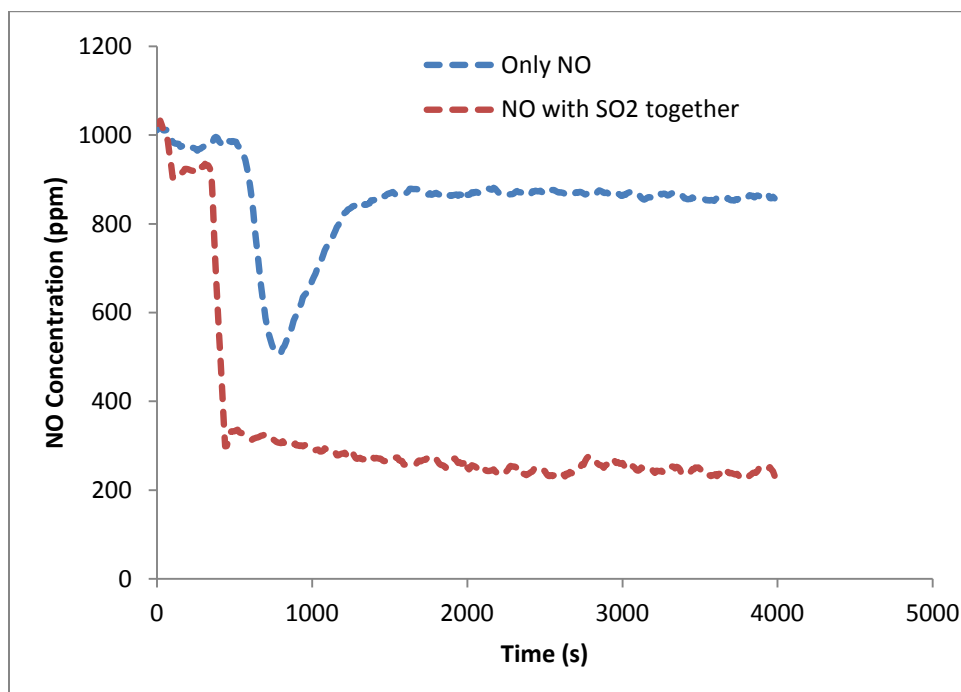
Figure 4.34. Effect of presence of 1550 ppm SO_2 gas on NO removal by 0.1 M persulfate at 23 °C
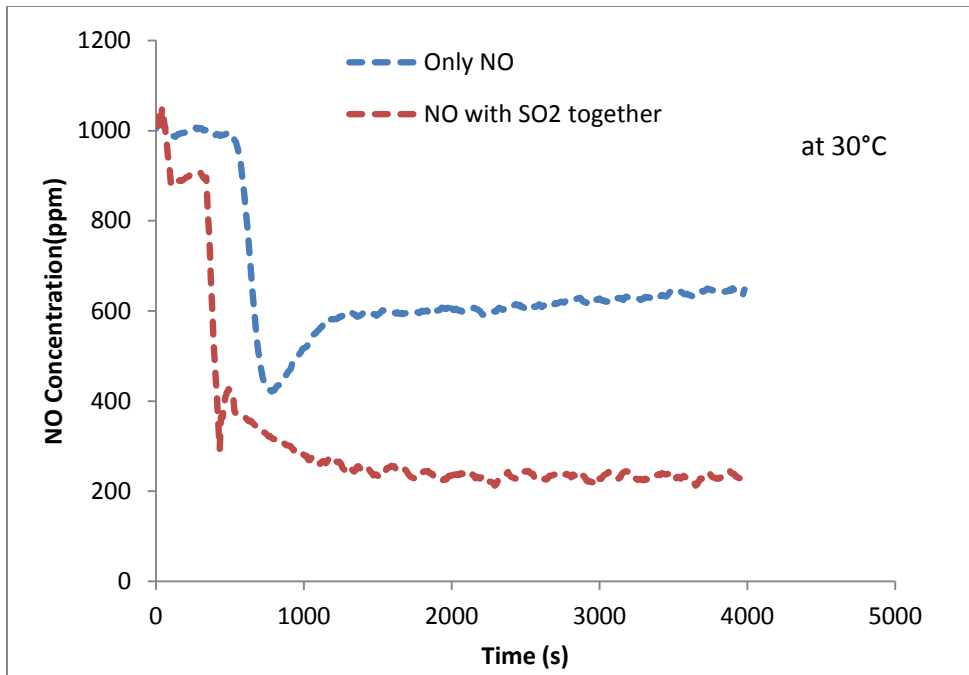
Figure 4.35. Effect of presence of 1550 ppm SO₂ gas on NO removal by 0.1 M persulfate at 30° C
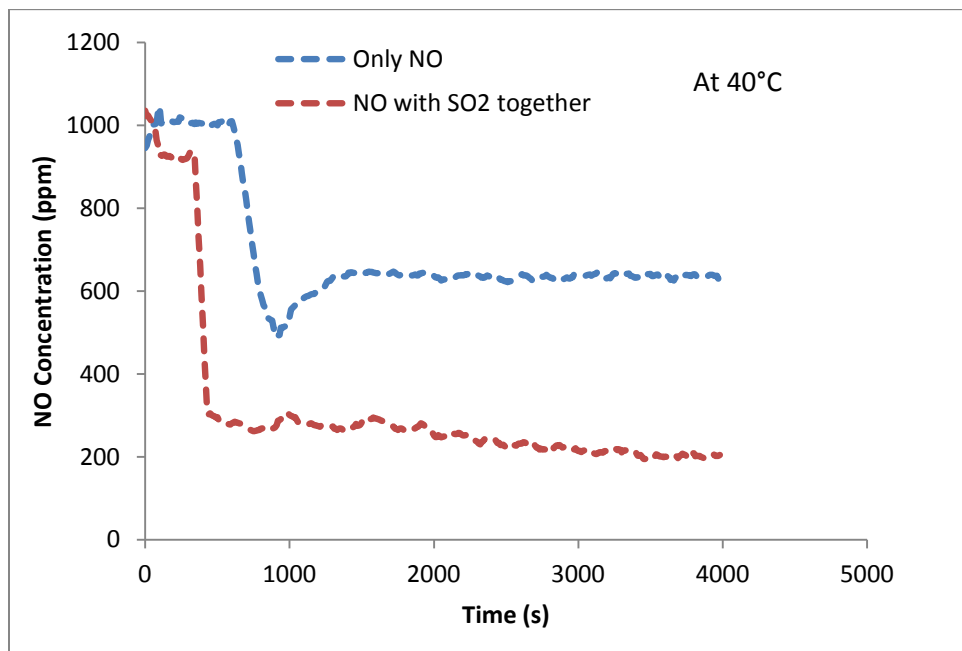
Figure 4.36. Effect of presence of 1550 ppm SO₂ gas on NO removal by 0.1 M persulfate at 40° C
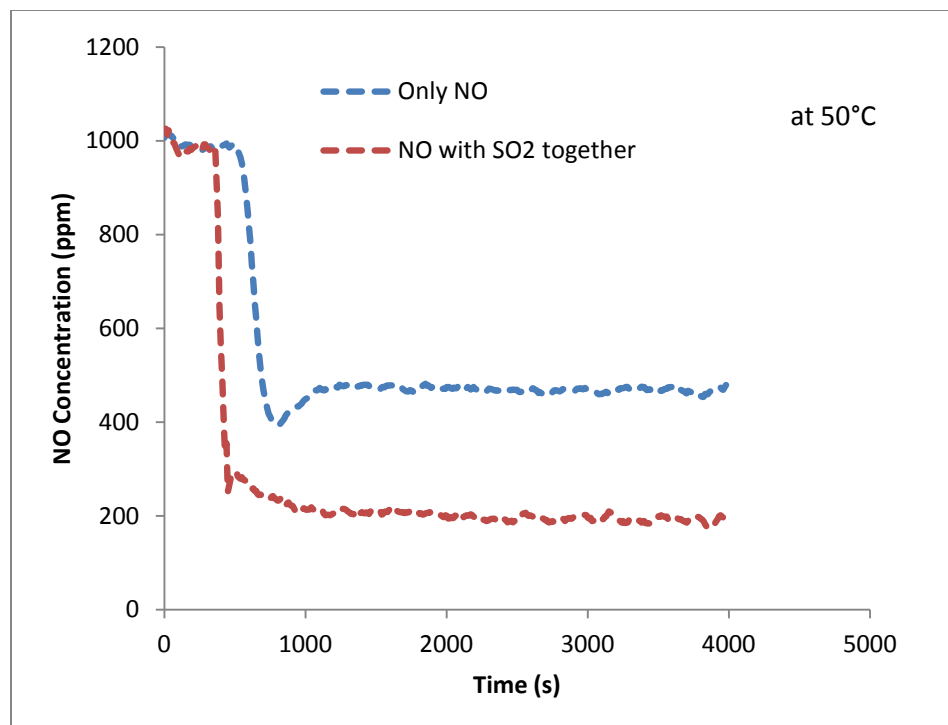
Figure 4.37. Effect of presence of 1550 ppm SO₂ gas on NO removal by 0.1 M persulfate at 50° C
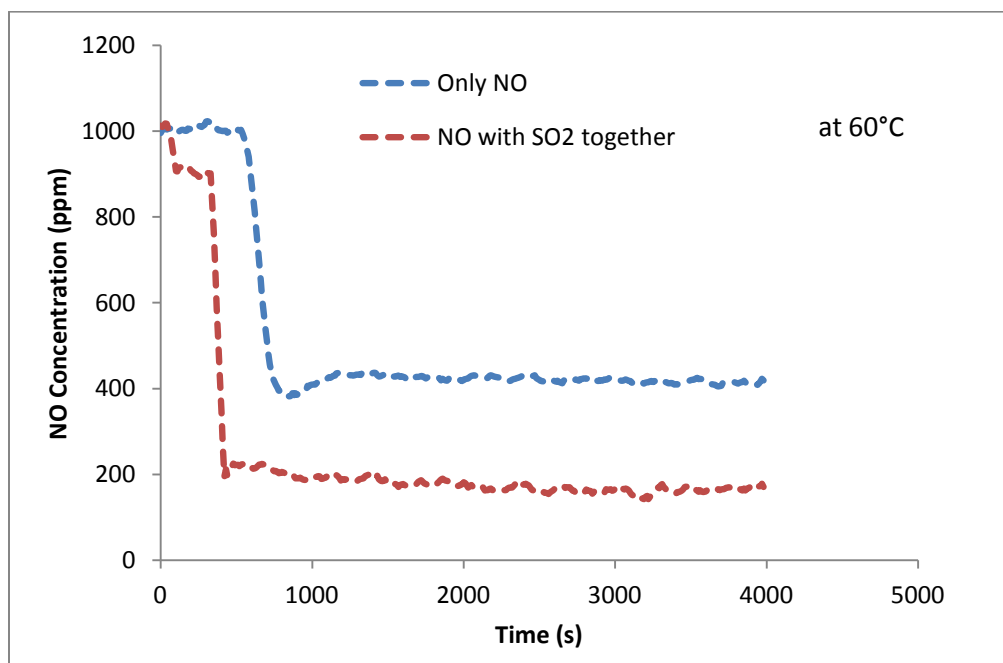
Figure 4.38. Effect of presence of 1550 ppm SO₂ gas on NO removal by 0.1 M persulfate at 60° C
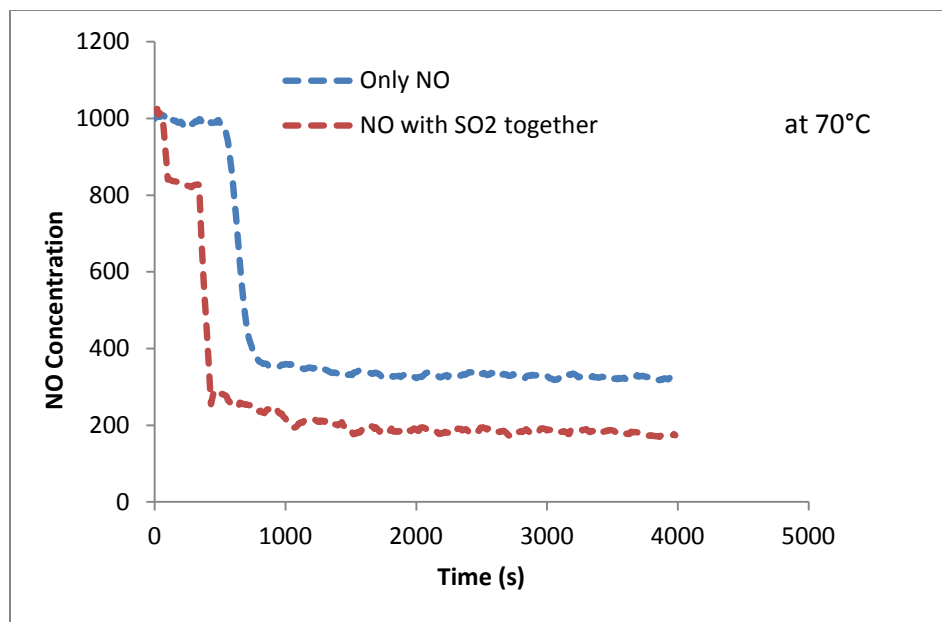
Figure 4.39. Effect of presence of 1550 ppm SO$_2$ gas on NO removal by 0.1 M persulfate at 70° C

A graph that combines all six individual temperatures to actually show the effect of temperature on NO conversion in the presence of SO$_2$ is shown in Figure 4.40. It can be inferred from this figure that presence of SO$_2$ enhanced NO removal by more than approximately 30%, and even about twice the gain in NO conversion at lower temperatures (23 and 30° C).
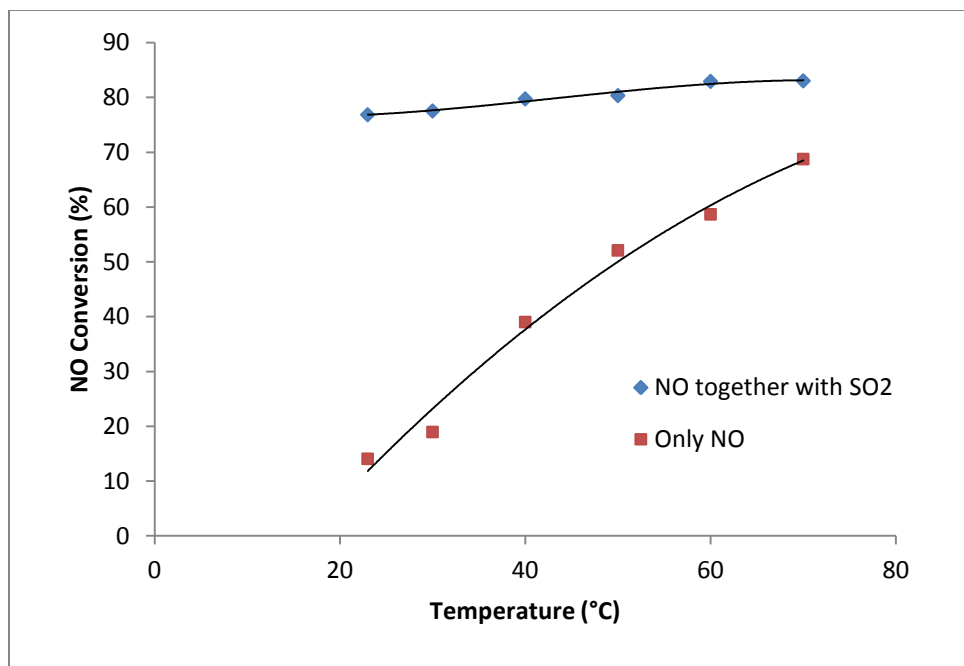
Figure 4.40. Effect of presence of 1550 ppm SO$_2$ gas on NO conversion over temperature

Persulfate is known to decompose faster under acidic conditions that can be described by a first order rate in following equation [3, 66]

$$-\frac{d[S_2O_8^{2-}]}{dt} = (k_1 + k_2[H^+])[S_2O_8^{2-}] = k_0[S_2O_8^{2-}] \qquad\qquad 4.28$$

From this rate expression, decrease in solution pH will accelerate persulfate decomposition. Therefore the observation with dramatic improvement in NO fractional conversions in the presence of SO$_2$ gas could be attributed to persulfate decomposing faster to produce highly reactive sulfate radicals responsible for NO oxidation and subsequent absorption. The necessary acidic medium might have come from SO$_2$ gas being more soluble than NO in aqueous solutions at lower temperatures, hence, the high NO fractional conversions increase recorded for 30 and 40°C in the presence of SO$_2$ gas.

Furthermore, formation of aqueous SO_2 species is much more rapid than formation of NO_2 species in aqueous solutions [65], therefore, in simultaneous removal of NO and SO_2 by aqueous persulfate solution, the SO_2 quickly gets absorbed into the aqueous medium providing immediate acidic conditions, with which high NO removal could be achieved.

In addition, SO_2 gas could interact with some of the $OH^\bullet$ radicals produced in equation 4.6 to form sulfuric acid according to the reaction shown below [6].

$$SO_2 + 2OH^\bullet \longrightarrow H_2SO_4 \qquad\qquad 4.29$$

Although SO_2 reacts with some of the $OH^\bullet$ radicals responsible for NO oxidation, figure 4.33 shows that 0.1 M $S_2O_8^{2-}$ is just enough for NO absorption by persulfate. Lower concentrations of persulfate (0.05 M and below) show lower NO conversions than when SO_2 is absent (Figure 4.33). These observations partially explain why the presence of SO_2 gas in our system showed great improvements in NO removal. The evidence is much clear from plots in Figures 4.34 to 4.39 which compare profiles of NO gas for presence and absence of SO_2 gas. While NO absorbs into aqueous persulfate around 800 seconds (Figure 4.34) during an actual experiment, presence of SO_2 gas lead to NO absorption into persulfate to within 500 seconds. Both profiles shown in Figure 4.34 to 4.39 are NO profiles except that one is in the presence of SO_2 gas and the other is not. In order to confirm this fact, individual plots of NO and SO_2 gas profiles have been put together on the same graph. Figure 4.41 through 4.46 shows the NO and SO_2 profiles for temperatures 23, 30, 40, 50, 60, and 70°C respectively.
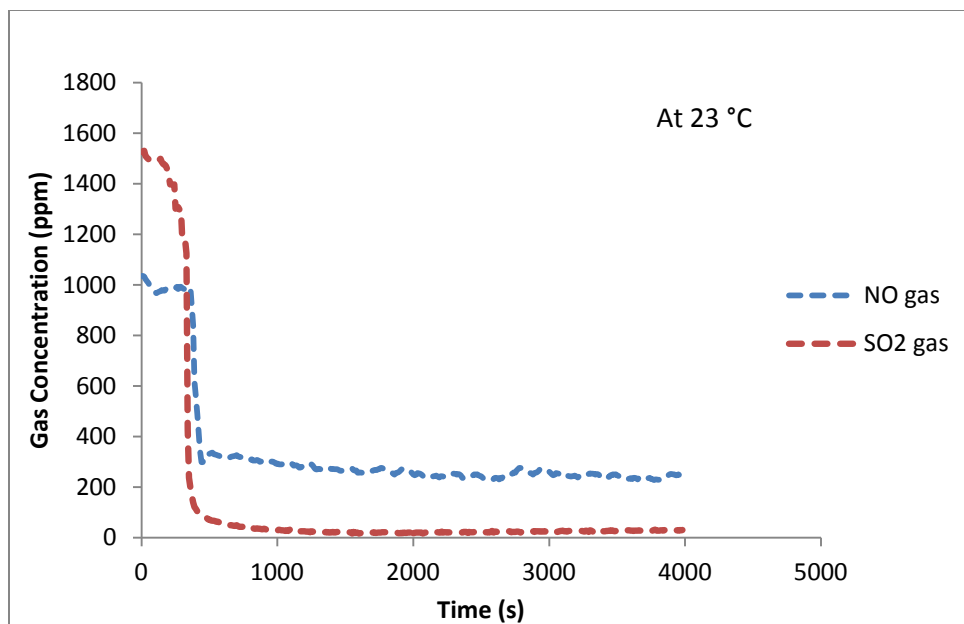
Figure 4.41. Profile of NO and SO$_2$ gas for simultaneous NO and SO$_2$ removal by 0.1 M persulfate at 23° C
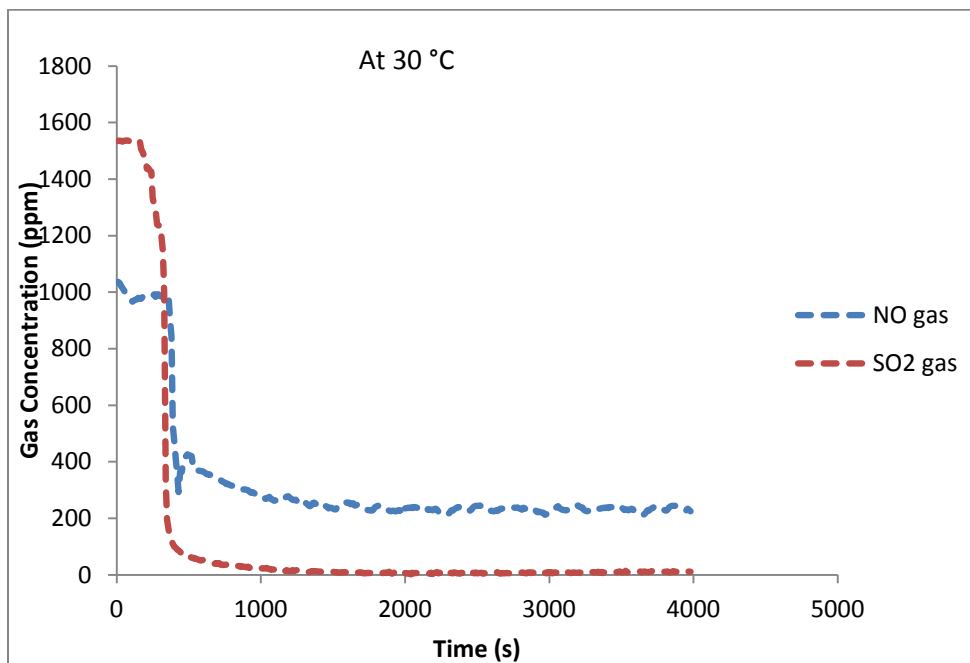
Figure 4.42. Profile of NO and SO$_2$ gas for simultaneous NO and SO$_2$ removal by 0.1 M persulfate at 30° C
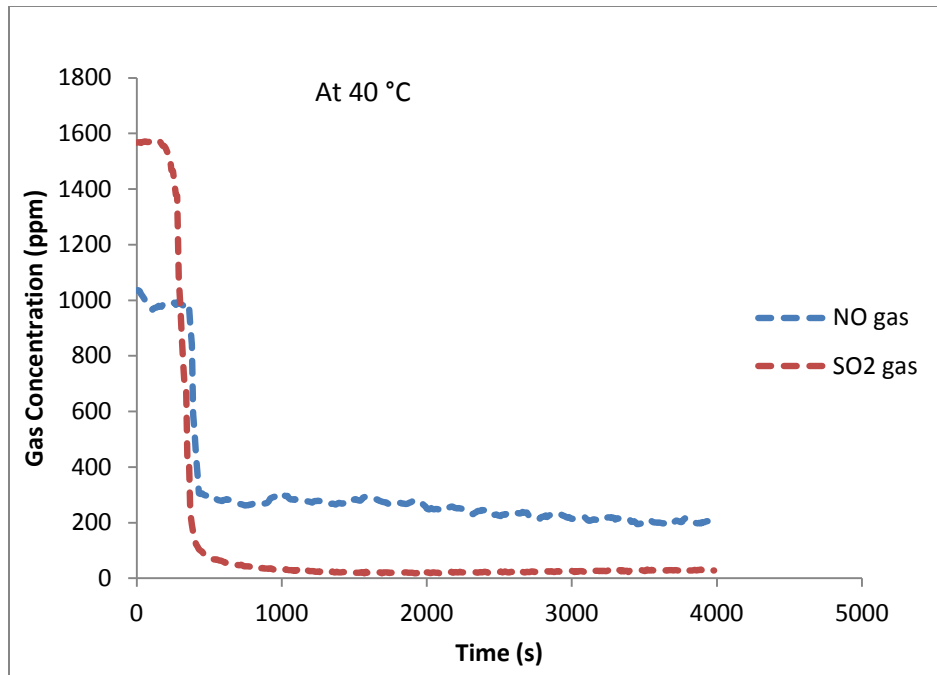
Figure 4.43. Profile of NO and SO₂ gas for simultaneous NO and SO₂ removal by 0.1 M persulfate at 40 °C
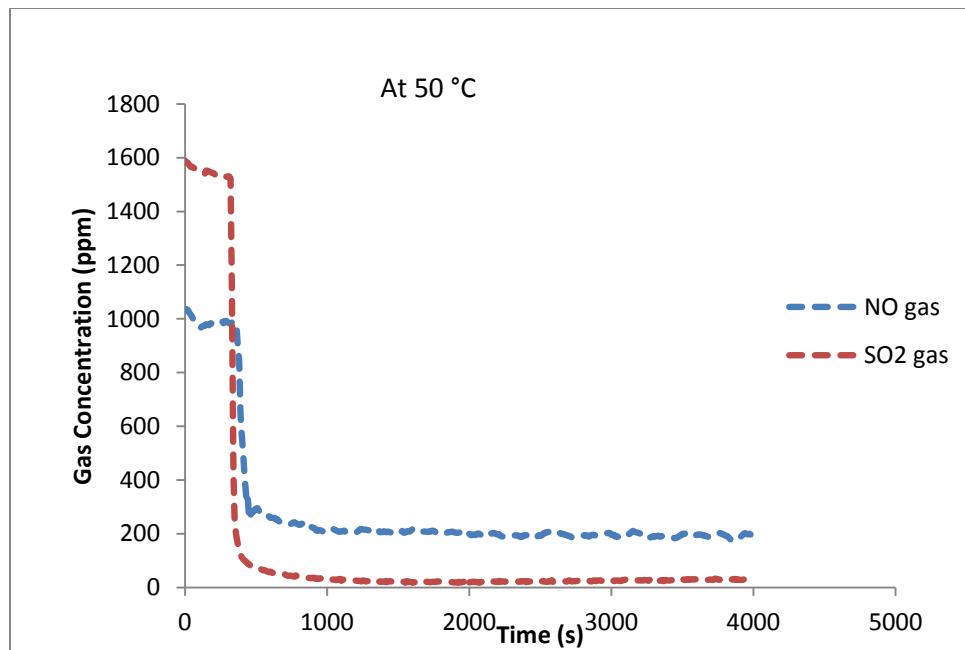
Figure 4.44. Profile of NO and SO₂ gas for simultaneous NO and SO₂ removal by 0.1 M persulfate at 50 °C
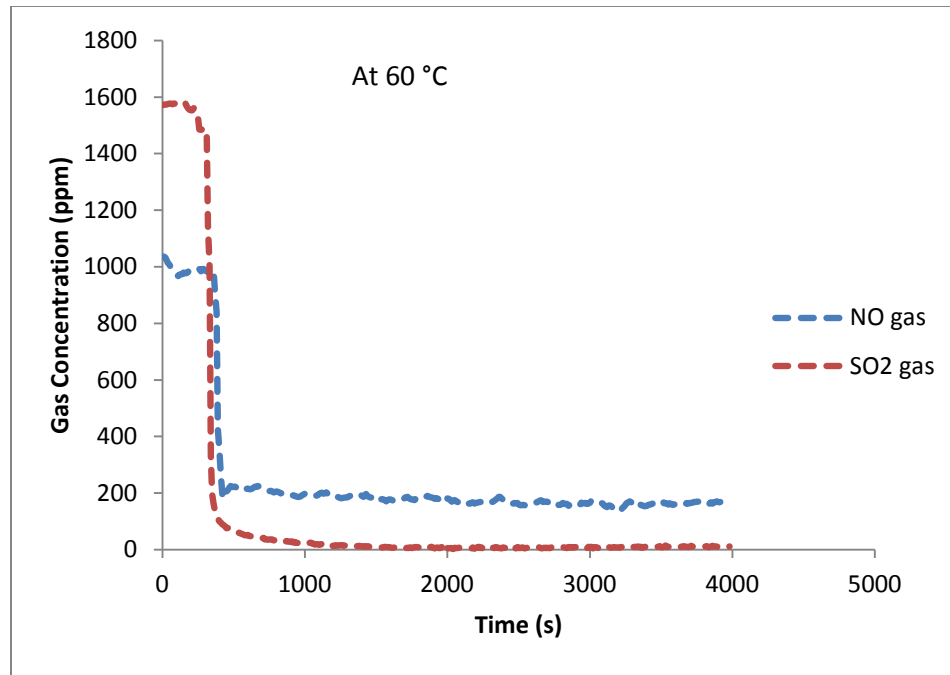
Figure 4.45. Profile of NO and SO$_2$ gas for simultaneous NO and SO$_2$ removal by 0.1 M persulfate at 60 °C
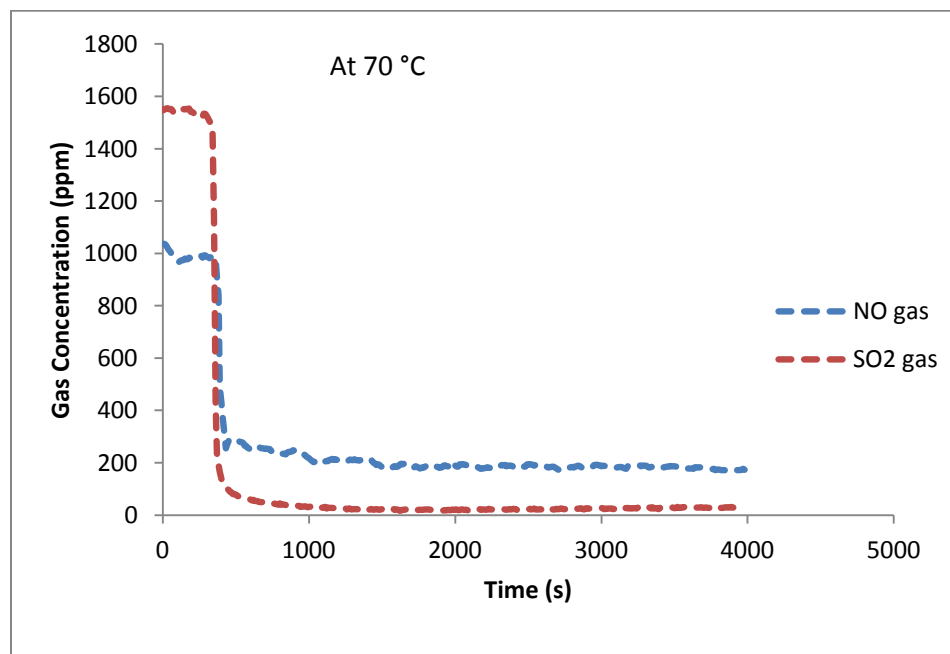
Figure 4.46. Profile of NO and SO$_2$ gas for simultaneous NO and SO$_2$ removal by 0.1 M persulfate at 70 °C

All experiments with SO_2 studies were conducted with 0.1 M persulfate concentration to enable comparison on the same platform. It is obvious from the plots in Figures 4.41 to 4.46 that both NO and SO_2 gases are being absorbed simultaneously and around 500 seconds. Notice that in the absence of SO_2 gas, NO gas absorbs into persulfate within 800 seconds. This indicates the possibility of formation of acidic conditions first by SO_2 which aids immediate and subsequent NO gas removal by aqueous persulfate. Indeed, presence of SO_2 gas induced faster NO gas absorption.

For some unknown reasons when presence of SO_2 gas was tested with 0.01 M Fe^{2+} activated persulfate, NO gas was poorly absorbed except at higher temperatures of 70° C. The plots for these observations are shown in Figures 4.47, 4.48 and 4.49 for 30, 50 and 70°C respectively. It could be that, instead of activating persulfate ions, Fe^{2+} ions were reacting with SO_3^{2-} which easily forms from SO_2 gas in aqueous solutions. However, at higher temperatures such as 70° C, more persulfate could be thermally activated, hence, the comparable NO fractional conversions recorded in the presence of both 0.1 M Fe^{2+} and SO_2 gas. The poor performance of Fe^{2+} activated persulfate for simultaneous absorption of NO and SO_2 could also stem from the fact that 0.01 M Fe^{2+} concentration was not the appropriate concentration level for NO-SO_2 gas blend, therefore optimization of Fe^{2+} might be required for NO-SO_2 gas mixture experiments.
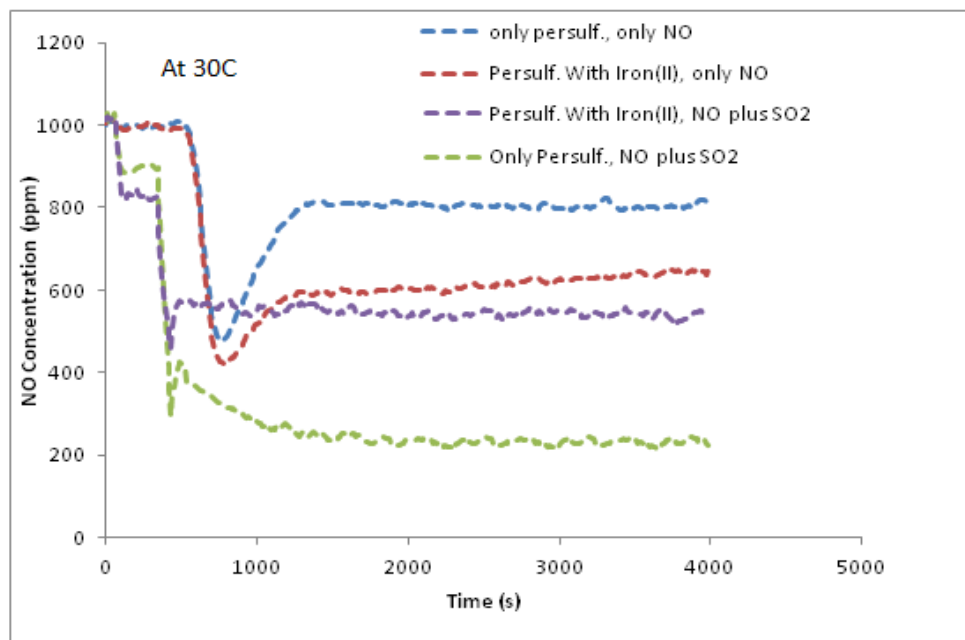
Figure 4.47. Effect of presence of SO₂ gas on NO removal by ferrous ion activated persulfate at 30 °C
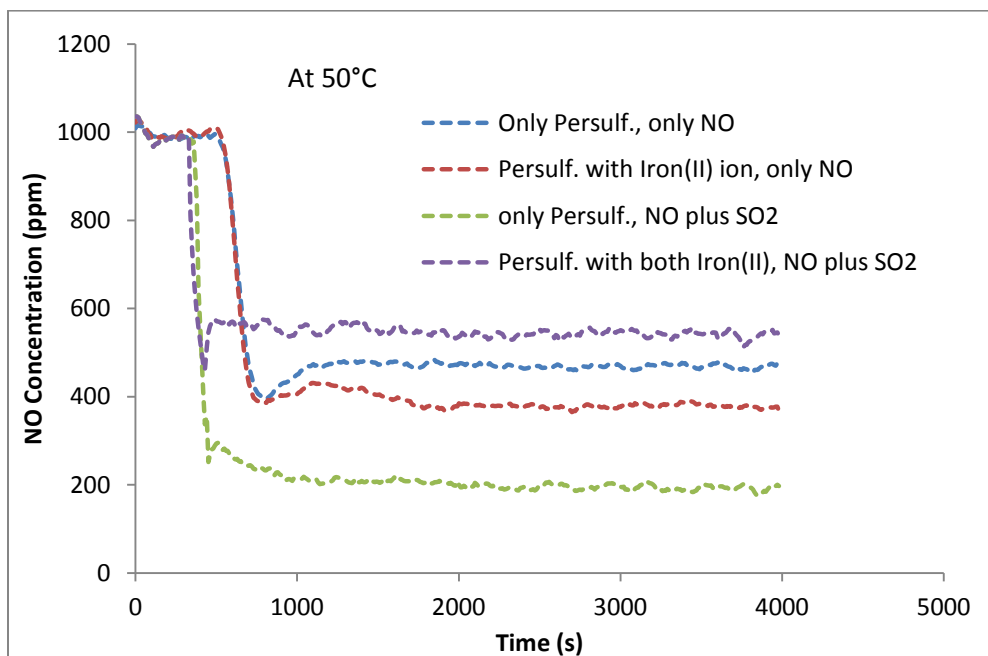
Figure 4.48. Effect of presence of SO₂ gas on NO removal by ferrous ion activated persulfate at 50 °C
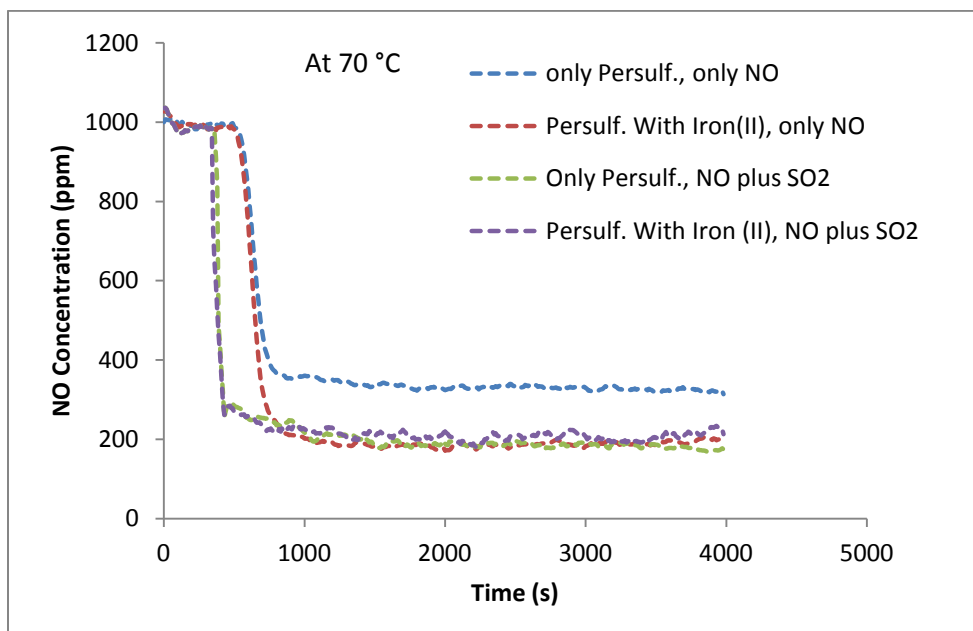
Figure 4.49. Effect of presence of SO$_2$ gas on NO removal by ferrous ion activated persulfate at 70 °C

4.9 Effect of pH

All experiments to investigate the influence of pH on NO gas absorption by aqueous persulfate were conducted at 50 °C, and without Fe^{2+} ions. 50 °C is known to be an average temperature for commercial flue gas control systems while Fe^{2+} precipitates at pHs greater than 3.5. The pH studies experiments were conducted by initially adding a standard buffer solution and continually adding NaOH to the reactor as needed to keep the pH at the desired level. Figure 4.50 shows NO gas absorption profiles for pH 4, 7, and 11. The NO fractional conversions recorded were 53.70, 43.61, and 24.95% for pH 7, 11, and 4 respectively. It can fairly be concluded that near neutral pH, neither acidic nor basic, provides the most suitable medium for simultaneous absorption of NO and SO$_2$ gases into aqueous solution of persulfate.
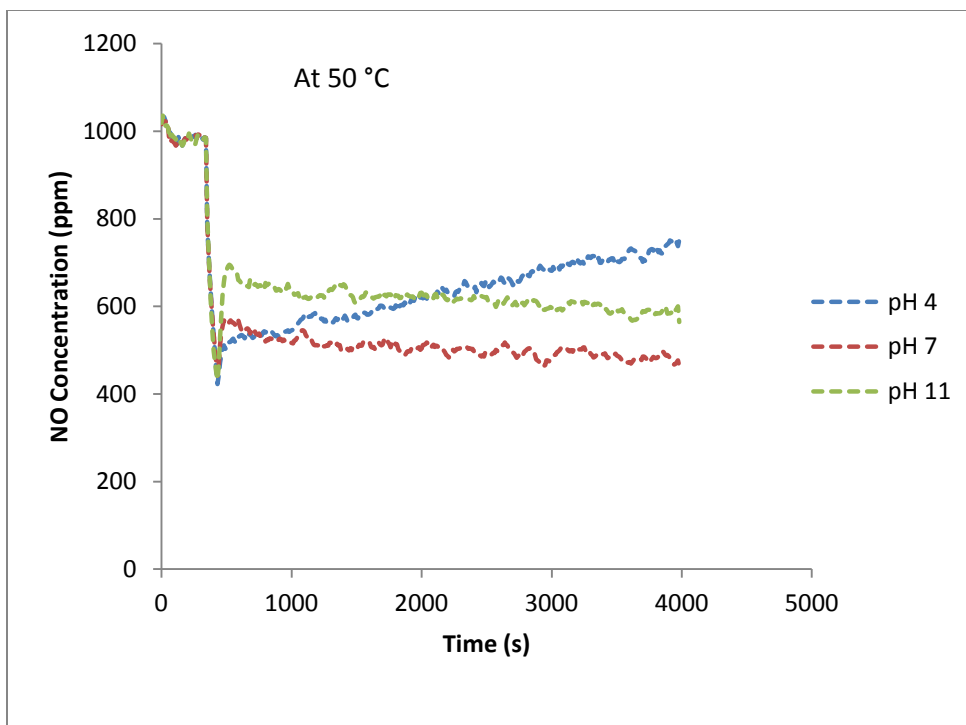
Figure 4.50. Effect of pH on NO removal in the presence of SO$_2$ gas at 50 °C

At pH 4, the NO profile appears to be increasing with time indicating saturation and inability of an aqueous solution to hold any more NO gas in solution. This is understandable because NO and SO$_2$ are responsible for acid rain formation at ambient conditions, therefore, it is unlikely for NO gas to absorb into a solution that is already acidic (pH 4). pH 11 which is more basic will probably hold some more acidic compounds, and its performance with higher NO fractional conversion than pH 4 in Figure 4.50 is expected. However, pH 7 recorded higher NO fractional conversion value over pH 11. This is because at pH 11, more OH• radicals could be produced than at neutral pH in thermal activated persulfate systems. Consequently more OH• radicals are scavenged by sulfate, hence reduced interaction of the radical species with the pollutant

90

[60]. Similar highest contaminant degradation at pH 7 have been documented by Liang et al., 2009 when they applied thermal activated persulfate to remove TCE from contaminated waters [60] Also, in the presence of SO2 gas, near neutral pH is ideal for NO absorption into oxone [32]. Nonetheless, in the absence of SO_2 gas, thus NO gas alone, pH does not seem to have any significant effect on NO gas removal by aqueous persulfate [3] . Both pH studies for presence and absence of SO_2 effect can be found in Figure 4.51.
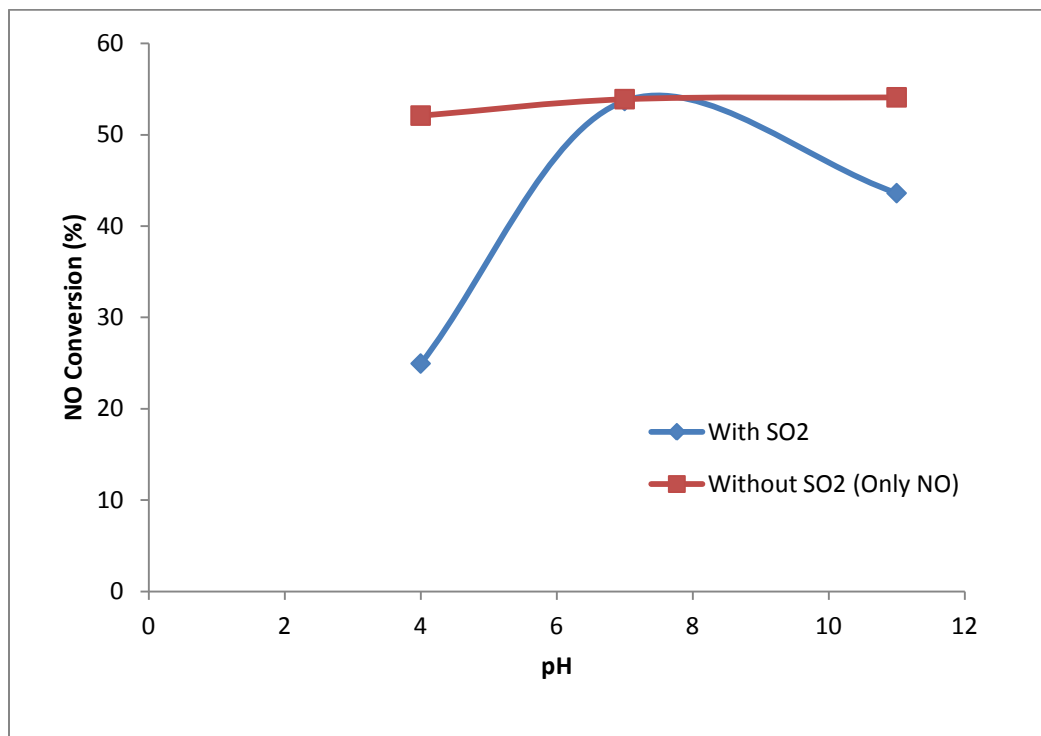
Figure 4.51. Effect of pH on NO removal in the presence and absence of SO$_2$ gas at 50 °C

CHAPTER 5

CONCLUSIONS AND RECOMMENDATIONS

5.1 Conclusions

The absorption and kinetics of NO by temperature-alone and combined temperature-Fe^{2+} activations have been studied at different persulfate concentrations. NO conversion increases with increasing temperature and persulfate concentrations. Previous studies reported 0.1 M persulfate as the optimum concentration for temperature activated persulfate absorption of NO. Same observation was made in the presence of 0.01 M Fe^{2+}, therefore, 0.1 M persulfate still remains the suitable concentration for NO removal by persulfate. Overall, presence of Fe^{2+} significantly improved NO removal by about 10% compared to temperature-alone activation. Excess Fe^{2+} truly acts as a scavenger to sulfate radicals, especially when 0.1 M Fe^{2+} was applied to 0.05 M persulfate, no NO removal was observed. However, addition of the required or minimum amount of Fe^{2+} in Fe^{2+} activated persulfate systems work well. Also, in the presence of 0.01 M Fe^{2+}, NO conversion increased with increase temperature (23-90 °C) persulfate (up to 0.1 M) concentration. This significantly shows a synergy for combined temperature and Fe^{2+} activations in NO removal by persulfate.

The presence of SO_2 gas did not work well for Fe^{2+} activated system, but greatly improved NO removal for temperature activated persulfate. SO_2 gas was completely absorbed in all SO_2 gas experiments. The rate of reaction of NO with persulfate ($S_2O_8^{2-}$)

was found to be first order with respect to NO and zero order with respect $S_2O_8{}^{2-}$ $(r_A = k_{mn}C_{NO})$ at 23, 40 and 50°C.

5.2 Recommendations

The results of this research demonstrate the feasibility of simultaneously removing NO_x and SO_2 by activated persulfate. The following recommendations may guide future work that will seek to improve upon this work or extend to other areas.

- Study Fe^{2+} activation with gradual addition of Fe^{2+} ions for NO absorption

- Optimize Fe^{2+} for simultaneous NO/SO_2 absorption by persulfate

- Look into the mechanism of NO absorption when SO_2 is present

- Extend persulfate activation to use of ultrasound and chelating agents

- Investigate the economics of the scrubbing process for possible industrial application

- Conduct studies on simultaneous NO, SO_2, CO_2 and Hg removal by activated persulfate

- Extend model work to include presence of SO_2 gas

REFERENCES

[1]   Adewuyi, Y. G. and Owusu, S. O., "Aqueous absorption and oxidation of nitric oxide with oxone for the treatment of tail gases: process feasibility, stoichiometry, reaction pathways, and absorption rate," *Industrial & Engineering Chemistry Research,* **42**, 4084 (2003).

[2]   Environmental Defense Fund. (2010, 20 May). Available: http://www.edf.org/page.cfm?tagID=78

[3]   Khan, N. E. and Adewuyi, Y. G., "Absorption and oxidation of nitric oxide (NO) by aqueous solutions of sodium persulfate in a bubble column reactor," *Industrial & Engineering Chemistry Research,* **49**, 8749 (2010).

[4]   Hosoi, J., Hiromitsu, N., Riechelmann, D., Fujii, A., and Sato, J., "Simple Low NOx Combustor Technology," *IHI engineering review,* **41**, 46 (2008).

[5]   Adewuyi, Y., He, X., Shaw, H., and Lolertpihop, W., "Simultaneous absorption and oxidation of NO and SO_2 by aqueous solutions of sodium chlorite," *Chem. Eng. Commun.,* **174**, 21 (1999).

[6]   Owusu, S. O. and Adewuyi, Y. G., "Sonochemical removal of nitric oxide from flue gases," *Industrial & Engineering Chemistry Research,* **45**, 4475 (2006).

[7]   Chien, T., Chu, H., and Hsueh, H., "Kinetic Study on Absorption of SO and NO with Acidic NaClO Solutions Using the Spraying Column," *Journal of environmental engineering,* **129**, 967 (2003).

[8]   Chu, H., Chien, T. W., and Li, S., "Simultaneous absorption of SO2 and NO from flue gas with KMnO4/NaOH solutions," *Science of the total environment,* **275**, 127 (2001).

[9]   Chu, H., Chien, T. W., and Twu, B. W., "The absorption kinetics of NO in NaClO2/NaOH solutions," *Journal of hazardous materials,* **84**, 241 (2001).

[10]   Gao, X., Du, Z., Ding, H., Wu, Z., Lu, H., Luo, Z., and Cen, K., "Kinetics of NO x Absorption into (NH4) 2SO3 Solution in an Ammonia-Based Wet Flue Gas Desulfurization Process," *Energy & Fuels,* (2010).

[11]   Sada, E., Kumazawa, H., Kudo, I., and Kondo, T., "Individual and simultaneous absorption of dilute NO and SO_2 in aqueous slurries of $MgSO_3$ with FeII-EDTA," *Industrial & Engineering Chemistry Process Design and Development,* **19**, 377 (1980).

[12]   Takeuchi, H., Ando, M., and Kizawa, N., "Absorption of nitrogen oxides in aqueous sodium sulfite and bisulfite solutions," *Industrial & Engineering Chemistry Process Design and Development,* **16**, 303 (1977).

[13]   Adewuyi, Y. and Owusu, S., "Ultrasound-induced aqueous removal of nitric oxide from flue gases: Effects of sulfur dioxide, chloride, and chemical oxidant," *J. Phys. Chem. A,* **110**, 11098 (2006).

[14]   Liang, C., Lin, Y. T., and Shih, W. H., "Treatment of trichloroethylene by adsorption and persulfate oxidation in batch studies," *Industrial & Engineering Chemistry Research,* **48**, 8373 (2009).

[15]   Sra, K. S., Thomson, N. R., and Barker, J. F., "Persistence of persulfate in uncontaminated aquifer materials," *Environmental science & technology,* **44**, 3098 (2010).

[16]   Bard, A. J., Parsons, R., and Jordan, J., Standard potentials in aqueous solution vol. 6, CRC, (1985).

[17]   Osgerby, I. T., "ISCO Technology Overview: Do You Really Understand the Chemistry?," *Contaminated Soils, Sediments and Water,* 287 (2006).

[18]   House, D. A., "Kinetics and mechanism of oxidations by peroxydisulfate," *Chem. Rev.,* **62**, 185 (1962).

[19]   Antoniou, M. G., De La Cruz, A. A., and Dionysiou, D. D., "Degradation of microcystin-LR using sulfate radicals generated through photolysis, thermolysis and e- transfer mechanisms," *Appl. Catal. B,* **96**, 290 (2010).

[20]   House, D. A., "Kinetics and Mechanism of Oxidations by Peroxydisulfate," *Chemical reviews,* **62**, 185 (1962).

[21]   Liang, C. and Lee, I., "In situ iron activated persulfate oxidative fluid sparging treatment of TCE contamination--A proof of concept study," *Journal of contaminant hydrology,* **100**, 91 (2008).

[22]   Liang, C., Lee, I., Hsu, I., Liang, C. P., and Lin, Y. L., "Persulfate oxidation of trichloroethylene with and without iron activation in porous media," *Chemosphere,* **70**, 426 (2008).

[23]   Cao, J., Zhang, W. X., Brown, D. G., and Sethi, D., "Oxidation of lindane with Fe (II)-activated sodium persulfate," *Environmental Engineering Science,* **25**, 221 (2008).

[24]   Kusic, H., Peternel, I., Koprivanac, N., and Bozic, A. L., "Iron-Activated Persulfate Oxidation of an Azo Dye in Model Wastewater: Influence of Iron Activator Type on Process Optimization," *Journal of environmental engineering,* **137**, 454 (2011).

[25]   Adewuyi, Y. G., "Sonochemistry in environmental remediation. 1. Combinative and hybrid sonophotochemical oxidation processes for the treatment of pollutants in water," *Environmental science & technology,* **39**, 3409 (2005).

[26]   Adewuyi, Y. G., "Sonochemistry in environmental remediation. 2. Heterogeneous sonophotocatalytic oxidation processes for the treatment of pollutants in water," *Environmental science & technology,* **39**, 8557 (2005).

[27]   Antoniou, M. G., De La Cruz, A. A., and Dionysiou, D. D., "Degradation of microcystin-LR using sulfate radicals generated through photolysis, thermolysis and transfer mechanisms," *Applied Catalysis B: Environmental,* **96**, 290 (2010).

[28]   Singh, U. C. and Venkatarao, K., "Kinetics of acid catalyzed and Ag (I) catalyzed decomposition of peroxodisulfate in aqueous medium," *International Journal of Chemical Kinetics,* **13**, 555 (1981).

[29]   Tsitonaki, A., Petri, B., Crimi, M., Mosbæk, H., Robert, L. S., and Bjerg, P. L., "In situ chemical oxidation of contaminated soil and groundwater using persulfate: A Review," *Critical Reviews in Environmental Science and Technology,* **40**, 55 (2010).

[30]   Block, P. A., Brown, R. A., and Robinson, D., "Novel activation technologies for sodium persulfate in situ chemical oxidation," (2004)

[31]   Group, W. B., "Pollution prevention and abatement handbook, 1998: toward cleaner production," (1999)

[32]   Adewuyi, Y. and Owusu, S., "Aqueous absorption and oxidation of nitric oxide with oxone for the treatment of tail gases: Process feasibility, stoichiometry, reaction pathways, and absorption rate," *Ind. Eng. Chem. Res,* **42**, 4084 (2003).

[33]   Sada, E., Kumazawa, H., Kudo, I., and Kondo, T., "Absorption of NO in aqueous mixed solutions of $NaClO_2$ and NaOH," *Chemical Engineering Science,* **33**, 315 (1978).

[34]   Brogren, C., Karlsson, H. T., and Bjerle, I., "Absorption of NO in an aqueous solution of $NaClO_2$," *Chemical engineering & technology,* **21**, 61 (1998).

[35]   Liu, Y., Zhang, J., and Sheng, C., "Study on the Kinetics of NO Removal from Simulated Flue Gas by a Wet Ultraviolet/H_2O_2 Advanced Oxidation Process," *Energy & Fuels,* (2011).

[36]   Cooper, C. D., Clausen Iii, C. A., Pettey, L., Collins, M. M., and De Fernandez, M. P., "Investigation of Ultraviolet Light-Enhanced HO Oxidation of NO Emissions," *Journal of environmental engineering,* **128**, 68 (2002).

[37]   Liu, Y., Zhang, J., Sheng, C., Zhang, Y., and Zhao, L., "Simultaneous removal of NO and SO_2 from coal-fired flue gas by UV/H_2O_2 advanced oxidation process," *Chemical Engineering Journal,* **162**, 1006 (2010).

[38]   Anipsitakis, G. P. and Dionysiou, D. D., "Degradation of organic contaminants in water with sulfate radicals generated by the conjunction of peroxymonosulfate with cobalt," *Environmental science & technology,* **37**, 4790 (2003).

[39] Rastogi, A., Al-Abed, S. R., and Dionysiou, D. D., "Sulfate radical-based ferrous-peroxymonosulfate oxidative system for PCBs degradation in aqueous and sediment systems," *Applied Catalysis B: Environmental,* **85**, 171 (2009).

[40] Anipsitakis, G. P. and Dionysiou, D. D., "Transition metal/UV-based advanced oxidation technologies for water decontamination," *Applied Catalysis B: Environmental,* **54**, 155 (2004).

[41] Khan, N. E. and Adewuyi, Y. G., "A new method of analysis of peroxydisulfate using ion chromatography and its application to the simultaneous determination of peroxydisulfate and other common inorganic ions in a peroxydisulfate matrix," *Journal of Chromatography A,* (2010).

[42] Liang, C., Wang, Z. S., and Bruell, C. J., "Influence of pH on persulfate oxidation of TCE at ambient temperatures," *Chemosphere,* **66**, 106 (2007).

[43] Furman, O. S., Teel, A. L., and Watts, R. J., "Mechanism of base activation of persulfate," *Environmental science & technology,* (2010).

[44] Liang, C. and Bruell, C. J., "Thermally activated persulfate oxidation of trichloroethylene: experimental investigation of reaction orders," *Industrial & Engineering Chemistry Research,* **47**, 2912 (2008).

[45] Waldemer, R. H., Tratnyek, P. G., Johnson, R. L., and Nurmi, J. T., "Oxidation of chlorinated ethenes by heat-activated persulfate: Kinetics and products," *Environmental science & technology,* **41**, 1010 (2007).

[46] Liang, C. J., Bruell, C. J., Marley, M. C., and Sperry, K. L., "Thermally activated persulfate oxidation of trichloroethylene (TCE) and 1, 1, 1-trichloroethane (TCA) in aqueous systems and soil slurries," *Soil and Sediment Contamination: An International Journal,* **12**, 207 (2003).

[47] Oh, S. Y., Kim, H. W., Park, J. M., Park, H. S., and Yoon, C., "Oxidation of polyvinyl alcohol by persulfate activated with heat, Fe^{2+}, and zero-valent iron," *Journal of hazardous materials,* **168**, 346 (2009).

[48]   Killian, P. F., Bruell, C. J., Liang, C., and Marley, M. C., "Iron (II) Activated persulfate oxidation of MGP contaminated soil," *Soil & Sediment Contamination,* **16**, 523 (2007).

[49]   Padmanabhan, A. R., "Novel Simultaneous Reduction/Oxidation Process for Destroying Organic Solvents," Worchester Polytechnic Institute, (2008).

[50]   Liang, C., Bruell, C. J., Marley, M. C., and Sperry, K. L., "Persulfate oxidation for in situ remediation of TCE. I. Activated by ferrous ion with and without a persulfate-thiosulfate redox couple," *Chemosphere,* **55**, 1213 (2004).

[51]   Liang, C. and Lai, M. C., "Trichloroethylene degradation by zero valent iron activated persulfate oxidation," *Environmental Engineering Science,* **25**, 1071 (2008).

[52]   Liang, C. and Guo, Y., "Mass Transfer and Chemical Oxidation of Naphthalene Particles with Zerovalent Iron Activated Persulfate," *Environmental science & technology,* (2010).

[53]   Liang, C., Guo, Y. Y., Chien, Y. C., and Wu, Y. J., "Oxidative Degradation of MTBE by Pyrite-Activated Persulfate: Proposed Reaction Pathways," *Industrial & Engineering Chemistry Research,* (2010).

[54]   Liang, C., Bruell, C. J., Marley, M. C., and Sperry, K. L., "Persulfate oxidation for in situ remediation of TCE. II. Activated by chelated ferrous ion," *Chemosphere,* **55**, 1225 (2004).

[55]   Rastogi, A., Al-Abed, S. R., and Dionysiou, D. D., "Effect of inorganic, synthetic and naturally occurring chelating agents on Fe (II) mediated advanced oxidation of chlorophenols," *Water research,* **43**, 684 (2009).

[56]   Owusu, S. and Adewuyi, Y., "Sonochemical removal of nitric oxide from flue gases," *Ind. Eng. Chem. Res,* **45**, 4475 (2006).

[57]   Adewuyi, Y. G. and Khan, N. E., "Modeling the ultrasonic cavitation-enhanced removal of nitrogen oxide in a bubble column reactor," *AIChE Journal,* **58**, 2397 (2012).

[58]   Liang, C., Chen, Y. J., and Chang, K. J., "Evaluation of persulfate oxidative wet scrubber for removing BTEX gases," *Journal of hazardous materials,* **164**, 571 (2009).

[59]   Ross, A., Mallard, W., Helman, W., Buxton, G., Huie, R., and Neta, P., NDRL-NIST Solution kinetics database: Version 3.0, (1998).

[60]   Liang, C., Liang, C. P., and Chen, C. C., "pH dependence of persulfate activation by EDTA/Fe (III) for degradation of trichloroethylene," *Journal of contaminant hydrology,* **106**, 173 (2009).

[61]   Buxton, G. V., Greenstock, C. L., Phillips Helman, W., and Ross, A. B., "Critical Review of rate constants for reacitons of hydrated electrons," *J. Phys. Chem. Ref. Data;(United States),* **17**, (1988).

[62]   Khan, N. E., "Chemical and Sonochemical Removal Of Nitric Oxide (NO) in a Bubble Column Reactor: Experimental and Modeling Studies," Masters in Chemical Engineering, Chemical and Bioengineering, North Carolina A&T State University, Greensboro (2010).

[63]   Charpentier, J. C., "Mass-Transfer Rates in Gas-Liquid Absorbers and Reactors," *Advances in chemical engineering,* **11**, 1 (1981).

[64]   Danckwerts, P. V. and Lannus, A., "Gas-liquid reactions," *Journal of The Electrochemical Society,* **117**, 369C (1970).

[65]   Ellison, T. and Eckert, C., "The oxidation of aqueous sulfur dioxide. 4. The influence of nitrogen dioxide at low pH," *The Journal of Physical Chemistry,* **88**, 2335 (1984).

[66]   Kolthoff, I. and Miller, I., "The Chemistry of Persulfate. I. The Kinetics and Mechanism of the Decomposition of the Persulfate Ion in Aqueous Medium1," *Journal of the American Chemical Society,* **73**, 3055 (1951).

[67]   Bird, R. and Stewart, W. E., "Lightfoot," *Transport phenomena,* **2**, (1960).

[68]   Sander, R., "Compilation of Henry's law constants for inorganic and organic species of potential importance in environmental chemistry," ed: Max-Planck Institute of Chemistry, Air Chemistry Department, 1999.

APPENDIX A

DETERMINATION OF DIFFUSION COEFFICIENTS

Gas Phase Diffusion Coefficient

The diffusivity of NO and SO_2 in nitrogen is determined from the Chapman-Enskog relation given by [67]:

$$D_{AB} = 0.0018583 \frac{\sqrt{T^3 \left(\frac{1}{M_A} + \frac{1}{M_B} \right)}}{p \sigma_{AB}^2 \Omega_{D,AB}}$$

Where D_{AB} = the diffusion coefficient of solute gas A in B [=] cm^2/s

P is the pressure if atm

σ_{AB} is the collision diameter in Å

$\Omega_{D,AB}$ is a dimensionless function of the temperature of te intermolecular potential field for one molecule of A and one of B

M_A and M_B are the molecular weights of the gases (g/mol), A = NO and B= nitrogen

The following physical values were used T = 25^oC = 298.16K, P = 1atm

For NO in Nitrogen,

M_A = 14 + 16 = 30g/mol

For N, M_B = 14.01 + 14.01 = 28.02

From table B-1 in appendix B of Bird and Lightfoot's book, $\sigma_A = 3.470$ and $\sigma_B = 3.681$

$[\varepsilon/k]_A = 119$ and

$[\varepsilon/k]_B = 91.5$

$\sigma_{AB} = \frac{1}{2}*(\sigma_A + \sigma_B) = 1/2*(3.47+3.681) = 3.5755$

$$\frac{\varepsilon_{AB}}{K} = \frac{\sqrt{\varepsilon_A * \varepsilon_B}}{K} = \sqrt{119*91.5} = 104.348$$

$$\frac{TK}{\varepsilon_{AB}} = \frac{298.16}{104.348} = 2.8574$$

From table B-2 Bird and Lightfoot [67], and using linear interpolation, Ω_{AB} is determined

to be 0.96617

Substituting all the values in D_{AB}, above gives

$$D_{NO,N} = 0.0018583 \frac{\sqrt{298.16^3 \left(\frac{1}{30} + \frac{1}{28} \right)}}{1*3.5755^2 *(0.96617)} = 0.20 cm^2 / \sec$$

Liquid Phase Diffusion Coefficient

The liquid phase diffusion coefficient of NO and SO_2 in water is determined from the

Wilke-Chang equation given by [67] $D_{AB} = \frac{7.4x10^{-8} \left(\psi_B M_B \right)^{\frac{1}{2}} T}{\mu \tilde{V}_A^{0.6}}$

Where $\tilde{V}_A$ is the molar volume of the solute gas in cm^3/gmole as liquid at its normal

boiling point = 23.6 cm^3/ g-mole for NO and 44.8 cm^3/ g-mole for SO_2 (Chapentier J,R)

μ is the dynamic viscosity of the solution in centipoises = 0.89cp for water at room temperature.

ψ_B is an association parameter for the solvent B = 2.6 for water

T is the absolute temperature in K.

M_B = Molecular weight of solvent B = 18 g/mole

From the parameters above the diffusion coefficient of NO at room temperature is obtained as:

$$D_{NO,W} = \frac{7.4x10^{-8}(2.6x18.0)^{0.5}x(273.16+23)}{0.89x23.6^{0.6}} = 2.526x10^{-5}cm^2s^{-1}$$

The values of $D_{NO,W}$ at other temperatures are shown in the table below:

Table A-1. Table of Dynamic viscosity and Diffusivity at different temperatures

temp, °C	temp, K	μ, cp	D_A, cm^2/s
20	293.15	1.002	6.27574E-06
30	303.15	0.798	8.14887E-06
40	313.15	0.653	1.02868E-05
50	323.15	0.547	1.26724E-05
60	333.15	0.467	1.53026E-05
70	343.15	0.404	1.82199E-05

APPENDIX B

ESTIMATION OF SOLUBILITY COEFFICIENT OR HENRY'S CONSTANT AT DIFFERENT TEMPERATURES

According to Sander, R. , 1999 [68]

$$-\frac{dlnk_H^o}{d\left(\frac{1}{T}\right)} = \frac{\Delta H_{soln}}{R} = 1400$$

where $k_H^o = 1.9 \ X \ 10^{-3} mol(L.atm)^{-1}$ at 25°C and

k_H (or H_{NO}) = Henry's constant or solubility coefficient

Therefore, $k_H = k_H^o \exp\{1400(\frac{1}{298} - \frac{1}{T})\}$ is the expression for finding Henry's

constants at different temperatures.

At 40 °C, H_{NO} = 2.384858 x 10^{-3} mol/L. atm

At 50 °C, H_{NO} = 2.738710 x 10^{-3} mol/L. atm

At 60 °C, H_{NO} = 3.119052 x 10^{-3} mol/L. atm

APPENDIX C

SUMMARY OF DATA FOR DETERMINING REACTION ORDERS AND RATE CONSTANT

Data set for determining interfacial concentration, C_{Ai}

Table C-1. Estimation of interfacial concentration, C_{Ai} for 0.1 M Persulfate at 23 °C

NO(ppm)	mole fraction	P_A (atm)	R_A/k_Ga	P_{Ai}(atm)	$C_{Ai}=P_{Ai}/H$	$\log C_{Ai}$
502	0.0005017	0.001387835	0.000143891	0.00124394	2.4053E-09	-8.6188392
753	0.0007524	0.002081231	0.000284285	0.00179695	3.4745E-09	-8.4591051
1004	0.001003	0.002774279	0.000401494	0.00237278	4.5879E-09	-8.3383819

Table C-2. Estimation of interfacial concentration, C_{Ai} for 0.2 M Persulfate at 23 °C

NO(ppm)	mole fraction	P_A (atm)	R_A/k_Ga	P_{Ai}(atm)	$C_{Ai}=P_{Ai}/H$	$\log C_{Ai}$
502	0.0005017	0.001387835	0.000216719	0.00117112	2.2644E-09	-8.6450402
753	0.0007524	0.002081231	0.000370902	0.00171033	3.307E-09	-8.4805606
1004	0.001003	0.002774279	0.000544687	0.00222959	4.3111E-09	-8.3654147

Table C-3. Estimation of interfacial concentration, C_{Ai} for 0.05M Persulfate at 40 °C

NO(ppm)	mole fraction	P_A (atm)	R_A/k_Ga	P_{Ai}(atm)	$C_{Ai}=P_{Ai}/H$	$\log C_{Ai}$
502	0.000501748	0.001387835	0.000288289	0.001099547	2.62226E-09	-8.5813238
753	0.000752433	0.002081231	0.000707753	0.001373478	3.27555E-09	-8.4847159
1004	0.001002993	0.002774279	0.000995432	0.001778846	4.2423E-09	-8.3723991

Table C-4. Estimation of interfacial concentration, C_{Ai} for 0.1 M Persulfate at 40 °C

NO(ppm)	mole fraction	P_A (atm)	R_A/k_Ga	P_{Ai}(atm)	$C_{Ai}=P_{Ai}/H$	$logC_{Ai}$
502	0.000501748	0.001387835	0.000437383	0.000950452	2.26669E-09	-8.6446072
753	0.000752433	0.002081231	0.000792273	0.001288958	3.07398E-09	-8.5122987
1004	0.001002993	0.002774279	0.001113455	0.001660823	3.96083E-09	-8.402214

Table C-5. Estimation of interfacial concentration, C_{Ai} for 0.2 M Persulfate at 40 °C

NO(ppm)	mole fraction	P_A (atm)	R_A/k_Ga	P_{Ai}(atm)	$C_{Ai}=P_{Ai}/H$	$logC_{Ai}$
502	0.000501748	0.001387835	0.000591379	0.000796456	1.89943E-09	-8.7213758
753	0.000752433	0.002081231	0.000966588	0.001114643	2.65827E-09	-8.5754016
1004	0.001002993	0.002774279	0.001424919	0.001349359	3.21803E-09	-8.4924098

Table C-6. Estimation of interfacial concentration, C_{Ai} for 0.05M Persulfate at 50 °C

NO(ppm)	mole fraction	P_A (atm)	R_A/k_Ga	P_{Ai}(atm)	$C_{Ai}=P_{Ai}/H$	$logC_{Ai}$
502	0.0005017	0.001388	0.00044335	0.00094448	2.5867E-09	-8.58726103
753	0.0007524	0.002081	0.00067607	0.001405158	3.8483E-09	-8.41472868
1004	0.001003	0.002774	0.00095866	0.001815618	4.9725E-09	-8.30342941

Table C-7. Estimation of interfacial concentration, C_{Ai} for 0.1 M Persulfate at 50 °C

NO(ppm)	mole fraction	P_A (atm)	R_A/k_Ga	P_{Ai}(atm)	$C_{Ai}=P_{Ai}/H$	$logC_{Ai}$
502	0.0005017	0.001388	0.00065636	0.000731475	2.0033E-09	-8.69825446
753	0.0007524	0.002081	0.00107656	0.001004673	2.7515E-09	-8.56042914
1004	0.001003	0.002774	0.0014867	0.001287579	3.5263E-09	-8.45268004

Table C-8. Estimation of interfacial concentration, C_{Ai} for 0.2 M Persulfate at 50 °C

NO(ppm)	mole fraction	P_A (atm)	R_A/k_Ga	P_{Ai}(atm)	$C_{Ai}=P_{Ai}/H$	$logC_{Ai}$
502	0.0005017	0.001388	0.00077404	0.000613796	1.681E-09	-8.77442958
753	0.0007524	0.002081	0.00121766	0.000863568	2.3651E-09	-8.6261576
1004	0.001003	0.002774	0.00176046	0.001013814	2.7765E-09	-8.55649569

Table C-9. Estimation of interfacial concentration, C_{Ai} for 0.05M Persulfate at 60 °C

NO(ppm)	mole fraction	P_A (atm)	R_A/k_Ga	P_{Ai}(atm)	$C_{Ai}=P_{Ai}/H$	$logC_{Ai}$
502	0.000501748	0.001388	0.000402	0.0009859	3.0666E-09	-8.513347
753	0.000752433	0.002081	0.0007	0.0013815	4.297E-09	-8.366831
1004	0.001002993	0.002774	0.001021	0.0017536	5.4545E-09	-8.263245

Table C-10. Estimation of interfacial concentration, C_{Ai} for 0.1M Persulfate at 60 °C

NO(ppm)	mole fraction	P_A (atm)	R_A/k_Ga	P_{Ai}(atm)	$C_{Ai}=P_{Ai}/H$	$logC_{Ai}$
502	0.000501748	0.001388	0.000676	0.0007119	2.2205E-09	-8.653547
753	0.000752433	0.002081	0.001172	0.0009092	2.8358E-09	-8.547319
1004	0.001002993	0.002774	0.001674	0.0010998	3.4304E-09	-8.464658

Table C-11. Estimation of interfacial concentration, C_{Ai} for 0.2M Persulfate at 60 °C

NO(ppm)	mole fraction	P_A (atm)	R_A/k_Ga	P_{Ai}(atm)	$C_{Ai}=P_{Ai}/H$	$logC_{Ai}$
502	0.000501748	0.001388	0.000217	0.0011711	3.6528E-09	-8.437377
753	0.000752433	0.002081	0.000371	0.0017103	5.3346E-09	-8.272898
1004	0.001002993	0.002774	0.000545	0.0022296	6.9542E-09	-8.157752

Data set for determining reaction order, *m*

Table C-12. Data for determining reaction order *m* at 23 °C

N_A	$P_A k_G - N_A$	$N_A k_G$	N'_A		$logN'_A$
		$[S_2O_8^{2-}] = 0.05M$			
1.10553E-14	7.2388E-11	5.81696E-25	2.9342E-09		-8.532517667
1.66199E-14	1.0855E-10	8.74488E-25	2.9414E-09		-8.531441675
2.23667E-14	1.447E-10	1.17687E-24	2.9696E-09		-8.527296788
		$[S_2O_8^{2-}] = 0.1M$			
1.18615E-14	7.2387E-11	6.24118E-25	3.1482E-09		-8.501942042
1.81318E-14	1.0855E-10	9.5404E-25	3.2091E-09		-8.493623146
2.43618E-14	1.447E-10	1.28185E-24	3.2346E-09		-8.490183299
		$[S_2O_8^{2-}] = 0.2M$			
1.22815E-14	7.2387E-11	6.40688E-25	3.2318E-09		-8.490559505
1.86281E-14	1.0855E-10	9.71773E-25	3.2687E-09		-8.485622913
2.53399E-14	1.447E-10	1.32191E-24	3.3357E-09		-8.476814737

Table C-13. Data for determining reaction order m at 40 °C

N_A	$P_A k_G - N_A$	$N_A k_G$	N'_A	$\log N'_A$
		$[S_2O_8^{2-}] = 0.05M$		
8.50743E-15	7.23907E-11	4.47635E-25	2.59286E-09	-8.58622077
1.35865E-14	1.08558E-10	7.14881E-25	2.76127E-09	-8.558890512
1.82668E-14	1.44708E-10	9.61144E-25	2.78506E-09	-8.555165243
		$[S_2O_8^{2-}] = 0.1M$		
8.96502E-15	7.23902E-11	4.71713E-25	2.73234E-09	-8.563465055
1.3857E-14	1.08558E-10	7.29112E-25	2.81625E-09	-8.550328732
1.86446E-14	1.44707E-10	9.81023E-25	2.84267E-09	-8.546273166
		$[S_2O_8^{2-}] = 0.2M$		
9.41964E-15	7.23898E-11	4.95633E-25	2.87092E-09	-8.541979637
1.43655E-14	1.08557E-10	7.55871E-25	2.91962E-09	-8.534673431
1.95595E-14	1.44706E-10	1.02916E-24	2.98217E-09	-8.525466937

Table C-14. Data for determining reaction order *m* at 50 °C

NA	PAkG-NA	NAkG	N′A	logN′A
see below				

NA	PAkG-NA	NAkG	N′A	logN′A
$[S_2O_8^{2-}] = 0.05M$				
1.54817E-11	4.6317E-11	8.0768E-19	3.37208E-11	-10.472103
2.34823E-11	6.9192E-11	1.2251E-18	3.42373E-11	-10.4655
3.19443E-11	9.1591E-11	1.6665E-18	3.51851E-11	-10.453642
$[S_2O_8^{2-}] = 0.1M$				
1.55284E-11	4.627E-11	8.1012E-19	3.38567E-11	-10.470356
2.37959E-11	6.8878E-11	1.2414E-18	3.48526E-11	-10.457764
3.1887E-11	9.1648E-11	1.6635E-18	3.51000E-11	-10.454693
$[S_2O_8^{2-}] = 0.2M$				
1.60594E-11	4.5739E-11	8.3782E-19	3.54208E-11	-10.450742
2.44217E-11	6.8253E-11	1.2741E-18	3.60971E-11	-10.442528
3.29247E-11	9.061E-11	1.7177E-18	3.66574E-11	-10.435839

Table C-15. Data for determining reaction order *m* at 60 °C

N_A	$P_A k_G - N_A$	$N_A k_G$	N'_A	$\log N'_A$
		$[S_2O_8^{2-}] = 0.05M$		
1.31645E-14	7.2386E-11	6.86754E-25	3.04175E-09	-8.516875993
2.01755E-14	1.0855E-10	1.0525E-24	3.10858E-09	-8.507437302
2.72868E-14	1.447E-10	1.42347E-24	3.154E-09	-8.501138524
		$[S_2O_8^{2-}] = 0.1M$		
1.44116E-14	7.2385E-11	7.51809E-25	3.32995E-09	-8.477562189
2.23255E-14	1.0855E-10	1.16466E-24	3.43992E-09	-8.463451643
3.02648E-14	1.447E-10	1.57882E-24	3.49829E-09	-8.456144529
		$[S_2O_8^{2-}] = 0.2M$		
2.51129E-14	7.2374E-11	1.31006E-24	5.80346E-09	-8.236312982
3.79282E-14	1.0853E-10	1.97872E-24	5.84516E-09	-8.23320373
5.11242E-14	1.4467E-10	2.66715E-24	5.9106E-09	-8.228368167

Data set for determining reaction order, n and rate constant k_{mn}

Table C-16. Data for determining reaction order *n* and rate constant k_{mn} at 23 °C

$C_{Bo}(M)$	N'_A	$N'_A/(D)^{0.5}$	$Log((N'_A/(D)^{0.5})$	$logC_{Bo}$
		[NO]= 502ppm		
0.05	1.25694E-11	2.50091E-09	-8.601901478	-1.30103
0.1	1.36657E-11	2.71904E-09	-8.565584901	-1
0.2	1.41265E-11	2.81073E-09	-8.551181635	-0.69897
		[NO]= 753ppm		
0.05	1.26062E-11	2.50824E-09	-8.600631483	-1.30103
0.1	1.39829E-11	2.78215E-09	-8.555618847	-1
0.2	1.43214E-11	2.8495E-09	-8.545230621	-0.69897
		[NO]= 1004ppm		
0.05	1.27492E-11	2.53668E-09	-8.59573394	-1.30103
0.1	1.41166E-11	2.80875E-09	-8.551486767	-1
0.2	1.46771E-11	2.92027E-09	-8.534577496	-0.69897

Table C-17. Data for determining reaction order *n* and rate constant k_{mn} at 40 °C

$C_{Bo}(M)$	N'_A	$N'_A/(D)^{0.5}$	$Log((N'_A/(D)^{0.5})$	$logC_{Bo}$
		[NO]= 502ppm		
0.05	1.07936E-11	3.36532E-09	-8.472973927	-1.30103
0.1	1.14562E-11	3.57191E-09	-8.447099354	-1
0.2	1.2124E-11	3.78013E-09	-8.422493008	-0.69897
		[NO]= 753ppm		
0.05	1.15948E-11	3.61514E-09	-8.441875048	-1.30103
0.1	1.18594E-11	3.69764E-09	-8.43207593	-1
0.2	1.23611E-11	3.85403E-09	-8.414084499	-0.69897
		[NO]= 1004ppm		
0.05	1.17091E-11	3.65078E-09	-8.437614837	-1.30103
0.1	1.19871E-11	3.73745E-09	-8.427424434	-1
0.2	1.26672E-11	3.9495E-09	-8.403458216	-0.69897

Table C-18. Data for determining reaction order *n* and rate constant k_{mn} at 50 °C

$C_{Bo}(M)$	N'_A	$N'_A/(D)^{0.5}$	$Log((N'_A/(D)^{0.5})$	$logC_{Bo}$
		[NO]= 502ppm		
0.05	3.37208E-11	6.70935E-09	-8.17331932	-1.30103
0.1	3.80568E-11	7.57208E-09	-8.120784566	-1
0.2	3.94744E-11	7.85415E-09	-8.104900718	-0.69897
		[NO]= 753ppm		
0.05	3.42373E-11	6.81213E-09	-8.166716862	-1.30103
0.1	3.89599E-11	7.75178E-09	-8.11059847	-1
0.2	4.00862E-11	7.97587E-09	-8.098222082	-0.69897
		[NO]= 1004ppm		
0.05	3.51851E-11	7.0007E-09	-8.154858266	-1.30103
0.1	3.9184E-11	7.79637E-09	-8.108107795	-1
0.2	4.05924E-11	8.0766E-09	-8.09277154	-0.69897

Table C-19. Data for determining reaction order *n* and rate constant k_{mn} at 60 °C

$C_{Bo}(M)$	N'_A	$N'_A/(D)^{0.5}$	$Log((N'_A/(D)^{0.5})$	$logC_{Bo}$
		[NO]= 502ppm		
0.05	1.36569E-11	3.49116E-09	-8.457030597	-1.30103
0.1	1.52721E-11	3.90406E-09	-8.40848356	-1
0.2	3.35633E-11	8.5799E-09	-8.066517578	-0.69897
		[NO]= 753ppm		
0.05	1.40254E-11	3.58535E-09	-8.445468191	-1.30103
0.1	1.59069E-11	4.06633E-09	-8.39079743	-1
0.2	3.29924E-11	8.43395E-09	-8.0739691	-0.69897
		[NO]= 1004ppm		
0.05	1.42778E-11	3.64989E-09	-8.437720336	-1.30103
0.1	1.62481E-11	4.15355E-09	-8.381580519	-1
0.2	3.35633E-11	8.5799E-09	-8.066517578	-0.69897

APPENDIX D

MATLAB CODE FOR MODELING WORK

The Matlab code used to fit the mathematical model in section 4.3.1 to the experimental data on NO concentration in the gas phase vs. time for different temperatures and persulfate concentrations is presented below. Each temperature has a separate m-file, and the excel files containing the experimental data were also different for different temperatures.

The code for 30$^{\text{o}}$C is presented below.

persulfatenanasakyi_30.m

```matlab
function persulfatenanasakyi_30()

    clc

        conc1=xlsread('\30deg.xls','e1','C:C')*1e-6;

        time30deg=xlsread('\30deg.xls','e1','D:D');



        conc2=xlsread('\30deg.xls','e1','F:F')*1e-6;

        time50deg=xlsread('\30deg.xls','e1','D:D');
```

```matlab
    conc3=xlsread('\30deg.xls','e1','G:G')*1e-6;

    time60deg=xlsread('\30deg.xls','e1','D:D');

%    conc4=xlsread('\40deg.xls','e1','F:F')*1e-6;

%    time40deg=xlsread('\40deg.xls','e1','D:D');

%

    figure(1)

     plot(time30deg, conc3,'-.r');

     hold on

%

figure(1)

   hold on

  %plot(time40deg, conc4,'-.r');


   figure(1)

    hold on

   plot(time30deg, conc2,'-.r');


   figure(1)

    hold on
```

```matlab
plot(time30deg, conc1,'-.r');


%Constants

  R = 8.314;       %universal gas constant, J/mol.K

  H = 5.223e4*1;    %henry's law constant, Pa/(mol/m^3)



 %Parameters

 q = 1.667e-6*1;   %gas flow rate, m^3/s

 V_gas = 1.96e-5*1; %gas holdup, m^3, based on 1 cm height increase

 V_liq = 1e-3;    %liquid volume, m^3



 P = 101325;      %pressure, Pa

 y_NO_in = 1010e-6; %mol fraction of NO, converted from mol fraction
of 0.105%



 V_1 = 1e-4*1;    %head space

 V_2 = 1e-4*0;



 T=303;  % = 30 degrees 1st copy
```

117

```matlab
    kLa = 1.57e-2*1.8;   %mass transfer coefficient, s^-1 1.6, .48

    k_1 = 1e-7*0.05;

    k_2 = 1e-4*1.90;

    k_3 = 2e-2*1.0;



    function dydt=odefun3(t, y)

        dydt = zeros(3,1);



        dydt(1)  =  kLa*P/H*y(2)  -  kLa*y(1)  -  y(4)*(2*k_1+k_2*y(1));
%C_NO_liq



        dydt(2)   =   q/V_gas*y_NO_in   -   y(2)*(q/V_gas)           -
(y(2)+y_NO_in)*0.5*(kLa*V_liq*R*T/(H*V_gas)) ...

            + kLa*V_liq*R*T/(P*V_gas)*y(1)*1; %y_NO_gas



        dydt(3) = q/V_1*(y(2) - y(3));



        dydt(4) = -(k_1+k_2*y(1)+k_3*y(5))*y(4);
```

```matlab
        dydt(5)     =     -k_3*y(5)*y(4);%+k_3*y(4)*y(5);%+k_3*y(4)*y(5);
%product of reaction 3



        dydt(6) = -2*k_1*y(4);




    end



    tspan = [0 3400];



M = [1 0 0 0 0 0% 0

     0 1 0 0 0 0 %0

     0 0 1 0 0 0 %0

     0 0 0 1 0 0 %0

     0 0 0 0 1 0% 0% 0

     0 0 0 0 0 1]; %0 %0

     %0 0 0 0 0 0 1];% 0 0

     %0 0 0 0 0 0 0 1];
```

```matlab
options = odeset('Mass', M, 'Refine', 4);




y_S2O8_ini = 0.05*1e3;   %concentration of persulfate, mol/m^3

y_fe_ini = 0.01e3;       %concentration of Iron(II), mol/m^3

y0 = [0 y_NO_in y_NO_in y_S2O8_ini y_fe_ini 0];% 0 0];




[t, y]=ode23s(@odefun3, tspan, y0, options);

figure(1);

t = t + 580;

plot(t,y(:,2));

hold on




%    T=303;  % = 30 degrees  2nd copy

%    kLa = 1.57e-2*1.8;  %mass transfer coefficient, s^-1 1.6, .48

%    k_1 = 1e-7*0.78;

%    k_2 = 1e-4*0.004;

%    k_3 = 3e-2*1.0;
```

```matlab
function dydt=odefun4(t, y)

    dydt = zeros(3,1);


    dydt(1)  =  kLa*P/H*y(2)  -  kLa*y(1)  -  y(4)*(2*k_1+k_2*y(1));
%C_NO_liq


    dydt(2)   =   q/V_gas*y_NO_in   -   y(2)*(q/V_gas)        -
(y(2)+y_NO_in)*0.5*(kLa*V_liq*R*T/(H*V_gas)) ...

        + kLa*V_liq*R*T/(P*V_gas)*y(1)*1; %y_NO_gas


    dydt(3) = q/V_1*(y(2) - y(3));


    dydt(4) = -(k_1+k_2*y(1)+k_3*y(5))*y(4);


    dydt(5)    =    -k_3*y(5)*y(4);%+k_3*y(4)*y(5);%+k_3*y(4)*y(5);
%product of reaction 3


    dydt(6) = -2*k_1*y(4);
```

```matlab
    end



    tspan = [0 3400];



M = [1 0 0 0 0 0% 0

     0 1 0 0 0 0 %0

     0 0 1 0 0 0 %0

     0 0 0 1 0 0 %0

     0 0 0 0 1 0% 0% 0

     0 0 0 0 0 1]; %0 %0

     %0 0 0 0 0 0 1];% 0 0

     %0 0 0 0 0 0 0 1];



    options = odeset('Mass', M, 'Refine', 4);
```

```matlab
    y_S2O8_ini = 0.1*1e3;  %concentration of persulfate, mol/m^3

    y_fe_ini = 0.01e3;      %concentration of Iron(II), mol/m^3

    y0 = [0 y_NO_in y_NO_in y_S2O8_ini y_fe_ini 0];% 0 0];



    [t, y]=ode23s(@odefun4, tspan, y0, options);

    figure(1);

    t = t + 580;

    plot(t,y(:,2));

    hold on




%    T=303;  % = 30 degrees   3rd copy

%    kLa = 1.57e-2*1.8;  %mass transfer coefficient, s^-1 1.6, .48

%    k_1 = 1e-7*0.78;

%    k_2 = 1e-4*0.004;

%    k_3 = 3e-2*1.0;



    function dydt=odefun5(t, y)
```

```matlab
dydt = zeros(3,1);



dydt(1)  =  kLa*P/H*y(2)  -  kLa*y(1)  -  y(4)*(2*k_1+k_2*y(1));
%C_NO_liq



dydt(2)   =   q/V_gas*y_NO_in   -   y(2)*(q/V_gas)        -
(y(2)+y_NO_in)*0.5*(kLa*V_liq*R*T/(H*V_gas)) ...

    + kLa*V_liq*R*T/(P*V_gas)*y(1)*1; %y_NO_gas



dydt(3) = q/V_1*(y(2) - y(3));



dydt(4) = -(k_1+k_2*y(1)+k_3*y(5))*y(4);



dydt(5)    =    -k_3*y(5)*y(4);%+k_3*y(4)*y(5);%+k_3*y(4)*y(5);
%product of reaction 3



dydt(6) = -2*k_1*y(4);
```

```matlab
    end


    tspan = [0 3400];


M = [1 0 0 0 0 0% 0

     0 1 0 0 0 0 %0

     0 0 1 0 0 0 %0

     0 0 0 1 0 0 %0

     0 0 0 0 1 0% 0% 0

     0 0 0 0 0 1]; %0 %0

     %0 0 0 0 0 0 1];% 0 0

     %0 0 0 0 0 0 0 1];



    options = odeset('Mass', M, 'Refine', 4);



    y_S2O8_ini = 0.2*1e3;   %concentration of persulfate, mol/m^3
```

```matlab
    y_fe_ini = 0.01e3;      %concentration of Iron(II), mol/m^3

    y0 = [0 y_NO_in y_NO_in y_S2O8_ini y_fe_ini 0];% 0 0];



    [t, y]=ode23s(@odefun5, tspan, y0, options);

    figure(1);

    t = t + 580;

    plot(t,y(:,2));

    hold on



    xlabel('Time(s)')

    ylabel('NO Concentration (ppm)')

  % Legend('at 30degC', 'at 40degC','at 50degC','at 60degC')

end
```

The code for 40°C is presented below.

persulfatenanasakyi_40.m

```matlab
function persulfatenanasakyi_40()

    clc



      conc1=xlsread('\40deg.xls','e1','C:C')*1e-6;

      time30deg=xlsread('\40deg.xls','e1','D:D');



      conc2=xlsread('\40deg.xls','e1','F:F')*1e-6;

      time50deg=xlsread('\40deg.xls','e1','D:D');



    conc3=xlsread('\40deg.xls','e1','G:G')*1e-6;

    time60deg=xlsread('\40deg.xls','e1','D:D');



    conc4=xlsread('\40deg.xls','e1','F:F')*1e-6;

    time40deg=xlsread('\40deg.xls','e1','D:D');
```

```matlab
  figure(1)

   plot(time30deg, conc3,'-.r');

    hold on

%


figure(1)

   hold on

  %plot(time40deg, conc4,'-.r');




   figure(1)

   hold on

  plot(time30deg, conc2,'-.r');



   figure(1)

   hold on

  plot(time30deg, conc1,'-.r');



  %Constants
```

```matlab
R = 8.314;        %universal gas constant, J/mol.K

H = 5.223e4*1;     %henry's law constant, Pa/(mol/m^3)



%Parameters

q = 1.667e-6*1;    %gas flow rate, m^3/s

V_gas = 1.96e-5*1; %gas holdup, m^3, based on 1 cm height increase

V_liq = 1e-3;      %liquid volume, m^3



P = 101325;        %pressure, Pa

y_NO_in = 1010e-6; %mol fraction of NO, converted from mol fraction
of 0.105%



V_1 = 1e-4*1;      %head space

V_2 = 1e-4*0;



T=313;   % = 40 degrees    first copy

kLa = 1.57e-2*1.8;  %mass transfer coefficient, s^-1 1.6, .48

k_1 = 1e-6*0.050;

k_2 = 1e-4*2.5;
```

```matlab
    k_3 = 2e-2*1.4;



    function dydt=odefun3(t, y)

        dydt = zeros(3,1);



        dydt(1)  =  kLa*P/H*y(2)  -  kLa*y(1)  -  y(4)*(2*k_1+k_2*y(1));
%C_NO_liq



        dydt(2)    =    q/V_gas*y_NO_in    -    y(2)*(q/V_gas)          -
(y(2)+y_NO_in)*0.5*(kLa*V_liq*R*T/(H*V_gas)) ...

            + kLa*V_liq*R*T/(P*V_gas)*y(1)*1; %y_NO_gas



        dydt(3) = q/V_1*(y(2) - y(3));



        dydt(4) = -(k_1+k_2*y(1)+k_3*y(5))*y(4);



        dydt(5)    =     -k_3*y(5)*y(4);%+k_3*y(4)*y(5);%+k_3*y(4)*y(5);
%product of reaction 3
```

```matlab
        dydt(6) = -2*k_1*y(4);



    end



    tspan = [0 3400];



M = [1 0 0 0 0 0% 0

     0 1 0 0 0 0 %0

     0 0 1 0 0 0 %0

     0 0 0 1 0 0 %0

     0 0 0 0 1 0% 0% 0

     0 0 0 0 0 1]; %0 %0

     %0 0 0 0 0 0 1];% 0 0

     %0 0 0 0 0 0 0 1];



    options = odeset('Mass', M, 'Refine', 4);
```

```matlab
    y_S2O8_ini = 0.05*1e3;   %concentration of persulfate, mol/m^3

    y_fe_ini = 0.01e3;       %concentration of Iron(II), mol/m^3

    y0 = [0 y_NO_in y_NO_in y_S2O8_ini y_fe_ini 0];% 0 0];



    [t, y]=ode23s(@odefun3, tspan, y0, options);

    figure(1);

    t = t + 580;

    plot(t,y(:,2));

    hold on



%     T=313;  % = 40 degrees    first copy

%     kLa = 1.57e-2*1.8;  %mass transfer coefficient, s^-1 1.6, .48

%     k_1 = 1e-7*0.90;

%     k_2 = 1e-4*0.175;

%     k_3 = 3e-2*1.6;



    function dydt=odefun4(t, y)

        dydt = zeros(3,1);
```

```matlab
        dydt(1)  =  kLa*P/H*y(2)  -  kLa*y(1)  -  y(4)*(2*k_1+k_2*y(1));
%C_NO_liq



        dydt(2)   =   q/V_gas*y_NO_in   -   y(2)*(q/V_gas)       -
(y(2)+y_NO_in)*0.5*(kLa*V_liq*R*T/(H*V_gas)) ...

        + kLa*V_liq*R*T/(P*V_gas)*y(1)*1; %y_NO_gas



        dydt(3) = q/V_1*(y(2) - y(3));



        dydt(4) = -(k_1+k_2*y(1)+k_3*y(5))*y(4);



        dydt(5)     =     -k_3*y(5)*y(4);%+k_3*y(4)*y(5);%+k_3*y(4)*y(5);
%product of reaction 3



        dydt(6) = -2*k_1*y(4);




    end
```

```matlab
tspan = [0 3400];


M = [1 0 0 0 0 0% 0

     0 1 0 0 0 0 %0

     0 0 1 0 0 0 %0

     0 0 0 1 0 0 %0

     0 0 0 0 1 0% 0% 0

     0 0 0 0 0 1]; %0 %0

     %0 0 0 0 0 0 1];% 0 0

     %0 0 0 0 0 0 0 1];


options = odeset('Mass', M, 'Refine', 4);


y_S2O8_ini = 0.1*1e3;  %concentration of persulfate, mol/m^3

y_fe_ini = 0.01e3;     %concentration of Iron(II), mol/m^3
```

```matlab
y0 = [0 y_NO_in y_NO_in y_S2O8_ini y_fe_ini 0];% 0 0];



[t, y]=ode23s(@odefun4, tspan, y0, options);

figure(1);

t = t + 580;

plot(t,y(:,2));

hold on



%    T=313;  % = 40 degrees    first copy

%    kLa = 1.57e-2*1.8;  %mass transfer coefficient, s^-1 1.6, .48

%    k_1 = 1e-7*0.90;

%    k_2 = 1e-4*0.175;

%    k_3 = 3e-2*1.6;



function dydt=odefun5(t, y)

    dydt = zeros(3,1);
```

```matlab
        dydt(1)  =  kLa*P/H*y(2)  -  kLa*y(1)  -  y(4)*(2*k_1+k_2*y(1));
%C_NO_liq



        dydt(2)    =    q/V_gas*y_NO_in    -    y(2)*(q/V_gas)        -
(y(2)+y_NO_in)*0.5*(kLa*V_liq*R*T/(H*V_gas)) ...

            + kLa*V_liq*R*T/(P*V_gas)*y(1)*1; %y_NO_gas



        dydt(3) = q/V_1*(y(2) - y(3));



        dydt(4) = -(k_1+k_2*y(1)+k_3*y(5))*y(4);



        dydt(5)    =    -k_3*y(5)*y(4);%+k_3*y(4)*y(5);%+k_3*y(4)*y(5);
%product of reaction 3



        dydt(6) = -2*k_1*y(4);



    end



    tspan = [0 3400];
```

```matlab
M = [1 0 0 0 0 0% 0

     0 1 0 0 0 0 %0

     0 0 1 0 0 0 %0

     0 0 0 1 0 0 %0

     0 0 0 0 1 0% 0% 0

     0 0 0 0 0 1]; %0 %0

     %0 0 0 0 0 0 1];% 0 0

     %0 0 0 0 0 0 0 1];




options = odeset('Mass', M, 'Refine', 4);




y_S2O8_ini = 0.2*1e3;  %concentration of persulfate, mol/m^3

y_fe_ini = 0.01e3;      %concentration of Iron(II), mol/m^3

y0 = [0 y_NO_in y_NO_in y_S2O8_ini y_fe_ini 0];% 0 0];
```

```matlab
    [t, y]=ode23s(@odefun5, tspan, y0, options);

    figure(1);

    t = t + 580;

    plot(t,y(:,2));

    hold on



    xlabel('Time(s)')

    ylabel('NO Concentration (ppm)')

  % Legend('at 30degC', 'at 40degC','at 50degC','at 60degC')

end
```

The code for 50°C is shown below.

persulfatenanasakyi_50.m

```matlab
function persulfatenanasakyi_50()

    clc



      conc1=xlsread('\50deg.xls','e1','C:C')*1e-6;

      time30deg=xlsread('\50deg.xls','e1','D:D');



      conc2=xlsread('\50deg.xls','e1','F:F')*1e-6;

      time50deg=xlsread('\50deg.xls','e1','D:D');



    conc3=xlsread('\50deg.xls','e1','G:G')*1e-6;

    time60deg=xlsread('\50deg.xls','e1','D:D');



    conc4=xlsread('\40deg.xls','e1','F:F')*1e-6;

    time40deg=xlsread('\40deg.xls','e1','D:D');



    figure(1)
```

```matlab
    plot(time30deg, conc3,'-.r');

    hold on

%



figure(1)

  hold on

 %plot(time40deg, conc4,'-.r');




  figure(1)

  hold on

 plot(time30deg, conc2,'-.r');



  figure(1)

  hold on

 plot(time30deg, conc1,'-.r');



 %Constants

  R = 8.314;       %universal gas constant, J/mol.K
```

```matlab
    H = 5.223e4*1;     %henry's law constant, Pa/(mol/m^3)


%Parameters

 q = 1.667e-6*1;    %gas flow rate, m^3/s

 V_gas = 1.96e-5*1; %gas holdup, m^3, based on 1 cm height increase

 V_liq = 1e-3;     %liquid volume, m^3



  P = 101325;      %pressure, Pa

 y_NO_in = 1010e-6; %mol fraction of NO, converted from mol fraction
of 0.105%



  V_1 = 1e-4*1;     %head space

  V_2 = 1e-4*0;



  T=323;  % = 50 degrees    4th copy

  kLa = 1.57e-2*1.8;   %mass transfer coefficient, s^-1 1.6, .48

  k_1 = 1e-6*0.11;

  k_2 = 1e-4*2.75;

  k_3 = 2e-2*1.65;
```

```matlab
function dydt=odefun3(t, y)

    dydt = zeros(3,1);


    dydt(1)  =  kLa*P/H*y(2)  -  kLa*y(1)  -  y(4)*(2*k_1+k_2*y(1));
%C_NO_liq


    dydt(2)   =   q/V_gas*y_NO_in   -   y(2)*(q/V_gas)        -
(y(2)+y_NO_in)*0.5*(kLa*V_liq*R*T/(H*V_gas)) ...

        + kLa*V_liq*R*T/(P*V_gas)*y(1)*1; %y_NO_gas


    dydt(3) = q/V_1*(y(2) - y(3));


    dydt(4) = -(k_1+k_2*y(1)+k_3*y(5))*y(4);


    dydt(5)   =   -k_3*y(5)*y(4);%+k_3*y(4)*y(5);%+k_3*y(4)*y(5);
%product of reaction 3


    dydt(6) = -2*k_1*y(4);
```

142

```matlab
    end


    tspan = [0 3400];


M = [1 0 0 0 0 0% 0

     0 1 0 0 0 0 %0

     0 0 1 0 0 0 %0

     0 0 0 1 0 0 %0

     0 0 0 0 1 0% 0% 0

     0 0 0 0 0 1]; %0 %0

     %0 0 0 0 0 0 1];% 0 0

     %0 0 0 0 0 0 0 1];



    options = odeset('Mass', M, 'Refine', 4);
```

```matlab
    y_S2O8_ini = 0.05*1e3;   %concentration of persulfate, mol/m^3

    y_fe_ini = 0.01e3;       %concentration of Iron(II), mol/m^3

    y0 = [0 y_NO_in y_NO_in y_S2O8_ini y_fe_ini 0];% 0 0];



    [t, y]=ode23s(@odefun3, tspan, y0, options);

    figure(1);

    t = t + 580;

    plot(t,y(:,2));

    hold on



%     T=323;   % = 50 degrees    4th copy

%     kLa = 1.57e-2*1.8;   %mass transfer coefficient, s^-1 1.6, .48

%     k_1 = 1e-7*1.20;

%     k_2 = 1e-4*1.5;

%     k_3 = 3.0e-2*1.85;



    function dydt=odefun4(t, y)

        dydt = zeros(3,1);
```

144

```matlab
        dydt(1)  =  kLa*P/H*y(2)  -  kLa*y(1)  -  y(4)*(2*k_1+k_2*y(1));
%C_NO_liq



        dydt(2)   =   q/V_gas*y_NO_in   -   y(2)*(q/V_gas)        -
(y(2)+y_NO_in)*0.5*(kLa*V_liq*R*T/(H*V_gas)) ...

        + kLa*V_liq*R*T/(P*V_gas)*y(1)*1; %y_NO_gas



        dydt(3) = q/V_1*(y(2) - y(3));



        dydt(4) = -(k_1+k_2*y(1)+k_3*y(5))*y(4);



        dydt(5)    =     -k_3*y(5)*y(4);%+k_3*y(4)*y(5);%+k_3*y(4)*y(5);
%product of reaction 3



        dydt(6) = -2*k_1*y(4);




    end
```

```matlab
tspan = [0 3400];


M = [1 0 0 0 0 0% 0

     0 1 0 0 0 0 %0

     0 0 1 0 0 0 %0

     0 0 0 1 0 0 %0

     0 0 0 0 1 0% 0% 0

     0 0 0 0 0 1]; %0 %0

     %0 0 0 0 0 0 1];% 0 0

     %0 0 0 0 0 0 0 1];


options = odeset('Mass', M, 'Refine', 4);


y_S2O8_ini = 0.1*1e3;  %concentration of persulfate, mol/m^3

y_fe_ini = 0.01e3;      %concentration of Iron(II), mol/m^3
```

```matlab
    y0 = [0 y_NO_in y_NO_in y_S2O8_ini y_fe_ini 0];% 0 0];



    [t, y]=ode23s(@odefun4, tspan, y0, options);

    figure(1);

    t = t + 580;

    plot(t,y(:,2));

    hold on




%    T=323;   % = 50 degrees    4th copy

%    kLa = 1.57e-2*1.8;   %mass transfer coefficient, s^-1 1.6, .48

%    k_1 = 1e-7*1.20;

%    k_2 = 1e-4*1.5;

%    k_3 = 3.0e-2*1.85;



    function dydt=odefun5(t, y)

        dydt = zeros(3,1);
```

147

```matlab
        dydt(1)  =  kLa*P/H*y(2)  -  kLa*y(1)  -  y(4)*(2*k_1+k_2*y(1));
%C_NO_liq



        dydt(2)    =    q/V_gas*y_NO_in    -    y(2)*(q/V_gas)         -
(y(2)+y_NO_in)*0.5*(kLa*V_liq*R*T/(H*V_gas)) ...

            + kLa*V_liq*R*T/(P*V_gas)*y(1)*1; %y_NO_gas



        dydt(3) = q/V_1*(y(2) - y(3));



        dydt(4) = -(k_1+k_2*y(1)+k_3*y(5))*y(4);



        dydt(5)    =    -k_3*y(5)*y(4);%+k_3*y(4)*y(5);%+k_3*y(4)*y(5);
%product of reaction 3



        dydt(6) = -2*k_1*y(4);




    end
```

```matlab
tspan = [0 3400];



M = [1 0 0 0 0 0% 0

     0 1 0 0 0 0 %0

     0 0 1 0 0 0 %0

     0 0 0 1 0 0 %0

     0 0 0 0 1 0% 0% 0

     0 0 0 0 0 1]; %0 %0

     %0 0 0 0 0 0 1];% 0 0

     %0 0 0 0 0 0 0 1];



options = odeset('Mass', M, 'Refine', 4);




y_S2O8_ini = 0.2*1e3;  %concentration of persulfate, mol/m^3

y_fe_ini = 0.01e3;      %concentration of Iron(II), mol/m^3

y0 = [0 y_NO_in y_NO_in y_S2O8_ini y_fe_ini 0];% 0 0];
```

```matlab
    [t, y]=ode23s(@odefun5, tspan, y0, options);

    figure(1);

    t = t + 580;

    plot(t,y(:,2));

    hold on



    xlabel('Time(s)')

    ylabel('NO Concentration (ppm)')

  % Legend('at 30degC', 'at 40degC','at 50degC','at 60degC')

end
```

The code for 60°C is shown below.

persulfatenanasakyi_60.m

```matlab
function persulfatenanasakyi_60()

    clc


        conc1=xlsread('\60deg.xls','e1','C:C')*1e-6;

        time30deg=xlsread('\60deg.xls','e1','D:D');


        conc2=xlsread('\60deg.xls','e1','F:F')*1e-6;

        time50deg=xlsread('\60deg.xls','e1','D:D');


        conc3=xlsread('\60deg.xls','e1','G:G')*1e-6;

        time60deg=xlsread('\60deg.xls','e1','D:D');


        conc4=xlsread('\40deg.xls','e1','F:F')*1e-6;

        time40deg=xlsread('\40deg.xls','e1','D:D');
```

```matlab
    figure(1)

     plot(time30deg, conc3,'-.r');

      hold on

%

figure(1)

   hold on

  %plot(time40deg, conc4,'-.r');




   figure(1)

    hold on

  plot(time30deg, conc2,'-.r');



   figure(1)

    hold on

  plot(time30deg, conc1,'-.r');



  %Constants
```

```matlab
R = 8.314;        %universal gas constant, J/mol.K

H = 5.223e4*1;    %henry's law constant, Pa/(mol/m^3)



%Parameters

q = 1.667e-6*1;   %gas flow rate, m^3/s

V_gas = 1.96e-5*1; %gas holdup, m^3, based on 1 cm height increase

V_liq = 1e-3;     %liquid volume, m^3



P = 101325;       %pressure, Pa

y_NO_in = 1010e-6; %mol fraction of NO, converted from mol fraction
of 0.105%



V_1 = 1e-4*1;     %head space

V_2 = 1e-4*0;



T=333;   % = 60 degrees

kLa = 1.57e-2*1.8;  %mass transfer coefficient, s^-1 1.6, .48

k_1 = 1e-6*.25;

k_2 = 1e-4*6.0;
```

```matlab
    k_3 = 2e-2*2.20;



    function dydt=odefun3(t, y)

        dydt = zeros(3,1);



        dydt(1)  =  kLa*P/H*y(2)  -  kLa*y(1)  -  y(4)*(2*k_1+k_2*y(1));
%C_NO_liq



        dydt(2)    =    q/V_gas*y_NO_in    -    y(2)*(q/V_gas)        -
(y(2)+y_NO_in)*0.5*(kLa*V_liq*R*T/(H*V_gas)) ...

            + kLa*V_liq*R*T/(P*V_gas)*y(1)*1; %y_NO_gas



        dydt(3) = q/V_1*(y(2) - y(3));



        dydt(4) = -(k_1+k_2*y(1)+k_3*y(5))*y(4);



        dydt(5)    =    -k_3*y(5)*y(4);%+k_3*y(4)*y(5);%+k_3*y(4)*y(5);
%product of reaction 3
```

```matlab
    dydt(6) = -2*k_1*y(4);



end



tspan = [0 3400];



M = [1 0 0 0 0 0% 0

     0 1 0 0 0 0 %0

     0 0 1 0 0 0 %0

     0 0 0 1 0 0 %0

     0 0 0 0 1 0% 0% 0

     0 0 0 0 0 1]; %0 %0

     %0 0 0 0 0 0 1];% 0 0

     %0 0 0 0 0 0 0 1];



options = odeset('Mass', M, 'Refine', 4);
```

```matlab
    y_S2O8_ini = 0.05*1e3;   %concentration of persulfate, mol/m^3

    y_fe_ini = 0.01e3;       %concentration of Iron(II), mol/m^3

    y0 = [0 y_NO_in y_NO_in y_S2O8_ini y_fe_ini 0];% 0 0];



    [t, y]=ode23s(@odefun3, tspan, y0, options);

    figure(1);

    t = t + 580;

    plot(t,y(:,2));

    hold on



%     T=333;  % = 60 degrees

%     kLa = 1.57e-2*1.8;  %mass transfer coefficient, s^-1 1.6, .48

%     k_1 = 1e-6*.35;

%     k_2 = 1e-4*9.5;

%     k_3 = 3e-2*2.0;



    function dydt=odefun4(t, y)
```
156

```
dydt = zeros(3,1);




dydt(1)  =  kLa*P/H*y(2)  -  kLa*y(1)  -  y(4)*(2*k_1+k_2*y(1));
%C_NO_liq




dydt(2)    =    q/V_gas*y_NO_in    -    y(2)*(q/V_gas)         -
(y(2)+y_NO_in)*0.5*(kLa*V_liq*R*T/(H*V_gas)) ...

     + kLa*V_liq*R*T/(P*V_gas)*y(1)*1; %y_NO_gas




dydt(3) = q/V_1*(y(2) - y(3));




dydt(4) = -(k_1+k_2*y(1)+k_3*y(5))*y(4);




dydt(5)    =    -k_3*y(5)*y(4);%+k_3*y(4)*y(5);%+k_3*y(4)*y(5);
%product of reaction 3




dydt(6) = -2*k_1*y(4);
```

```matlab
end


tspan = [0 3400];


M = [1 0 0 0 0 0% 0

    0 1 0 0 0 0 %0

    0 0 1 0 0 0 %0

    0 0 0 1 0 0 %0

    0 0 0 0 1 0% 0% 0

    0 0 0 0 0 1]; %0 %0

    %0 0 0 0 0 0 1];% 0 0

    %0 0 0 0 0 0 0 1];



options = odeset('Mass', M, 'Refine', 4);



y_S2O8_ini = 0.1*1e3;  %concentration of persulfate, mol/m^3
```

```matlab
    y_fe_ini = 0.01e3;        %concentration of Iron(II), mol/m^3

    y0 = [0 y_NO_in y_NO_in y_S2O8_ini y_fe_ini 0];% 0 0];


    [t, y]=ode23s(@odefun4, tspan, y0, options);

    figure(1);

    t = t + 580;

    plot(t,y(:,2));

    hold on



%    T=333;  % = 60 degrees

%    kLa = 1.57e-2*1.8;  %mass transfer coefficient, s^-1 1.6, .48

%    k_1 = 1e-6*.35;

%    k_2 = 1e-4*9.5;

%    k_3 = 3e-2*2.0;


    function dydt=odefun5(t, y)

        dydt = zeros(3,1);
```

```
        dydt(1)  =  kLa*P/H*y(2)  -  kLa*y(1)  -  y(4)*(2*k_1+k_2*y(1));
%C_NO_liq



        dydt(2)    =    q/V_gas*y_NO_in    -    y(2)*(q/V_gas)         -
(y(2)+y_NO_in)*0.5*(kLa*V_liq*R*T/(H*V_gas)) ...

            + kLa*V_liq*R*T/(P*V_gas)*y(1)*1; %y_NO_gas



        dydt(3) = q/V_1*(y(2) - y(3));



        dydt(4) = -(k_1+k_2*y(1)+k_3*y(5))*y(4);



        dydt(5)     =     -k_3*y(5)*y(4);%+k_3*y(4)*y(5);%+k_3*y(4)*y(5);
%product of reaction 3



        dydt(6) = -2*k_1*y(4);




    end
```

```matlab
tspan = [0 3400];


M = [1 0 0 0 0 0% 0

     0 1 0 0 0 0 %0

     0 0 1 0 0 0 %0

     0 0 0 1 0 0 %0

     0 0 0 0 1 0% 0% 0

     0 0 0 0 0 1]; %0 %0

     %0 0 0 0 0 0 1];% 0 0

     %0 0 0 0 0 0 0 1];


options = odeset('Mass', M, 'Refine', 4);

y_S2O8_ini = 0.2*1e3;   %concentration of persulfate, mol/m^3

y_fe_ini = 0.01e3;      %concentration of Iron(II), mol/m^3

y0 = [0 y_NO_in y_NO_in y_S2O8_ini y_fe_ini 0];% 0 0];


[t, y]=ode23s(@odefun5, tspan, y0, options);

figure(1);

t = t + 580;
```

```matlab
    plot(t,y(:,2));

    hold on

    xlabel('Time(s)')

    ylabel('NO Concentration (ppm)')

   % Legend('at 30degC', 'at 40degC','at 50degC','at 60degC')

end
```

APPENDIX E

SUMMARY OF EXPERIMENTAL DATA

Table E-1. Summary of Experimental Runs (#1-8)

Conditions/Run Num.	1	2	3	4	5	6	7	8
Temp., °C	50	50	50	50	50	50	50	50
Inlet NO Conc., ppm	1004	1004	1004	1004	1004	1004	1004	1004
Inlet SO_2 Conc., ppm	None	None	None	None	None	None	None	None
Conc. Of Persulfate, M	0.1	0.1	0.1	0.1	0.1	0.1	0.1	0.1
Conc. Of Iron(II), M	0.004	0.008	0.01	0.02	0.04	0.06	0.08	0.1
Initial pH	2.54	2.58	2.37	2.61	2.62	2.56	2.54	2.49
Final pH	2.53	2.55	2.19	2.58	2.52	2.45	2.46	2.43
Fractional NO conver.,%	49.70	61.38	63.37	63.47	59.38	51.20	45.31	43.81
Fractional SO_2 conver., %	N/A	N/A	N/A	N/A	N/A	N/A	N/A	N/A

Table E-2. Summary of Experimental Runs (#9-16)

Conditions/Run Num.	9	10	11	12	13	14	15	16
Temp., °C	50	50	50	50	50	50	50	50
Inlet NO Conc., ppm	1004	1004	1004	1004	1004	1004	1004	1004
Inlet SO_2 Conc., ppm	None	None	None	None	None	None	None	None
Conc. Of Persulfate, M	0.05	0.05	0.05	0.05	0.05	0.05	0.05	0.05
Conc. Of Iron(II), M	0.004	0.008	0.01	0.02	0.04	0.06	0.08	0.1
Initial pH	2.65	2.66	2.66	2.56	2.57	2.52	2.51	2.46
Final pH	2.60	2.62	2.60	2.52	2.55	2.48	2.48	2.45
Fractional NO conver.,%	34.83	36.93	41.62	46.11	47.01	45.01	41.22	0
Fractional SO_2 conver., %	N/A	N/A	N/A	N/A	N/A	N/A	N/A	N/A

Table E-3. Summary of Experimental Runs (#17-24)

Conditions/Run Num.	17	18	19	20	21	22	23	24
Temp., °C	23	23	30	30	40	40	50	50
Inlet NO Conc., ppm	1004	1004	1004	1004	1004	1004	1004	1004
Inlet SO_2 Conc., ppm	None	None	None	None	None	None	None	None
Conc. Of Persulfate, M	0.05	0.05	0.05	0.05	0.05	0.05	0.05	0.05
Conc. Of Iron(II), M	None	0.01	None	0.01	None	0.01	None	0.01
Initial pH	4.14	2.65	4.68	2.73	4.79	2.38	2.68	2.41
Final pH	3.92	2.66	4.17	2.66	4.15	2.35	2.59	2.35
Fractional NO conver.,%	9.58	20.66	10.48	24.84	25.65	37.33	33.37	41.62
Fractional SO_2 conver., %	N/A	N/A	N/A	N/A	N/A	N/A	N/A	N/A

Table E-4. Summary of Experimental Runs (#25-32)

Conditions/Run Num.	25	26	27	28	29	30	31	32
Temp., °C	60	60	70	70	23	23	30	30
Inlet NO Conc., ppm	1004	1004	1004	1004	1004	1004	1004	1004
Inlet SO_2 Conc., ppm	None	None	None	None	None	None	None	None
Conc. Of Persulfate, M	0.05	0.05	0.05	0.05	0.1	0.1	0.1	0.1
Conc. Of Iron(II), M	None	0.01	None	0.01	None	0.01	None	0.01
Initial pH	4.19	2.26	3.49	1.78	3.89	2.73	3.70	2.59
Final pH	2.90	2.15	2.33	1.83	3.78	2.75	3.44	2.57
Fractional NO conver., %	35.53	56.39	37.03	70.36	14.07	27.05	18.96	35.33
Fractional SO_2 conver., %	N/A	N/A	N/A	N/A	N/A	N/A	N/A	N/A

Table E-5. Summary of Experimental Runs (#33-40)

Conditions/Run Num.	33	34	35	36	37	38	39	40
Temp., °C	40	40	50	50	60	60	70	70
Inlet NO Conc., ppm	1004	1004	1004	1004	1004	1004	1004	1004
Inlet SO_2 Conc., ppm	None	None	None	None	None	None	None	None
Conc. Of Persulfate, M	0.1	0.1	0.1	0.1	0.1	0.1	0.1	0.1
Conc. Of Iron(II), M	None	0.01	None	0.01	None	0.01	None	0.01
Initial pH	4.72	2.35	4.50	2.37	3.76	2.38	3.19	2.26
Final pH	2.99	1.69	3.38	2.19	2.70	2.11	2.16	1.85
Fractional NO conver.,%	39.02	47.70	52.10	63.37	58.68	75.95	68.76	79.14
Fractional SO_2 conver., %	N/A	N/A	N/A	N/A	N/A	N/A	N/A	N/A

Table E-6. Summary of Experimental Runs (#41-48)

Conditions/Run Num.	41	42	43	44	45	46	47	48
Temp., °C	23	23	30	30	40	40	50	50
Inlet NO Conc., ppm	1004	1004	1004	1004	1004	1004	1004	1004
Inlet SO_2 Conc., ppm	None	None	None	None	None	None	None	None
Conc. Of Persulfate, M	0.2	0.2	0.2	0.2	0.2	0.2	0.2	0.2
Conc. Of Iron(II), M	None	0.01	None	0.01	None	0.01	None	0.01
Initial pH	4.77	2.78	4.69	2.78	4.76	2.67	4.49	2.44
Final pH	4.42	2.79	4.20	2.80	3.96	2.66	3.28	2.36
Fractional NO conver.,%	18.96	31.14	32.53	39.12	49.60	56.79	61.28	70.96
Fractional SO_2 conver., %	N/A	N/A	N/A	N/A	N/A	N/A	N/A	N/A

Table E-7. Summary of Experimental Runs (#49-56)

Conditions/Run Num.	49	50	51	52	53	54	55	56
Temp., °C	60	60	70	70	23	23	30	30
Inlet NO Conc., ppm	1004	1004	1004	1004	502	502	502	502
Inlet SO_2 Conc., ppm	None	None	None	None	None	None	None	None
Conc. Of Persulfate, M	0.2	0.2	0.2	0.2	0.05	0.05	0.05	0.05
Conc. Of Iron(II), M	None	0.01	None	0.01	None	0.01	None	0.01
Initial pH	4.07	2.33	4.11	2.89	5.86	3.54	5.73	3.58
Final pH	2.78	2.17	2.48	1.90	5.17	3.55	4.81	3.57
Fractional NO conver., %	64.17	80.04	71.86	85.03	9.64	17.13	20.52	37.25
Fractional SO_2 conver., %	N/A	N/A	N/A	N/A	N/A	N/A	N/A	N/A

Table E-8. Summary of Experimental Runs (#57-64)

Conditions/Run Num.	57	58	59	60	61	62	63	64
Temp., °C	40	40	50	50	60	60	70	70
Inlet NO Conc., ppm	502	502	502	502	502	502	502	502
Inlet SO_2 Conc., ppm	None	None	None	None	None	None	None	None
Conc. Of Persulfate, M	0.05	0.05	0.05	0.05	0.05	0.05	0.05	0.05
Conc. Of Iron(II), M	None	0.01	None	0.01	None	0.01	None	0.01
Initial pH	5.52	3.32	5.38	3.45	5.26	3.27	4.78	3.14
Final pH	4.67	3.29	4.10	3.36	3.80	3.11	3.27	2.98
Fractional NO conver.,%	34.06	53.39	36.85	58.76	57.97	66.53	65.34	80.68
Fractional SO_2 conver., %	N/A	N/A	N/A	N/A	N/A	N/A	N/A	N/A

Table E-9. Summary of Experimental Runs (#65-72)

Conditions/Run Num.	65	66	67	68	69	70	71	72
Temp., °C	23	23	30	30	40	40	50	50
Inlet NO Conc., ppm	502	502	502	502	502	502	502	502
Inlet SO_2 Conc., ppm	None	None	None	None	None	None	None	None
Conc. Of Persulfate, M	0.1	0.1	0.1	0.1	0.1	0.1	0.1	0.1
Conc. Of Iron(II), M	None	0.01	None	0.01	None	0.01	None	0.01
Initial pH	4.51	2.93	4.45	3.11	5.01	2.96	3.84	2.89
Final pH	3.10	2.94	4.24	3.09	4.25	2.92	3.41	2.83
Fractional NO conver.,%	16.33	27.69	30.28	45.62	40.64	51.20	53.98	63.15
Fractional SO_2 conver., %	N/A	N/A	N/A	N/A	N/A	N/A	N/A	N/A

Table E-10. Summary of Experimental Runs (#73-80)

Conditions/Run Num.	73	74	75	76	77	78	79	80
Temp., °C	60	60	70	70	23	23	30	30
Inlet NO Conc., ppm	502	502	502	502	502	502	502	502
Inlet SO_2 Conc., ppm	None	None	None	None	None	None	None	None
Conc. Of Persulfate, M	0.1	0.1	0.1	0.1	0.2	0.2	0.2	0.2
Conc. Of Iron(II), M	None	0.01	None	0.01	None	0.01	None	0.01
Initial pH	5.55	2.79	4.13	2.76	7.60	3.65	7.38	3.67
Final pH	4.86	2.65	2.64	2.49	6.61	3.69	6.18	3.68
Fractional NO conver., %	62.35	65.94	69.92	75.10	10.49	13.28	15.01	25.37
Fractional SO_2 conver., %	N/A	N/A	N/A	N/A	N/A	N/A	N/A	N/A

Table E-11. Summary of Experimental Runs (#81-88)

Conditions/Run Num.	81	82	83	84	85	86	87	88
Temp., °C	40	40	50	50	60	60	23	23
Inlet NO Conc., ppm	502	502	502	502	502	502	753	753
Inlet SO_2 Conc., ppm	None	None	None	None	None	None	None	None
Conc. Of Persulfate, M	0.2	0.2	0.2	0.2	0.2	0.2	0.1	0.1
Conc. Of Iron(II), M	None	0.01	None	0.01	None	0.01	None	0.01
Initial pH	7.17	3.63	6.43	3.55	5.88	3.40	7.77	3.45
Final pH	5.67	3.57	5.10	3.54	4.41	3.17	6.02	3.39
Fractional NO conver.,%	22.84	33.20	25.37	36.52	32.40	57.77	15.80	20.85
Fractional SO_2 conver., %	N/A	N/A	N/A	N/A	N/A	N/A	N/A	N/A

Table E-12. Summary of Experimental Runs (#89-96)

Conditions/Run Num.	89	90	91	92	93	94	95	96
Temp., °C	30	30	40	40	50	50	60	60
Inlet NO Conc., ppm	753	753	753	753	753	753	753	753
Inlet SO_2 Conc., ppm	None	None	None	None	None	None	None	None
Conc. Of Persulfate, M	0.1	0.1	0.1	0.1	0.1	0.1	0.1	0.1
Conc. Of Iron(II), M	None	0.01	None	0.01	None	0.01	None	0.01
Initial pH	7.54	3.61	7.35	3.55	5.93	3.43	5.52	3.36
Final pH	5.52	3.58	4.98	3.43	4.32	3.22	3.57	3.06
Fractional NO conver.,%	17.13	25.90	47.01	53.65	60.29	72.11	61.75	82.20
Fractional SO_2 conver., %	N/A	N/A	N/A	N/A	N/A	N/A	N/A	N/A

Table E-13. Summary of Experimental Runs (#97-104)

Conditions/Run Num.	97	98	99	100	101	102	103	104
Temp., °C	23	23	30	30	40	40	50	50
Inlet NO Conc., ppm	753	753	753	753	753	753	753	753
Inlet SO_2 Conc., ppm	None	None	None	None	None	None	None	None
Conc. Of Persulfate, M	0.05	0.05	0.05	0.05	0.05	0.05	0.05	0.05
Conc. Of Iron(II), M	None	0.01	None	0.01	None	0.01	None	0.01
Initial pH	7.74	3.68	7.60	3.77	7.29	3.67	6.45	3.50
Final pH	6.27	3.69	5.93	3.72	5.43	3.56	4.67	3.34
Fractional NO conver., %	10.49	13.28	15.01	25.37	22.84	33.20	25.37	36.52
Fractional SO_2 conver., %	N/A	N/A	N/A	N/A	N/A	N/A	N/A	N/A

Table E-14. Summary of Experimental Runs (#105-112)

Conditions/Run Num.	105	106	107	108	109	110	111	112
Temp., °C	60	60	23	23	30	30	40	40
Inlet NO Conc., ppm	753	753	753	753	753	753	753	753
Inlet SO_2 Conc., ppm	None	None	None	None	None	None	None	None
Conc. Of Persulfate, M	0.05	0.05	0.2	0.2	0.2	0.2	0.2	0.2
Conc. Of Iron(II), M	None	0.01	None	0.01	None	0.01	None	0.01
Initial pH	5.58	3.40	7.93	3.75	7.73	3.75	7.34	3.55
Final pH	4.03	3.15	6.04	3.77	5.66	3.72	4.98	3.47
Fractional NO conver.,%	32.40	57.77	15.05	29.75	20.04	31.87	54.85	62.68
Fractional SO_2 conver., %	N/A	N/A	N/A	N/A	N/A	N/A	N/A	N/A

Table E-15. Summary of Experimental Runs (#113-120)

Conditions/Run Num.	113	114	115	116	117	118	119	120
Temp., °C	50	50	60	60	23	30	40	50
Inlet NO Conc., ppm	753	753	753	753	1004	1004	1004	1004
Inlet SO_2 Conc., ppm	None	None	None	None	~1550	~1550	~1550	~1550
Conc. Of Persulfate, M	0.2	0.2	0.2	0.2	0.1	0.1	0.1	0.1
Conc. Of Iron(II), M	None	0.01	None	0.01	None	None	None	None
Initial pH	6.45	3.48	5.18	3.36	4.74	5.12	5.43	5.24
Final pH	4.21	3.36	3.51	3.07	3.35	4.30	4.27	4.35
Fractional NO conver.,%	57.64	75.30	75.50	83.67	76.85	77.54	79.74	80.34
Fractional SO_2 conver., %	N/A	N/A	N/A	N/A	99.99	99.99	99.99	99.99

Table E-16. Summary of Experimental Runs (#121-128)

Conditions/Run Num.	121	122	123	124	125	126	127	128
Temp., °C	60	70	80	50	50	50	50	50
Inlet NO Conc., ppm	1004	1004	1004	1004	1004	1004	1004	1004
Inlet SO_2 Conc., ppm	~1550	~1550	~1550	~1550	~1550	~1550	~1550	~1550
Conc. Of Persulfate, M	0.1	0.1	0.1	0.1	0.1	0.1	0.02	0.05
Conc. Of Iron(II), M	None	None	None	None	None	None	None	None
Initial pH	4.82	4.57	4.21	4.64	7.74	11.15	4.89	4.13
Final pH	2.95	2.74	2.22	4.59	7.50	11.83	3.42	3.27
Fractional NO conver., %	82.93	83.03	87.92	24.95	53.70	43.61	17.60	19.56
Fractional SO_2 conver., %	99.99	99.99	99.99	99.99	99.99	99.99	99.99	99.99

Table E-17. Summary of Experimental Runs (#129-136)

Conditions/Run Num.	129	130	131	132	133	134	135	136
Temp., °C	50	30	50	70	90	70	40	60
Inlet NO Conc., ppm	1004	1004	1004	1004	1004	502	500	750
Inlet SO_2 Conc., ppm	1550	1550	1550	1550	None	None	None	None
Conc. Of Persulfate, M	0.2	0.1	0.1	0.1	0.1	0.1	0.02	0.02
Conc. Of Iron(II), M	None	0.01	0.01	0.01	0.01	None	0.01	0.01
Initial pH	4.93	3.59	3.48	3.08	2.27	4.78	3.43	3.33
Final pH	2.91	3.26	3.29	2.54	2.15	3.13	3.31	3.10
Fractional NO conver.,%	73.65	46.21	54.19	78.74	~100	50.80	37.25	42.51
Fractional SO_2 conver., %	99.99	99.99	99.99	99.99	N/A	N/A	N/A	N/A